INTERNAL REPORT

HIP - 2009 - 02

GEANT4 HADRONIC CASCADE MODELS AND CMS DATA ANALYSIS – COMPUTATIONAL CHALLENGES IN THE LHC ERA

Aatos Heikkinen

Helsinki Institute of Physics,
P.O. Box 64, FIN-00014 University of Helsinki, Finland

HELSINKI INSTITUTE OF PHYSICS
P.O. Box 64 • FIN-00014 UNIVERSITY OF HELSINKI • FINLAND

INTERNAL REPORT

HIP - 2009 - 02

Geant4 Hadronic Cascade Models and CMS Data Analysis – Computational Challenges in the LHC era

Aatos Heikkinen

Helsinki Institute of Physics,
P.O. Box 64, FIN-00014 University of Helsinki, Finland

ACADEMIC DISSERTATION

To be presented, with the permission of the Faculty of Science of the University of Helsinki, for public criticism in the University Main Building, Auditorium XII, Unioninkatu 34 (3rd floor), on Thursday, 13th of August 2009, at 12 o'clock.

Helsinki 2009

ISBN 978–952–10–5675–8 (paperback)
ISBN 978–952–10–5676–5 (pdf)
ISSN 1455–0563
http://ethesis.helsinki.fi
Helsinki University Print 2009

Acknowledgments

This thesis is based on research carried out during the years 2000-2007 as a member of the CMS Software and Physics group of the Helsinki Institute of Physics (HIP). Part of the work was done at CERN, TRIUMF, and SLAC.

During these years I was a member of the CMS experiment and Geant4 collaboration. In the CMS Tracker Project I participated in the development activities of tracker test beam software and data analysis using LHC test beam data and Geant4 simulated CMS events. In Geant4 my responsibilities were to translate existing hadronic models to Geant4 and develop them further. I was a representative of HIP on the Geant4 technical steering board, and in 2005–2007 I was coordinating the activities of the Geant4 Hadronic Physics Working Group.

I am grateful to my instructor, adjunct professor Veikko Karimäki, for introducing the subject of this thesis and providing a pleasant and informal atmosphere for the research. I also acknowledge the guidance of professor Jorma Tuominiemi.

Software development in high-energy physics is a collaborative effort. I want to acknowledge particularly Hans-Peter Wellisch for introducing me to the Geant4 hadronic framework, Nikita Stepanov for providing the original INUCL code, and Pekka Kaitaniemi for preparing an elastic interface to it. I acknowledge Dennis Wright for developing the kaon extension to the Bertini code, Jukka Heinonen and Mika Haapakorpi for developing software for the Helsinki Silicon Beam Telescope, Sami Lehti for providing simulated CMS data, and Tomas Lindén for providing Linux cluster computing support.

Special thanks go to my colleagues and friends for sharing so many memorable moments during these years - Juha Kalliopuska, Makoto Asai, Barbara Machiano, Tapio Lampén, Tomas Lindén, Sami Lehti, Jaakko Härkönen, Jukka Heinonen, Mika Haapakorpi, and Jukka Nysten.

This work was supported financially by the Stanford Linear Accelerator Center (SLAC), KEK, the CERN IT division, UNESCO, ESA, the Magnus Ehnrooth Foundation, and the Waldemar von Frenckell Foundation. Being able to share the excitement of LHC-era physics computing with colleagues from different cultures has been the most enjoyable part of my work.

CERN, July 17th, 2009

Aatos Heikkinen

Abstract

The simulation and data analysis of the CERN Large Hadron Collider (LHC) experiments, such as the CMS, will be a major challenge because of the complexity of the experimental setups and enormous volumes of data involved. As the computer industry has moved to an object-oriented paradigm and a related methodology, the high-energy physics (HEP) community has followed the trend, looking for the benefits that object-oriented technology can offer.

The general-purpose detector simulation toolkit Geant4 has been developed following the object-orientation philosophy, and many previously scattered models for physics generators have been remodelled, improved, and included in this de facto standard LHC physics modelling tool.

This thesis presents studies related to the development of hadronic cascade models, used for the accurate simulation of medium-energy hadron-nucleus reactions, up to 10 GeV. These models are typically needed in hadronic calorimeter studies and in the estimation of radiation backgrounds. Various applications outside HEP include the medical field (such as hadron treatment simulations), space science (satellite shielding), and nuclear physics (spallation studies). We discuss several significant improvements released in Geant4 version 9.1, compared with older Geant4 physics models and the FORTRAN -based GEANT3 (the predecessor of Geant4 and de facto standard for HEP detector simulation before the LHC era). Validation results are presented, and the significance of the new models for computing in the LHC era is estimated. In particular, we estimate the ability of the Bertini cascade to simulate CMS hadron calorimeter HCAL.

LHC test beam activity has a tightly coupled cycle of simulation-to-data analysis. Typically, a Geant4 computer experiment is used to understand test beam measurements, but at the same time new data can be used to improve models in Geant4. The data and simulation are used, for example, to optimise hadronic calorimeter setups and perform energy calibration. Similarly, in tracking, we want to understand the experimental setup, how particles scatter from tracker material, or how the misalignment of detector elements affects signal reconstruction.

Following this line of thought, another aspect of this thesis is a description of studies related to developing new CMS H2 test beam data analysis tools and performing data analysis on the basis of CMS Monte Carlo events. These events have been simulated in detail using Geant4 physics models, full CMS detector description, and event reconstruction.

We have made extensive use of the ROOT data analysis framework, which provides a new approach and exciting functionality to cope with computing challenges in the LHC era. For example, several artificial neural network (ANN) implementations are integrated in ROOT, together with advanced parallel processing features needed in grid computing. With the help of the ROOT framework we have developed an offline ANN-based approach to tag b-jets associated with heavy neutral Higgs particles, and we show that this kind of NN methodology can be successfully used to separate the Higgs signal from the background in the CMS experiment.

List of Publications

This thesis consists of an overview and the following publications, which are referred to in the text by their Roman numerals.

I **A. Heikkinen** with Geant4 collaboration, *Geant4 – a simulation toolkit*, Nuclear Instruments and Methods in Physics Research A 506 (2003) 250–303

II **A. Heikkinen**, N. Stepanov, and J. P. Wellisch, *Bertini intra-nuclear cascade implementation in Geant4*, Proceedings of the Conference for Computing in High Energy and Nuclear Physics, CHEP03, La Jolla, USA, SLAC-R-636, [arXiv:nucl-th/0306008], 2003

III **A. Heikkinen** with Geant4 collaboration, *Geant4 Developments and Applications*, IEEE Transactions on Nuclear Science, Vol. 53, No. 1, February 2006

IV D. H. Wright, T. Koi, G. Folger, V. Ivantchenko, M. Kossov, N. Starkov, **A. Heikkinen**, and J. P. Wellisch, *Recent Developments and Validations in Geant4 Hadronic Physics*, 12^{th} International Conference on Calorimetry in High Energy Physics, CALOR'06, SLAC-PUB-12348, 2006

V K. Banzuzi, M. Haapakorpi, **A. Heikkinen**, J. V. Heinonen, A. Honkanen, V. Karimäki, T. Mäenpää, E. Pietarinen, T. Salomäki, and J. Tuominiemi, *Performance and calibration studies of silicon strip detectors in a test beam*, Nuclear Instruments and Methods in Physics Research A 453 (2000) 536–544

VI K. Banzuzi, S. Czellar, **A. Heikkinen**, J. Härkönen, V. Karimäki, M. Leppänen, P. Luukka, S. Nummela, E. Pietarinen, E. Tuominen, J. Tuominiemi, and L. Wendland, *Test beam results with upgraded Helsinki Silicon Beam Telescope*, HIP-2001-08, December 2001

VII **A. Heikkinen** and S. Lehti, *Tagging b jets associated with heavy neutral MSSM Higgs bosons*, Nuclear Instruments and Methods in Physics Research A 559 (2006) 195–198

VIII T. Lindén, F. García, **A. Heikkinen**, and S. Lehti, *Optimizing Neural Network Classifiers with ROOT on a Rocks Linux Cluster*, Revised Selected Papers of 8th International Workshop, PARA 2006. Applied Parallel Computing, Lecture Notes in Computer Science, LNCS 4699 (2007) 1065–1073

Brief description of the contents of Publications

Publications [**I**]–[**IV**] discuss work done with hadronic physics models in Geant4 collaboration, while Publications [**V**]–[**VIII**] represent a development of CMS collaboration data analysis tools, utilising LHC test beam- or Geant4- generated Monte Carlo data. The arrangement of the papers closely follows the chronology of original publication.

Publication I is the very first general paper of Geant4, published collectively by the collaboration. This extended paper introduces and describes all the key features built into the Geant4 framework for detector simulation. For hadronic physics modelling the requirements span more than 15 orders of magnitude in energy. Publication explains how Geant4 manages the complex nature of LHC experiment requirements and specific subdetector questions, such as pion nuclear interactions in calorimeter simulations.

Publication II describes a Bertini cascade implementation in Geant4. The following sub-models are discussed: an intra-nuclear cascade model with excitons, pre-equilibrium model, nucleus explosion model, fission model, an evaporation model, and gamma de-excitation. Physics performance is reviewed.

Publication III is a second general Geant4 paper, the emphasis of which is on describing the major Geant4 developments during the years 2003–2006.

Publication IV presents Geant4 hadronic physics developments and validations from the perspective of high-energy physics calorimetry and shower shape studies. An example of the performance of the Bertini cascade is presented, and the longitudinal shower profile in the CMS H2 test beam calorimeter is compared with Geant4 simulation.

Publication V describes the performance studies of silicon strip detectors at the CERN H2 test beam. Emphasis is placed on the calibration of the response of the Helsinki Silicon Beam Telescope (SiBT). In this paper the geometric alignment of the detector planes is investigated.

Publication VI extends the research reported in Publication [**V**] by presenting test beam results for the upgraded SiBT operating at the CERN H2 test beam. The architecture and configuration of the object-oriented, online, and offline software in terms of the Unified Modeling Language is described. Cluster finding and track reconstruction results obtained with 225 GeV muon beams are presented.

Publication VII demonstrates an artificial neural network application for tagging b-jets associated with heavy neutral MSSM Higgs bosons in the CMS detector. The data set in this study is produced using full CMS simulation based on Geant4 geometry description and physics models, as described in Publication [**I**]. The possibility of distinguishing a Higgs signal from a QCD background with multi-layer perceptrons (MLP) is investigated. An unsupervised learning algorithm of self-organising maps is used to separate Higgs events from the LHC Drell-Yan background.

Publication VIII elaborates the neural network approach introduced in Publication [**VII**] to b-tagging, by optimising MLP classifiers with the ROOT data analysis tool on a Linux Cluster. Advanced features of the object-oriented ROOT data analysis framework are utilised.

Author's contribution

The author played an active role in all the published papers. Since the year 2001 until 2008 he was a representative of HIP on the Geant4 Technical Steering Board, and during the years 2005-2007 he co-coordinated the Geant4 Hadronic Physics Working Group. The author also coordinated software development for the Helsinki Silicon Beam Telescope at the CMS H2 test beam.

I The author coordinated the implementation of the INUCL Bertini cascade into Geant4, participated in the further development and implementation of Bertini sub-models, and helped, through his activity in the Geant4 Hadronic Physics Working Group, to prepare the hadronic physics section of Publication.

II The author wrote Publication and was the developer responsible for the object-oriented software described in the paper.

III The author developed further Bertini cascade models, validated isotope production, and extended the applicability of the model up to 10 GeV for incoming hadrons.

IV The author developed Bertini software based on the INUCL code utilised in shower shape studies. He initiated the development of the elastic scattering interface for the Bertini model, coordinated the further development of its sub-models, and participated in the development of the Bertini cascade kaon extension and Geant4 hadronic physics validation efforts.

V As a part of the CMS H2 test beam activity, the author coordinated a project to redesign the old FORTRAN-based monitoring software using the C++ -language and participated in the data collection and offline data analysis.

VI The author coordinated the development of the architecture and configuration of the object-oriented online and offline software used in test beam experiments with the SiBT. The author edited the offline section of the paper.

VII The author was the main author of Publication, developed a neural network method and carried out the analysis, and introduced the usage of unsupervised learning with self-organising maps.

VIII The author outlined Publication and wrote a significant part of the paper. He performed runs in the Linux cluster to optimise the neural networks and prepared the plots for Publication.

Contents

0 Computing Challenges in the LHC era **13**
0.1 Software engineering and object-orientation 14
0.2 Monte Carlo method and cluster computing 16
0.3 Data analysis with artificial neural networks 17

I INTRA-NUCLEAR CASCADE MODELS FOR GEANT4 **19**

1 Geant4 and its Applications **20**
1.1 Geant4 toolkit 20
1.2 Physics modelling 23
1.3 Simulation of detector systems using Geant4 30

2 Bertini Intra-Nuclear Cascade Models **34**
2.1 Bertini cascade 35
2.2 Cross-sections 39
2.3 Design of Bertini sub-models 39

3 Applications for Geant4 Bertini Cascade **44**
3.1 Kaon extension 44
3.2 Quasi-elastic K^+ scattering from lead 45
3.3 Simulation of the CMS hadronic calorimeter 46

4 Validation of Geant4 Hadronic Models **50**
4.1 Validation suite for intermediate energy interactions 50
4.2 Validation of Bertini cascade models 50
4.3 Isotope production 55

II ANALYSIS OF THE SiBT DATA AND HIGGS EVENTS IN THE CMS EXPERIMENT **59**

5 Helsinki Silicon Beam Telescope for the CMS H2 Beam Line **60**
5.1 Helsinki Silicon Beam Telescope (SiBT) 60

5.2 SiBT cluster analysis 61
5.3 Detector response calibration and resolution 62

6 H2 Test Beam Software for the SiBT **65**
6.1 Geant4 simulation of the SiBT 65
6.2 Online software for the SiBT 66
6.3 Offline monitoring 68

7 Neural Networks for Higgs Signal b-tagging in the CMS Experiment **73**
7.1 Tagging of b-jets in $\mathrm{pp} \rightarrow \mathrm{b\bar{b}H_{SUSY}} \rightarrow \tau\tau$ channel 73
7.2 Multi-layer perceptrons for a signal vs. background classification 74
7.3 Separation of Higgs signal from the QCD -background with self-organising maps . 79

8 Cluster Computing and the CMS Data Analysis **83**
8.1 ROOT-based CMS data analysis in a cluster environment 83
8.2 Computational environment for the Ametisti Linux cluster 84
8.3 Optimising Higgs neural network event -classifiers 84

9 Conclusions **87**

Chapter 0

Computing Challenges in the LHC era

This work belongs to the field of computational high-energy physics (HEP).

The arrangement of the material will follow the chronology of the original publication dates of Publications **[I]**–**[VIII]**, and the main body of the work we are going to describe falls into two parts.

In Part I, covering Chapters 1–4, we present work done in the Geant4 collaboration while developing medium-energy hadronic cascade models for use in the next generation of HEP experiments. The discussion is based on Publications **[I]**–**[IV]**. We start by introducing Geant4 in Chapter 1. Chapter 2 will introduce the Bertini cascade models prepared for Geant4. Chapter 3 discusses the Bertini cascade kaon extension and a simulation of the CMS hadronic calorimeter, and Chapter 4 shows examples of various validations performed to ensure the quality of the physics models.

In Part II we describe the work done in the Compact Muon Solenoid (CMS) collaboration, and the discussion is based on Publications **[V]**–**[VIII]**. We start in Chapters 5 and 6 with a description of the CMS H2 test beam activity from the perspective of online and offline software development for the Helsinki Silicon Beam Telescope (SiBT). Data analysis using these tools, including Geant4-based detector simulation, is discussed. Additionally, in Chapter 7 we utilise an increasingly important statistical data analysis methodology based on neural networks. We continue with work on signal background discrimination studies performed with neural classifiers to separate Higgs boson signal from the dominating QCD background in the Compact Muon Solenoid (CMS) detector. This analysis uses Monte Carlo data produced with a full CMS simulation chain with a detailed Geant4 detector description. Chapter 8 will focus on the cluster computing environment used for Higgs physics simulation studies. In Chapter 9 we draw conclusions.

Our aim is to demonstrate the fruitful interplay between different aspects of HEP experiments, namely:

Theory In this work intra-nuclear cascade models for Geant4 represent the theoretical aspect (Chapter 2).

Experiments CMS H2 test beam activity with the Helsinki Silicon Beam Tracker (Chapters 5 and 6).

Computing Geant4 Monte Carlo simulation, and artificial neural network-based data analysis (Chapters 1, 3, 4, and 6–8).

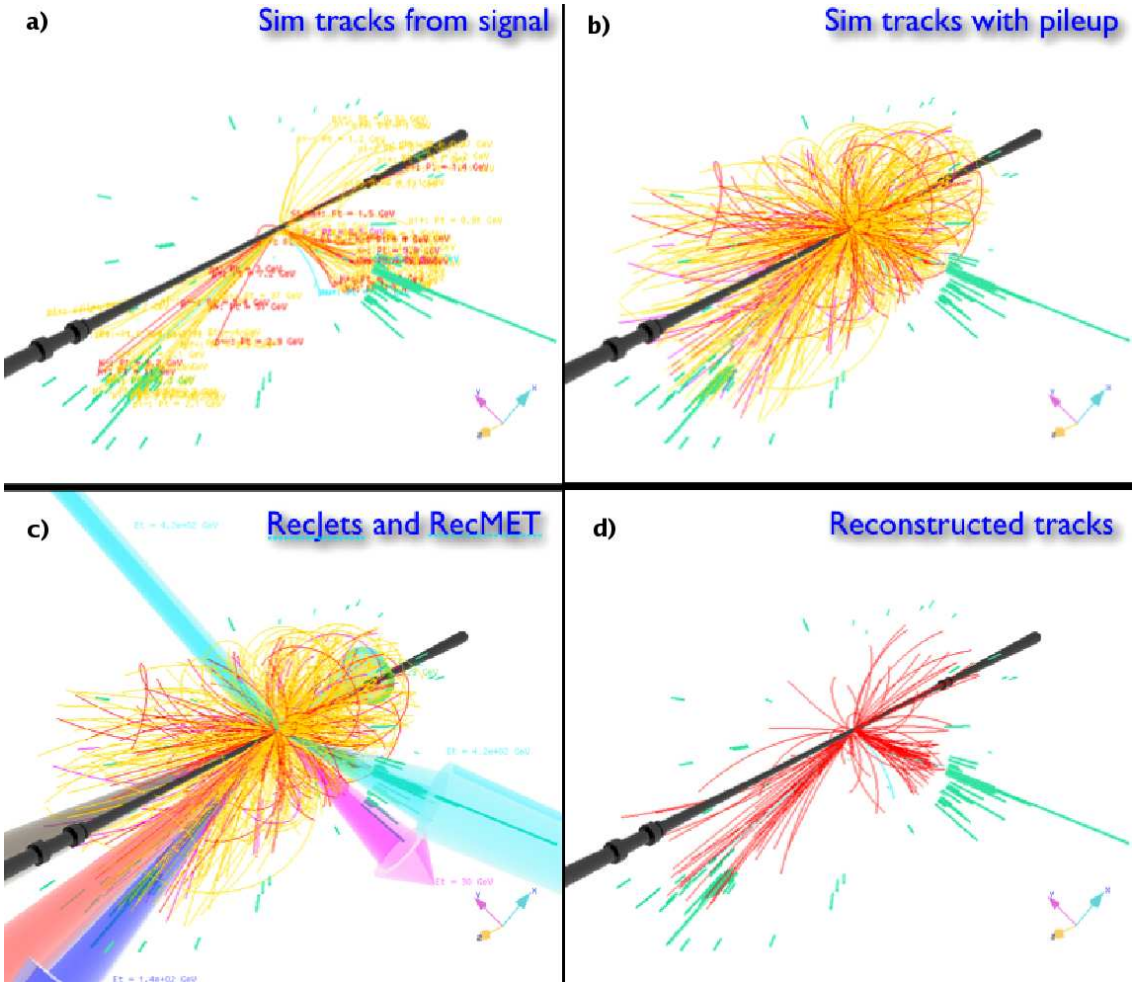

Figure 1: Simulation–data analysis cycle demonstrated with Geant4-based Iguana [24] visualisation of SUSY particle production in the CMS detector. **a)** A SUSY signal event before adding pile-up. **b)** The same event with high-luminosity pile-up added. **c)** Reconstructed Jets and Missing transverse energy of the full event. **d)** Reconstructed tracks of the full event. (Courtesy of Iguana group, I. Osborne, S. Spiropulu, and S. Wynhoff)

In this work these aspects are present in CMS detector development and test beam activity, which has a tightly coupled cycle of simulation-to-data analysis, which is demonstrated in Fig. 1.

Before going further, we want briefly to introduce the key methods used in this thesis work to meet the challenges raised by the Large Hadron Collider (LHC) era experiments: object-orientation with software engineering, Monte Carlo simulation, the computer technology of clusters, and artificial neural networks.

0.1 Software engineering and object-orientation

The LHC era, with its large multidisciplinary computing projects, have raised a need to coordinate a traditionally informal scientific programming practice, so in recent years software engineering aspects have become increasingly important. The CMS collaboration, for example, has

taken formal actions to improve the software process to address critical issues: efficiency, usability, reliability, and maintainability. In a similar fashion the Geant4 collaboration has emphasised formal engineering practices, such as defining the software requirements [113].

These aspects of the software process should be reflected against key techniques for the advancement of scientific software in general [1]:

- developing and publishing the algorithms themselves,
- open publication of well-documented, refereed, and tested programs, and
- producing portable universal modules supporting standards.

Further, ideals in using a programming language include directness (representing concepts directly) and independence (representing independent concepts independently). Ideas and thoughts should be reflected directly in the code.

On a practical level, we have to find a way to map the modern software process and technology to the real-world HEP software environment, where many programmers are physicists. The most critical decision was made in the mid-'90s, when it was decided to use object-orientation and C++ as the language of the LHC experiments. This meant that practically all the scientific software used at CERN needed to be re-invented, or at least translated according to the demands of the chosen programming paradigm. This radical methodological shift has enabled modelling of LHC physics with many new and previously unavailable language constructs.

The object-oriented language supports and implements [4]:

- encapsulation (information hiding and data abstraction);
- message passing (means for objects to communicate; polymorphism), and
- the inheritance of attributes by a subclass from a class higher in the hierarchy (dynamic binding).

These are powerful techniques used nowadays in LHC software engineering to manage problem domain complexity.

C++ is an object-oriented multiparadigm programming language, with great flexibility in programming styles and notational convenience. C++ supports an ability to create types that are optimal for specific applications (data abstraction), and programming using parametrised types (generic programming). In C++ the class contract is used to express different kinds of concepts [106]. C++ supports a rich set of logical design alternatives, which raises a new requirement, to carefully consider different design aspects. For example, the object-orientation paradigm naturally supports the reuse of a common component. However, the coupling implied by reuse in itself is undesirable, since subsystems should not be tied to a large block of unnecessary code [88].

Large projects, such as LHC, benefit from their implementers' knowing when to make code reusable (typically, when clients attempt to reuse a common component for different purposes), and when to reuse code (independent clients using the standard components without requiring functional changes).

Typically, when modelling a physical phenomenon, a computational physicist approaches the problem by dividing it into interacting agents. These agents or objects are defined as a collection of data, called its *state*, and the procedures capable of altering that state. Further, using the services provided by an object should be restricted to accessing encapsulated features through a well-defined interface [4].

With object-orientation techniques developers try to maintain scientific software libraries of reusable objects, with clearly defined specifications. Users can combine and further specialise

objects provided by a framework such as the Geant4 software for general particle detector simulations into applications that meet their particular needs. Other examples of software fulfilling these requirements are the CERN-originated Common Libraries for High-Energy Physics (CLHEP) and the ROOT data analysis framework.

In this thesis work, the clearest example of advanced object-orientation techniques can be found in the design of the SiBT software. Publication [**VI**] and Chapter 6 demonstrate this work accomplished with a CASE tool, Rational Rose, using a unified modelling language, UML.

0.2 Monte Carlo method and cluster computing

The Monte Carlo method was pioneered by S. Ulam and J. von Neuman for the development of thermonuclear weapons [1]. The Monte Carlo method is a numerical solution to problems that model objects (particles in our applications) interacting with other objects (or their environment), based upon the most essential relationships. The solution is obtained by the random sampling of these relationships and iterating until the result converges. This method exploits computers to maximum advantage and readily absorbs all the computer power that one may have at one's disposal.

The minimal requirements for the use of the Monte Carlo method in particle physics are quite simple, including:

- the tabulation or modelling of cross-sections and particle relationships;
- sampling from probability distributions;
- the definition of geometries and particle tracing through geometries;
- the scoring and accumulation of results, and
- an interface to facilitate human interaction.

The uncertainties in the cross-sections and modelling of particle relationships define the accuracy of the Monte Carlo method [63].

Computational issues in experimental particle physics are closely linked to the fast development of computer technology and software engineering technologies, making new Monte Carlo simulation and data analysis techniques available.

The exponential increase in computing power available in high-performance computing cluster environments is likely to continue in the future through evolutionary changes in computing technology (e.g. recent development in multi-core processors). These changes may sometimes hinder the actual research activities, since great effort and expense are often required in translating, porting, and optimising codes. If possible, such changes should be anticipated and incorporated into the future plans for the development of scientific software.

The impact of efficient computers and software systems on particle physics has been tremendous, making possible the simulation and optimisation of the complicated detector systems built for LHC. Massive Monte Carlo production runs utilise thousands of CPUs and the future LHC data analysis efforts have been distributed in computing centers all around the globe. The management of simulated or measured data for the millions of channels that typical modern large-scale HEP detectors consist of is a challenging task [116].

D. Filges and W. Gudowski have argued in [63] that a high-energy transport code should aim at:

- implementing better physics;

- promoting precise validation processes;
- improving the modularity of models;
- providing user-friendly interfaces to transport code functionality, and
- developing common utilities for input/output analysis.

The following chapter, Chapter 1 will describe how the Geant4 Monte Carlo toolkit has addressed these goals.

0.3 Data analysis with artificial neural networks

A traditional method used to separate signal and background in high-energy physics (HEP) is to make cuts in a multidimensional parameter space. This analysis is often done without taking into account all the correlations between the variables, which means that useful information is lost.

The need for efficient analysis methods has led to the use of multivariate techniques and alternative data analysis methods, such as artificial neural networks, to distinguish between signal and background events [35, 41, 90]. The artificial neural network (ANN) approach is in general resistant to noise in data samples, and hence it is suitable for LHC-era HEP experiments in which high fluxes of particles and event pile-up raise serious data analysis challenges.

ANNs have successfully been used in a wide variety of HEP tasks, including:

- classification of particles and final states,
- track reconstruction,
- triggering,
- particle identification (e.g. flavour tagging and Higgs detection),
- reconstruction of invariant masses, and
- offline analysis.

Several studies have shown that neural network classifiers can be helpful in HEP [23, 37]. ANNs have been used in the discrimination of Higgs production from background at LHC using quark-gluon separation and heavy quark tagging [53, 83, 94].

The ANN has several notable features, including high processing speed, high fault tolerance (the data may be incomplete, inconsistent, or noisy), inherently parallel algorithms, and the ability to learn a solution to the problem from a set of examples. Many of these features can be regarded as complementary to those of more conventional approaches.

Training algorithms for ANNs are divided into two distinctive groups:

- **Supervised learning**. In this case ANNs are trained with data containing complete input-output information or patterns, and the class of data is known a-priori.
- **Unsupervised learning**. This self-organised algorithm uses only input information, so the classes in the data are unlabelled. Unsupervised algorithms usually employ competitive learning, in which output neurons compete with each other to become activated.

In Chapter 7 we will describe training algorithms for both of these ANN types.

The principal disadvantages of ANNs stem from the need to provide a suitable set of example data for network training. Additionally, it is often difficult to analyse the internal representation of the ANN.

A trained network should be able to model data it has never seen before. This critical property of a trained network is called generalisation. The problem of teaching a neural network that performs well is quite a subtle issue, especially when only a limited number of training samples are available. Thus specific care is needed to gain optimal generalisation and avoid problems, such as over-training [11, 16].

Part I

INTRA-NUCLEAR CASCADE MODELS FOR GEANT4

Chapter 1

Geant4 and its Applications

The Geant4 toolkit provides a versatile and comprehensive software package for modern simulation applications that involve the interactions and passage of particles through matter. This chapter will introduce Geant4 mainly on the basis of Publication [**I**]. Our perspective is to introduce particularly those Geant4 concepts that were essential in the thesis work by focusing on hadronic physics.

1.1 Geant4 toolkit

Background

Modern particle physics experiments pose enormous challenges to the creation of complex yet robust software frameworks and applications. The demand is driven by the escalating size, complexity, and sensitivity of the detectors. The ever-increasing demand for large-scale, accurate and comprehensive simulations of the particle detectors used in these experiments is of particular importance.

In response to this, an object-oriented simulation toolkit, Geant4, has been developed. The origin of the development of Geant4 can be traced back to two studies carried out at CERN and KEK in 1993. Both groups sought to investigate how modern computing techniques could be applied to improve what was offered by the existing GEANT3 program.

Geant4, with its collaboration members: BaBar, CMS, ATLAS, LHCb, and HARP, was the first large-scale software project to pioneer the adoption of object-oriented technology in high-energy physics. The first public version of Geant4 was released at the end of 1998. The Geant4 toolkit was first reviewed in the year 2003 in Publication [**I**]. A second general review from the year 2006, Publication [**III**], discussed recent developments and applications.

The Geant4 documentation includes installation, user and reference guides, and a range of training kits. The code and documentation, as well as tutorials and examples, are available from collaboration web site. Data and expertise have been drawn from many sources and in this respect Geant4 acts as a repository that incorporates a large part of all that is known about particle interactions. All aspects of the simulation process have been included:

- geometry and materials;
- particle interactions in matter;
- tracking management,

- digitisation and hit management,
- event and track management,
- visualisation and a visualisation framework, and
- the user interface.

The Geant4 toolkit provides a diverse, wide-ranging, and yet cohesive set of software components which can be employed in a variety of settings.

The overall problem decomposition and the high-level design of Geant4 were based on an analysis of the user requirements. A typical HEP software system contains components, such as an event generator, detector simulation, reconstruction and analysis, that can be used separately or in combinations. The requirements led to the concept of a toolkit, which implies that a user may assemble her program at the time of compilation from components chosen from the toolkit or self-supplied. This ultimately led to a modular and hierarchical structure for the toolkit, where sub-domains are linked by a uni-directional flow of dependencies, and where class categories with coherent interfaces are provided [**I**].

Geometrical models and graphics

The Geant4 toolkit offers the user the ability to create a geometrical model with a large number of components of different shapes and materials, and to define sensitive elements that record the information (called hits) needed to simulate detector responses (digitisation). An example of the graphical user interface of a Geant4 simulation is shown Fig. 1.1a.

For the description of a detector geometrical setup the geometry description markup language (GDML) is provided. This module enables a user to save a Geant4 geometry description by writing it into a text file using the extensible markup language (XML) [**III**].

The efficient and compact handling of complex geometries is supported with visualisation through a variety of interfaces [28]. For example, the Geant4 HepRep graphics systems is a generic and hierarchical format for the description of graphic representables. The HepRep output of detector geometry, particle trajectories, and hits and their digitisation includes a great deal of useful HepRep attribute information, such as material names, densities, particle ID numbers, and momenta [**III**]. With the HepRep browser it is possible to view this information by selecting the relevant objects from the display. The WIRED3 browser can write any such attributes as visible labels on the display, as is demonstrated in Fig. 1.1b.

Modularity and flexibility

A serious limitation of GEANT3 simulation system was the difficulty of adding geometry components and new physics models. Development became difficult because of the complexity and interdependency of the procedure-based code.

Exploiting object-oriented technology has enabled Geant4 to establish a clear and customisable correspondence between particles and processes, and offer a choice of models for each process in a highly granular implementation. This is a completely new situation, since object-oriented methods have allowed us to manage complexity effectively and limit dependencies by defining a uniform interface and common organisational principles for all physics models. In the technology adapted by Geant4, the functionality of models can be more easily seen and understood. The implementation of Geant4 physics is transparent and open to user validation, allowing the user to understand, customise, and extend it in all domains. The creation and addition of new models is a well-defined procedure and refinement of the toolkit is possible without affecting the existing code used in production mode by LHC experiments.

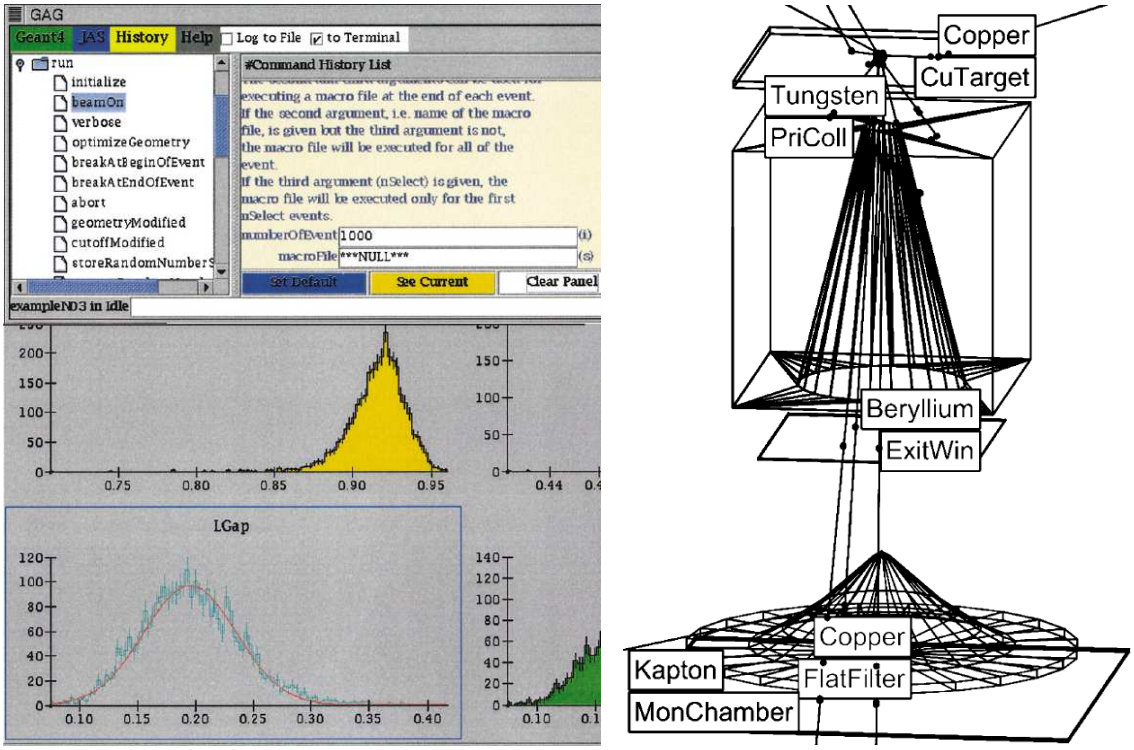

Figure 1.1: **a)** Java-based Geant4 Adaptive GUI starts a run in collaboration with Java Analysis Studio allowing real-time histogramming [**I**]. **b)** Geant4 Visualisation using the WIRED3 HepRep browser enables a user to label an image with attributes such as material or energy [**III**].

The use of state-of-the-art software technology is the key that permits the distributed development of Geant4 hadronic physics. In a very short time it has led to an unexpectedly wide range of modelling possibilities in Geant4, and unprecedented ease and flexibility of the usage of models and cross-sections. The keys to its success are its careful design, adopting an object-oriented methodology, and the early decision to use the practical C++ language. The choice of this novel technology has made possible the initial development of a powerful toolkit with rich functionality, and its further extension and refinement without affecting the original kernel.

Using Geant4

In any Geant4 simulation the user must specify the following three mandatory user base classes [**I**]:

- *G4VUserDetectorConstruction* for defining the material and geometrical setup of the detector. Several other properties, such as detector sensitivities and visualisation attributes, are also defined in this class.
- *G4VUserPhysicsList* for defining all the particles, physics processes, and cut-off parameters. (Geant4 defines no default physics process.)
- *G4VUserPrimaryGeneratorAction* for generating the primary vertices and particles. (Geant4 supports HEPMC format, a HEP standard for the Monte Carlo event generators.)

Listing 1.1 demonstrates how the user can control all aspects of Geant4 simulation with macro commands, such as verbosity levels, the physics models, how to modify the configuration for target materials, and how to manage the simulation runs.

```
# PHYSICS LIST:
#  Decay:
#    * Decay of all unstable particles
#
#  Electromagnetic Physics
#    * Livermore-based models for photons, electrons
#    * ICRU49-based models for charged hadrons, ions
#    * Standard models for positrons, muons
#
#  Hadronic Physics (elastic)
#    * LEP elastic scattering model for hadrons (protons,
#      neutrons, pions), ions (deuterons, tritons, alphas)
#
#  Hadronic Physics (inelastic)
#    * Bertini model for protons, neutrons
#    * Fission and capture models for neutrons
#    * LEP model for ions (deuterons, tritons, alphas)
#    * LEP model for pions (pions+, pions-)
#
#  Hadronic Physics (inelastic)
#    * Capture model for muons-
### VERBOSITY LEVELS #
/control/verbose 1
/tracking/verbose 0
/run/verbose 0
/event/verbose 0

###  A) EM PHYSICS AND DECAY
/physics/addPhysics Decay
/physics/addPhysics EM-Photon-EPDL
/physics/addPhysics EM-Electron-EEDL
/physics/addPhysics EM-Positron-Standard
/physics/addPhysics EM-HadronIon-LowE
/physics/addPhysics EM-Muon-Standard

###  B) HADRONIC PHYSICS
/physics/addPhysics HadronicEl-HadronIon-LElastic
/physics/addPhysics HadronicInel-ProtonNeutron-Bert
/physics/addPhysics HadronicInel-Ion-LEP
/physics/addPhysics HadronicInel-Pion-LEP
/physics/addPhysics HadronicAtRest-MuonMinus-Capture

### BEAM LINE SETTINGS AND RUN #
/run/initialize

###  SETTING FOR THE RANGE SHIFTER
/beamLine/RangeShifter/thickness 4 cm
#/beamLine/RangeShifter/RSMat Water

/run/beamOn 200
```

Listing 1.1: A Geant4 macro used to control Monte Carlo simulation. (From `geant4.9.1.p01/-examples/advanced/hadrontherapy/physicsHadronicBertini.mac`).

1.2 Physics modelling

Model vs. process

For particle interaction or decay, Geant4 distinguishes between the process, i.e. a particular initial and final state, which therefore has a well-defined cross-section or mean life, and the model that implements the production of secondary particles. Process classes utilise model classes to deter-

mine the secondaries produced in the interaction and to calculate the momenta of the particles. This mechanism allows the possibility of offering multiple models for the same process.

The tracking code is common to all processes of all particle types. This unified model for physics processes gives flexibility in the design of a physics process. Depending on its nature, a physics process possesses one or more characteristics represented by the following actions handled by the tracking:

- at rest, for particles at rest (e.g. decay at rest);
- along-step, which implements behaviours such as energy loss or secondary particle production that happen continuously along a step (e.g. Cherenkov radiation);
- post-step, which is invoked at the end of the step (e.g. secondary particle production by a decay or interaction).

These actions and the corresponding virtual methods are defined in the base class *G4VProcess*, and all physics processes conform to this basic interface [**I**]. Each process can perform any combination of these three actions with the *DoIt*-method.

In Geant4, the concept of particle change, represented by the class *G4VParticleChange*, is introduced to keep the results of the *DoIt*-method, i.e. the final state of the track and secondary tracks. Only these objects know which properties the physics process has updated.

As a result, a clear separation between process and tracking functionality has been realised, ensuring that new physics processes can be easily developed and the functionality of existing processes extended [**I**].

Interactions and decays

A particle in flight is subject to many competing processes. Moreover, in a detector, it will often travel through many volumes of different materials with various shapes before interacting or decaying. In Geant4 simulation, the particle propagates in steps, so an efficient and unbiased way of choosing what limits the step has to be defined.

Consider the interaction or decay of a particle in flight, and the distance to the point of interaction or decay. This is characterised by the mean free path λ. The probability of surviving a distance l is

$$P(l) = e^{-n_\lambda},$$

where

$$n_\lambda = \int_0^l \frac{dl}{\lambda(l)}.$$

For a decay, $\lambda = \gamma v \tau$, where v is the velocity and τ the mean life. For an interaction, if the cross-section on isotope i of mass m_i that has a fraction x_i by mass in the current material of density ρ is σ_i, then

$$\frac{1}{\lambda} = \rho \sum_i x_i \sigma_i / m_i.$$

Notice that λ varies as particle loses energy and changes discontinuously at a geometrical boundary. The probability distribution of n_λ is independent of material and energy, and at the point of production of the particle

$$n_\lambda = -\ln \eta,$$

where η is a random number uniformly distributed in the range (0,1). This is used in Geant4 to determine the distance to the point of interaction or decay in the current material. This information from all processes for the particle is used to decide what happens.

Processes other than interaction or decay also compete to limit the step. For example, continuous energy loss may limit the step. Additionally, transportation requires that the step should not cross a geometrical boundary between two volumes. The user can also request a maximum allowed step. The process which returns the smallest distance is selected and its post-step action is invoked. If this is an interaction or decay, the particle is killed and secondaries are generated.

A large variety of interactions are experienced by particles passing through matter. In Geant4 these interactions are divided into major process categories: electromagnetic, hadronic, transportation, decay, optical, photo-lepton hadron, and parameterisation. In addition, several ion-ion interaction models are provided [121]. The electromagnetic package, for example, is organised as a set of class categories:

- standard: handling basic processes for electron, positron, photon, and hadron interactions;
- low-energy: providing alternative models extended down to lower energies than the standard category;
- muons: handling muon interactions;
- X-rays: providing specific code for X-ray physics, and
- optical: handling optical photons.

Geant4 hadronic framework

The basic requirements for the physics modelling of hadronic interactions in Geant4 span more than 15 orders of magnitude in energy. The energy ranges from thermal for neutron cross-sections and interactions, through 7 TeV in the laboratory for LHC experiments, to even higher for cosmic ray physics. Depending on the setup being simulated, the full range or only a small part of the toolkit functionality might be needed in a single application.

The complex nature of hadronic showers requires the user to be able easily to vary the models for particular particles and materials. A viable approach adopted by Geant4 is to use simplified models, whose validity is often restricted. An inventory of hadronic models available in Geant4 is shown Figure 1.2.

Given the vast number of possible modelling approaches, Geant4 has chosen to design an additional set of implementation frameworks to help generate the corresponding code in a distributed manner, and allow significant flexibility to the final user. The so-called Russian dolls - approach to the design of the implementation framework is followed. In this approach, an abstract top-level framework provides the basic interface to other Geant4 categories. It satisfies the most general use-case for a hadronic shower simulation, namely to provide inclusive cross-sections and final state generation. The framework is then refined for more specific use-cases by implementing a hierarchy of frameworks. Figure 1.3 illustrates the various framework levels in an annotated package dependency diagram.

The Geant4 hadronic physics platform [112] defines both an inter-code communication standard and an intra-code specification to facilitate the extension of functionalities (Fig. 1.3). Each sub-level implements the interface specification of the previous framework level. It adds an implementation for the common logic of a particular use-case package, such as the information flow between parton string models and codes simulating the de-excitation of nuclear matter into hadrons. Also, it provides abstract interfaces for the associated use-case package. The granularity of abstraction and delegation is refined at each framework level.

The requirements for the second framework level are the following:

- the ability to add user-defined data sets and models in a seamless manner;

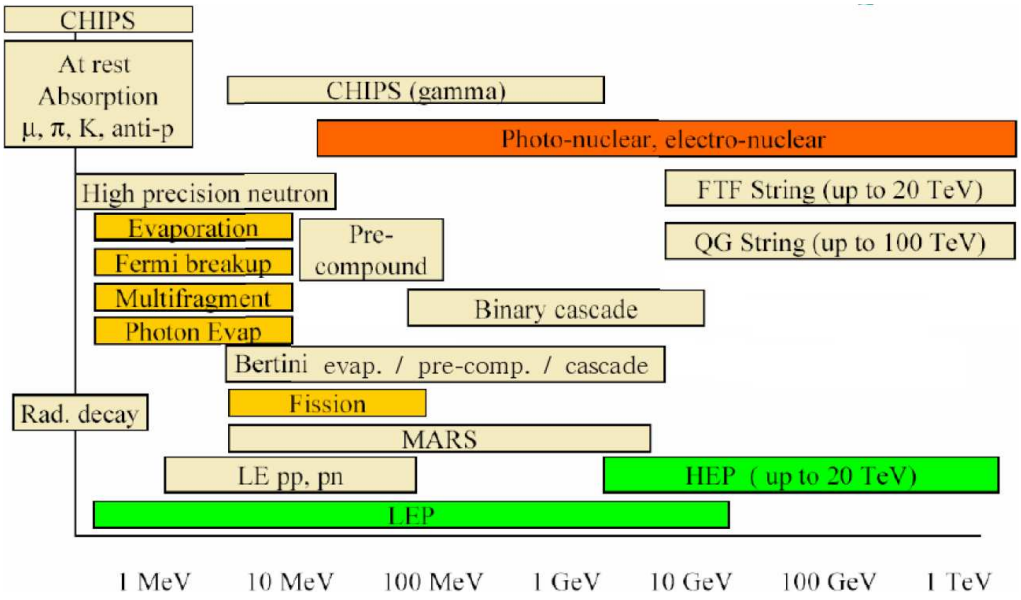

Figure 1.2: A collection of optional Geant4 hadronic physics models.

- the ability to use different data sets and final state production depending on the conditions at the point of interaction, and

- allow a flexible choice of cross-sections, final state production models and isotope production models, to run in parasitic mode to any kind of transport model [**I**].

These requirements are integrated in the *G4HadronicProcess* class, which serves as the base-class for all hadronic processes of particles in flight. Each process holds a list of cross-section data sets, which encapsulates methods and data for calculating the total cross-sections for a given process in a certain range of validity. The way cross-sections are calculated – via formulae, parameterisations, or the interpolation of databases – is exposed. The information extracted from the database is separated from the way it is accessed and used, creating the possibility of using different databases and allowing their applicability to be tailored by particle, energy, and material. Figure 1.4 shows how the loading sequence affects the cross-sections used in the Geant4 simulation.

Three classes of models are distinguished for modelling final states. There are models that are largely based on theory, models that are predominantly based on parameterisations and the extrapolation of experimental data under some theoretical assumptions, and models that are predominantly based on evaluated or measured data [112].

Theory-based models. In the medium-energy cascade region the user can select from various models using a theoretical approach:

Bertini cascade The Bertini-style intra-nuclear cascade [9, 93] is one of the most-used Geant4 hadronic medium energy models, representing a theoretical approach to simulating hadronic interactions. This model will be discussed in detail in Chapter 2.

Binary cascade. Instead of the Bertini cascade the user can select an alternative modelling approach based on a time-like Binary cascade. A comparison between a Binary and Bertini cascade physics performance is shown in Fig. 4.3.

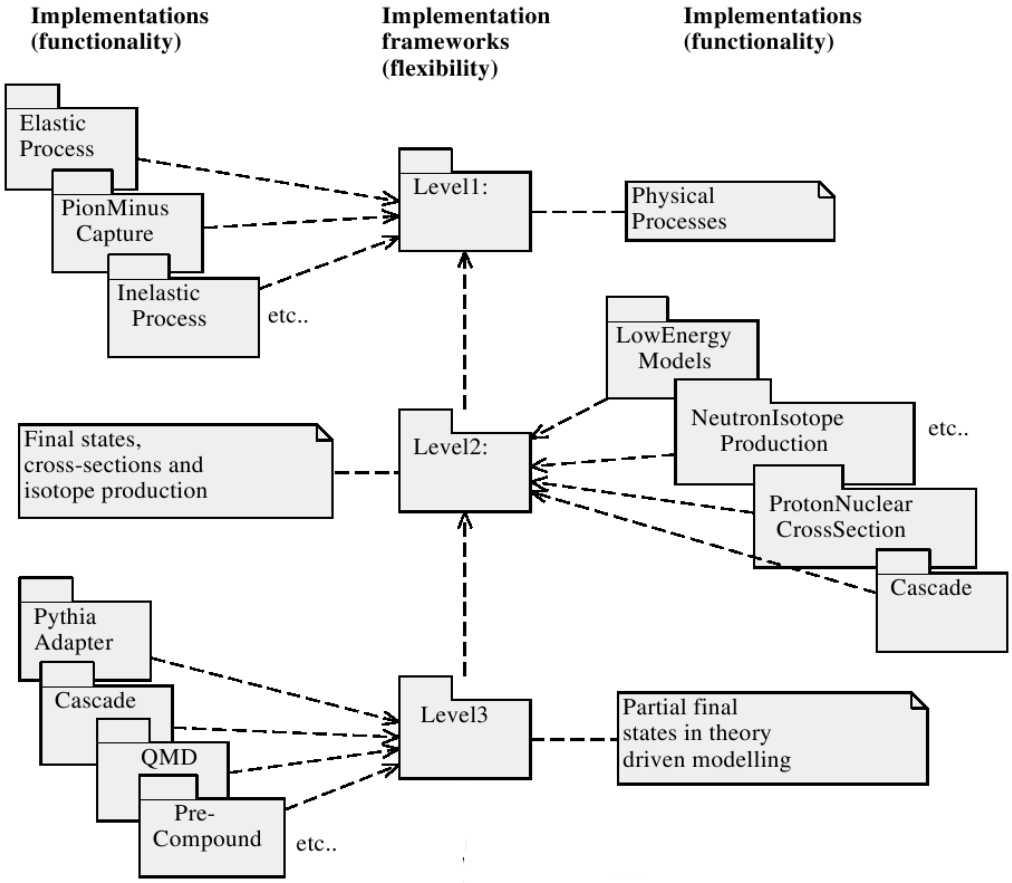

Figure 1.3: Geant4 hadronic physics organisation with the Russian dolls -approach. In this approach an abstract top-level framework provides the basic interface to other categories, and more specific use-cases are refined level by level. A package diagram of implementation frameworks above Level 3 is shown, together with sample implementations available for the hadronic physics category [**I**].

Liége cascade This is the latest major theory-based model, added to Geant4 9.0 in December 2007, after the FORTRAN intra-nuclear cascade code INCL4.2 and ABLA evaporation-fission code were cast into C++ and interfaced with the hadronic framework [2].

Geant4 provides a default pre-compound model to be used when the reaction energy is below the validity range of the intra-nuclear cascade (Fig. 1.5). The Bertini cascade also contains an independent implementation of a pre-compound model (Fig. 4.3b).

The last phase of a nuclear interaction is nuclear evaporation. In order to model the behaviour of excited, thermalised nuclei, variants of the classical Weisskopf–Ewing model are used. Specialised improvements such as Fermi's break-up model for light nuclei and multi-fragmentation for very high excitation energies are employed. Fission and photon evaporation can be treated as competitive channels in the evaporation model. Internal conversion is used as a competitive channel in photon evaporation.

At the end of the reaction chain, the electron configuration on the residual atom is estimated, and the necessary atomic relaxation is performed. Again, Geant4 provides default models for this functionality. Optional models are also available. For example, the Bertini cascade provides a corresponding sub-model for Fermi break-up, multi-fragmentation, and evaporation.

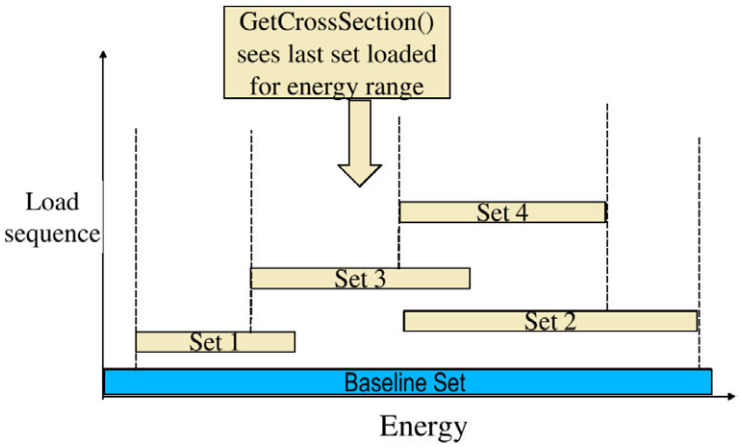

Figure 1.4: Effect of cross-section data set loading sequence to actual cross-section used in specific Geant4 simulation.

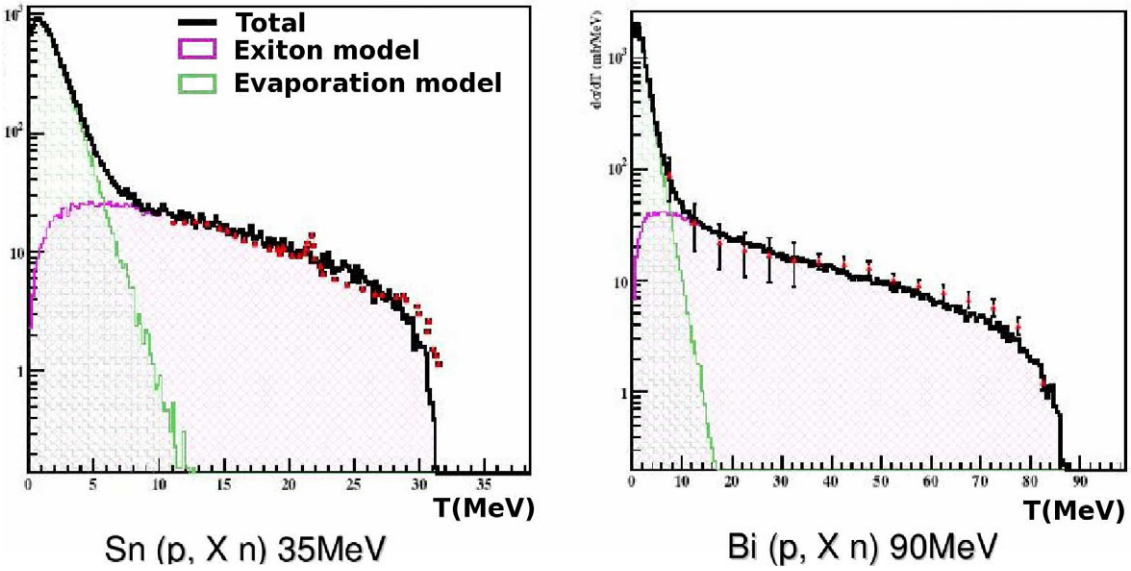

Figure 1.5: Secondary neutrons created in proton-induced Sn and Bi interactions. A comparison between measurements and standard Geant4 pre-compound and evaporation modelling, producing low-energy neutrons, is shown [124]. In Chapter 4 Fig. 4.3b we show the corresponding performance using Bertini models developed in this thesis work.

As a final example of theory-based models we will mention the Chiral Invariant Phase Space (CHIPS) model. Figure 1.6 demonstrates the performance of CHIPS for a two-particle final states in proton antiproton annihilation.

Parametrised models. Parameterisations and extrapolations of cross-sections and interactions are widely used in the full range of hadronic shower energies, and for all kinds of reactions. They are the result of re-writes of models available from GEANT3, predominantly GHEISHA [64], and they include induced fission, capture, and elastic scattering, as well as inelastic final state production.

In Geant4 GHEISHA FORTRAN code was cast into C++, re-engineered, and split into the current high- and low-energy parts. These LEP and HEP models are fast, cover all long-lived

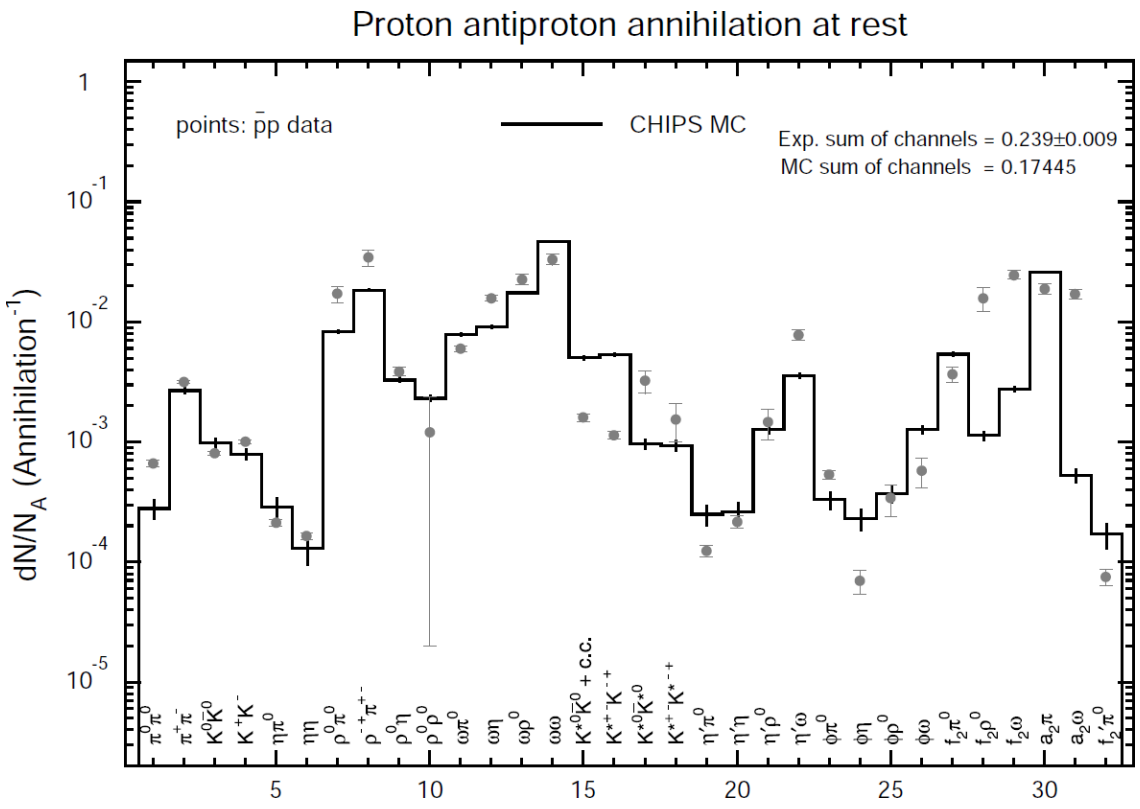

Figure 1.6: Comparison of the branchings in two-particle final states in proton antiproton annihilation with the predictions of CHIPS [**I**].

particles at all energies, and describe hadronic showers reasonably well. They conserve energy and momentum on average but not event by event.

Data-driven models. The main data-driven models in Geant4 deal with neutron- and proton-induced isotope production and with the detailed transport of neutrons at low energies. The codes for neutron interactions are generic sampling codes, based on the ENDF/B-VI data format, and evaluated neutron data libraries such as ENDF/B-VI, JENDL, and FENDL.

The data-driven isotope production models that run in parasitic mode to the transport codes are based on the MENDL data libraries for proton- and neutron-induced production. Data-driven modelling is known to provide the best, if not only, approach to low-energy neutron transport for radiation studies in large detectors [**I**].

Often the most critical choice before speed optimisation is the choice of the physics models used, since they have significant differences in CPU requirements. A key advantage associated with data-parametrised and data-driven models is their execution speed.

Optimising Geant4 Monte Carlo simulation

One of the most significant Geant4 optimisation capabilities is the possibility of defining regions in the experimental setup, and setting a different particle production threshold in each region. This reflects the real-life design of most experiments, which are characterised by detectors of very different precision capabilities, e.g. an inner micro-vertex detector and a coarse-grained hadronic calorimeter or muon detector.

Geant4 offers the possibility of introducing event biasing in a simulation through user code. The Geant4 kernel offers access to user code through the user action and user initialisation base classes. To facilitate the usage of variance reduction techniques, general-purpose biasing methods have been introduced into the toolkit. Many applications, including radiation shielding studies, can profit from this functionality to achieve large gains in time efficiency.

Importance sampling is supported, with splitting and Russian roulette; an importance value is associated with each volume. Either conventional mass geometry (that used for physics and tracking) or a dedicated artificial parallel geometry can be used for biasing [**I**].

Other biasing capabilities include an implementation of the weight-window method and of the related, but simpler, weight-cutoff method. Leading particle and cross-section biasing are provided for hadronic processes in the corresponding physics package. Biasing options for physics processes are also available [**III**].

Charged particles in Geant4 are tracked in external electromagnetic fields, and the intersection of their curved trajectories with geometrical boundaries is approximated within a user-specified precision. Thus the user can attach the same or a different field to a geometrical volume and specialise the integration accuracy parameters for each field. It is also possible, utilising the track's properties, to select different values for the accuracy parameters for tracking in a field. This functionality allows a user, for example, to undertake precise tracking for all muons, or for any tracks with energy above a given threshold, while tracking electrons in a calorimeter more coarsely.

Running Geant4 as a parallel application often involves the generation of a large number of events and requires significant computing resources. Execution in a parallel mode contributes to adequate simulation statistics in a reduced time frame. The use of job-level parallelism, using independent jobs on farms of computers, is well established and well suited when there is experience in distributing jobs and gathering the results. Yet in other domains different types of parallelism provide an alternative with simpler ways to launch jobs and obtain results. An extended Geant4 example is provided to show how to use the task-oriented parallel package TOP-C to parallelise simulation using event-level parallelism. Even though the application actually runs in parallel on distributed computers, it appears to run as a single process with a single Geant4 library, storing and analysing a single collection of hits [**III**].

1.3 Simulation of detector systems using Geant4

The choice of object-oriented technology has enabled Geant4 toolkit to possess a rich functionality, and made possible further extensions without affecting the original kernel.

The Geant4 toolkit is used by a wide scientific community worldwide in diverse experimental domains. Apart from particle physics, it is employed for accurate simulations in astrophysics, space science, radiation protection, and nuclear medicine [**I**]. In fact, Geant4 has become a showcase example of technology transfer from particle physics to other fields [97].

Next we briefly introduce some examples of this technology transfer, with emphasis on applications using Bertini cascade.

Simulating LHC detectors

Simulation and computing in the Large Hadron Collider experiments is a major challenge because of the enormous data volumes involved. The CMS front end electronics will receive signals from millions of particle detection channels, each at the frequency of 40 MHz. From this huge information flux the online trigger and data acquisition system will resolve the potentially interesting events for output onto a mass storage device. The events of some 1 MB of storage size will

be recorded at the rate of 50-100 Hz, yielding raw data volumes of the order of a PB (1000 TB) a year to be analysed offline [17]. An example of Geant4 event in the Compact Muon Solenoid (CMS) experiment is shown in Fig. 1.7.

Previously, background radiation studies for LHC detectors were mainly performed using FLUKA. Now Geant4 can be used to do similar studies. The LHCb experiment, for example, has used Geant4 scoring planes and tracking optimisation of the geometry, called voxelisation, with a resolution of $\sim$10 cm, added to the LHCb geometry to this purpose. The LHEP_BERT_HP physics list was used to provide proper treatment for low-energy neutrons and to evaluate the $\sim$1 keV region in the neutron energy spectrum. The scoring planes in the simulation, corresponding to the Si detectors in LHCb, were prepared to estimate a 1 MeV-neutron equivalent fluence for silicon (calculated as a sum of the weighted fluence contributions of each particle type) [14]. The QGSP_BERT_HP physics list was also used in OSCAR-based neutron background studies in CMS to count the number of neutron interactions in the sensitive muon chamber gas [104].

Another recent example of the usage of Geant4 is a simulation of an LHC beam loss [95]. The role of the beam loss measurement BLM system is to protect the LHC from damage and dump the beam to avoid magnet quenches. It is also a diagnostic tool to improve the performance of LHC. To understand the LHC beam dump, a comparison with HERA beam dump measurements was performed, in which Geant4 and FLUKA agreed with each other within error bars at 39 GeV and 920 GeV and a discrepancy of factor 2 between the measurements and the simulation. A 50% systematic error for the LHC simulation is expected. As a consequence, Geant4 QGSP_BERT_HP physics list and FLUKA were qualified for the LHC beam dump secondary shower simulation, needed particularly for far transverse tails.

In Chapter 3 we discuss a CMS hadronic calorimeter simulation based on Geant4 and the Bertini cascade models developed in this work.

TARC simulation

The aims of the TARC experiment (Neutron-Driven Nuclear Transmutation by Adiabatic Resonance Crossing) [100] are to understand neutron transport properties, on the distance scale relevant to industrial applications of reactor size, and to study neutron production by GeV protons hitting a large volume of lead (334 tons of lead in a cylindrical 3.3x3.3x3 m^3 block). Sample holes inside the Pb volume are used to measure a number of specific isotopes relevant to the efficiency of transmutation.

In Ref. [81] spallation neutron production was validated for 2.5–3.5 GeV/c protons on pure lead (Fig. 1.8). Geant4 simulation using the Bertini cascade gives good agreement for transportation energy-time correlation and the number of neutrons. Agreement is particularly good with the TARC data radial distribution. Neutrons in the 0.8–1.6 GeV energy region are slightly overproduced [80].

Geant4 physics potential for space applications

Interest in the Geant4 toolkit from the space community has been strong since the beginning of the Geant4 project. International organisations such as ESA value key Geant4 features [85]: open source software with strong support, a large collection of physics models, and a modern approach to the design and use of components.

A typical application in the space domain deals with shielding and radiation protection. An example of the use of Geant4 in dosimetry for interplanetary manned missions comes from the European AURORA programme. In the Ref. [47] Geant4 Monte Carlo simulations were performed to estimate a total equivalent dose for an astronaut living on the Moon. Comparisons between Geant4 Bertini and Binary models showed only small differences.

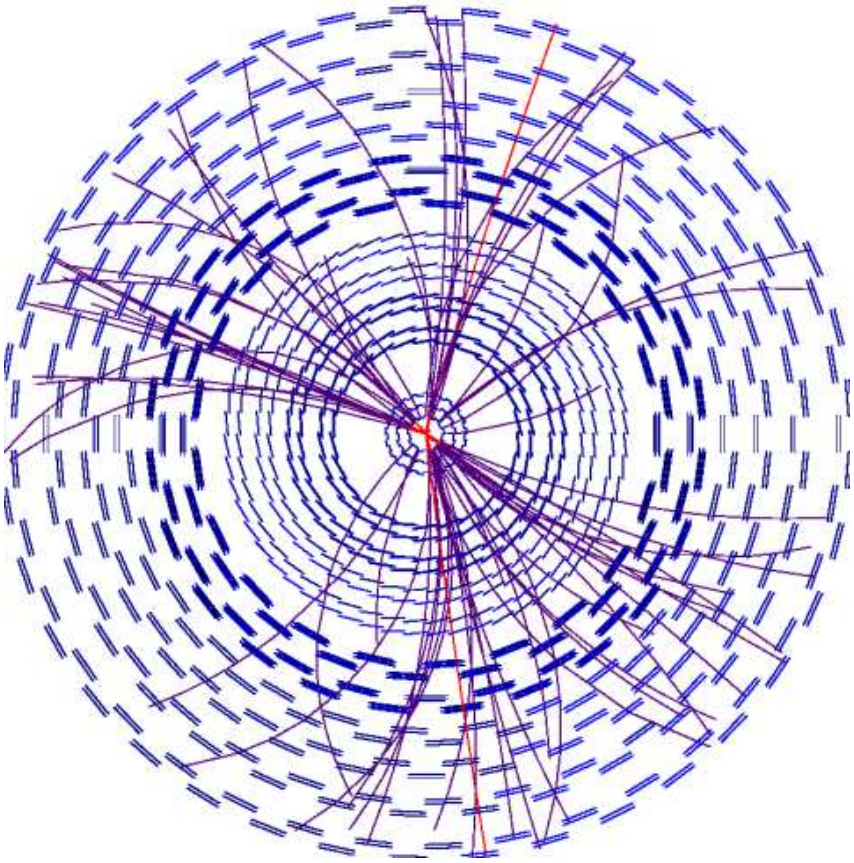

Figure 1.7: An event in the CMS detector simulated with Geant4. Reconstructed tracks from $t\bar{t}H(120\ GeV) \rightarrow b\bar{b}$ and vertices are shown in the CMS Tracker barrel.

The last example is a Geant4 shielding simulation of graphite-epoxy composite material for a satellite electronic housing [107]. In this project the Laboratory of Lightweight Structures at Helsinki University of Technology participated in an ESA-funded Advanced Equipment Design project. The goal was to evaluate the feasibility of composite materials in space applications, and design a composite housing that was relatively light, while providing good shielding against cosmic radiation.

Geant4 was used to simulate a multi-layer laminate structure (1 mm graphite – 50 μm tungsten – 1 mm graphite) in low and medium Earth orbits. Comparisons between Monte Carlo and test beam measurements were made against a standard 2-mm aluminium wall thickness. Results on shielding characteristics indicated that the proposed low Z – high Z – low Z graphite-epoxy composite material can be used successfully as a main housing component for satellite electronics.

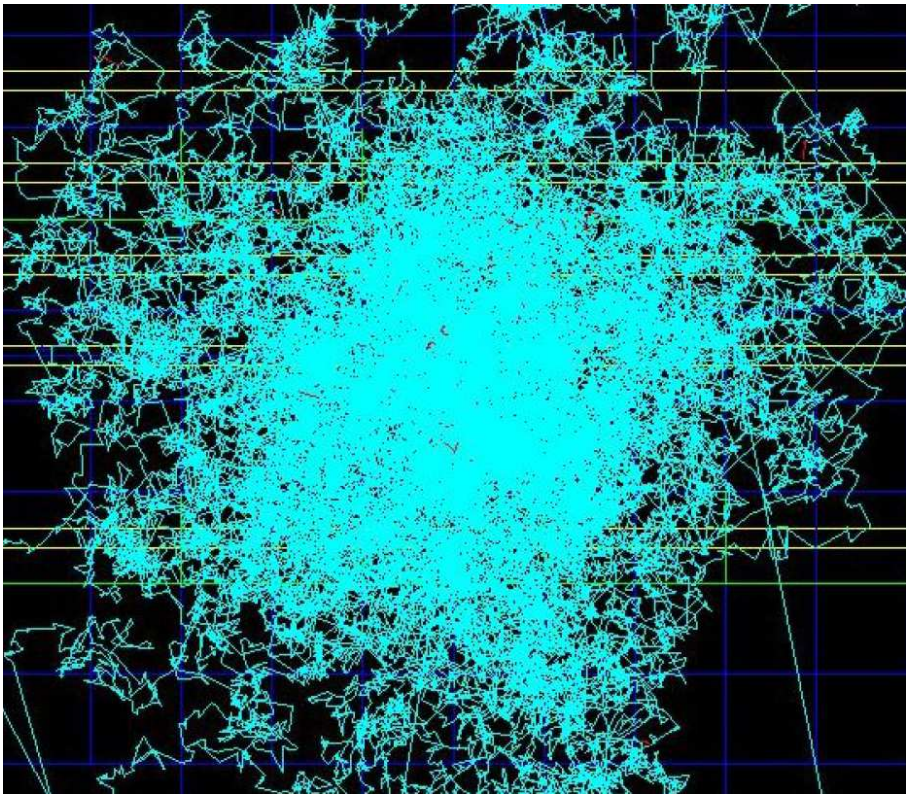

Figure 1.8: Geant4 Bertini hadronic cascade in action. A validation of neutron spallation production in the TARC experiment. (Courtesy of A. Howard [80])

Chapter 2

Bertini Intra-Nuclear Cascade Models

This chapter discusses the hadronic physics modelling of Bertini intra-nuclear cascades implemented in the hadronic framework of the Geant4 toolkit. We also describe how the Geant4 Bertini models are made available to users through validated physics lists. The discussion is based mainly on Publication [**II**].

Background

The intra-nuclear cascade model (INC) was first proposed by Serber in 1947 [103]. Serber noticed that in particle nuclear collisions the de Broglie wavelength of the incident particle is comparable to (or shorter than) the average intra-nucleon distance, hence the justification for describing the interactions in terms of particle-particle collisions.

Goldberger made the first INC calculations by hand in 1947 [68], and generating a few dozen events took days to compute by hand. Figure 2.1 gives a schematic presentation of the Bertini intra-nuclear process based on the original visualisation by Bernardini *et al.* in the year 1952 [67]. It was only with the computer era that this approach came feasible for physics studies, and it was H. W. Bertini *et al.* who popularised INC with computer codes in the 1960s [8, 9, 93]. Today, a typical Monte Carlo simulation of one INC takes a few ms to compute. For LHC production runs, with detailed calorimetry geometry, even this speed can be too slow so parametrised models are often used.

The necessary condition of validity of the INC model is $\lambda_B/v \ll \tau_c \ll \Delta t$, where λ_B is the de Broglie wavelength of the nucleons, v is the average relative N-N velocity and Δt is the time interval between collisions. When the physical foundation becomes approximate at energies less than 0.2 GeV, it needs to be supported with the pre-equilibrium model. Additionally, at energies higher than $\sim$10 GeV the INC picture breaks down [18].

In inelastic particle-nucleus collisions a fast phase (10^{-23} - 10^{-22} s) of INC can result into a highly excited nucleus, and is possibly followed by fission and pre-equilibrium emission. A slower (10^{-18} - 10^{-16} s) compound nucleus phase follows with evaporation. A Boltzman equation must be solved to treat the physical process of collisions in detail. The intra-nuclear cascade model developed by Bertini [9, 10, 93], solves the Boltzman equation on the average. This model has been implemented in several codes, such as HETC [3].

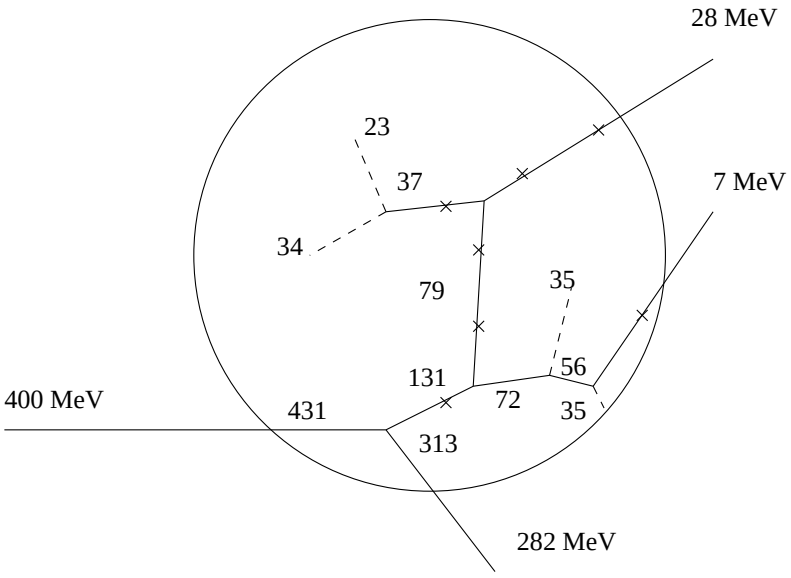

Figure 2.1: Schematic presentation of an intra-nuclear cascade. A hadron with 0.4 GeV energy is forming an INC history. Crosses represent the Pauli exclusion principle in action. For this event the potential well depth is 31 MeV and the thermal excitation 66 MeV [**II**].

2.1 Bertini cascade

Introduction

The implementation of the Bertini cascade in Geant4 is based in a re-engineered version of Stepanovs INUCL code [105] and employs many of the standard intra-nuclear cascade features developed by Bertini [9, 93]:

- classical scattering without matrix elements;
- free hadron-nucleon cross-sections and angular distributions which are taken from experiments, and
- step-like nuclear density distributions and potentials.

The implementation contains intra-nuclear cascade, pre-equilibrium with exitons, Fermi-breakup, fission, evaporation, and gamma de-excition models. The Bertini cascade and its latest extensions provide inelastic treatment between hadronic projectile particle and target atoms up to a maximum energy of 15 GeV. In addition to hadron scattering from a target nucleus, capture on the nucleus is also treated. Table 2.1 summarises the Bertini sub-models available in Geant4 version 9.1.

The Bertini cascade can handle incident protons, neutrons, pions, kaons, and hyperons. The range of targets allowed is arbitrary. With the help of an internal pre-compound de-excitation handler, this code has been extended down to zero initial energy. Elastic scattering is also provided through a separate interface. The upper limit for Bertini is roughly 10 GeV. Some of the internal cross-sections are provided up to 15 GeV, but since many of the original assumptions of INC are not valid, the performance of the model gets increasingly worse above 10 GeV.

The modelling sequence is similar to many other cascade codes. The projectile enters the nucleus at a point sampled over the projected area of the nucleus. The projectile is then transported

along straight lines through the nuclear medium. The projectile interacts according to the mean free path determined by the free hadron-nucleon total cross-section. The nuclear medium is approximated by up to three concentric, constant-density shells. The initial nucleon momenta are distributed according to the Fermi gas model, and Pauli blocking is invoked for the nucleons. For the most part the projectile interacts with a single nucleon, but some nucleon-nucleon correlation is included by allowing pions to be absorbed on quasi-deuterons.

Relativistic kinematics is applied throughout the cascade. The cascade is stopped when all the particles which can escape the nucleus have done so. Then conformity with the energy-conservation law is checked.

Nuclear model

The Bertini nuclear model consists of a three-region approximation to the continuously changing density distribution of nuclear matter within a nucleus [**II**].

Nucleons are assumed to have a Fermi gas momentum distribution. The Fermi energy is calculated in a local density approximation, i.e. it is made radius-dependent with the Fermi momentum

$$p_f(r) = (\frac{3\pi^2\rho(r)}{2})^{\frac{1}{3}}. \tag{2.1}$$

Nucleon-binding energies $BE_N(A,Z)$ are calculated using a mass formula. A parametrisation of the BE_N uses a combination of the Kummel mass formula and experimental data. An asymptotic high temperature mass formula is also used if it is impossible to use experimental data.

If the target is hydrogen ($A = 1$), a direct particle-particle collision is performed, and no nuclear modelling is used. If $1 < A < 4$, a model of the nucleus consisting of one layer with a radius of 8.0 fm is created. For $4 \leq A \leq 11$, the model is composed of three concentric spheres, defined by logarithmic radial term $\alpha_i = \{0.01, 0.3, 0.7\}$, with the radius

$$r_i(\alpha_i) = \sqrt{C_1^2(1 - \frac{1}{A}) + 6.4}\sqrt{-\log(\alpha_i)}, \tag{2.2}$$

where $i = \{1,2,3\}$, and $C_1 = 3.3836\,A^{1/3}$. If $A > 11$, a nuclear model with three concentric spheres is used, and the radius is defined as

$$r_i(\alpha_i) = C_2 \log(\frac{1 + e^{-\frac{C_1}{C_2}}}{\alpha_i} - 1) + C_1, \tag{2.3}$$

where $C_2 = 1.7234$.

The potential energy V for nucleon N is

$$V_N = \frac{p_f^2}{2m_N} + BE_N(A,Z), \tag{2.4}$$

where p_f is a Fermi momentum and BE_N a binding energy.

The momentum distribution in each region follows Fermi distribution with zero temperature

$$f(p) = cp^2, \tag{2.5}$$

where

$$\int_0^{p_f} f(p)dp = n_p \quad \text{or} \quad n_n. \tag{2.6}$$

In Eq. (2.6) n_p and n_n are the number of protons or neutrons in a region. A p_f is the momentum corresponding to the Fermi energy

$$E_f = \frac{p_f^2}{2m_N} = \frac{\hbar^2}{2m_N}(\frac{3\pi^2}{v})^{\frac{2}{3}}, \tag{2.7}$$

which depends on the density n/v of particles, and which is different for each particle and region.

The Pauli exclusion principle forbids interactions where the products would already be in occupied states. Following an assumption of completely degenerate Fermi gas, the levels are filled from the lowest level. The minimum energy allowed for the product of the collision corresponds to the lowest unfilled level of the system, which is the Fermi energy in the region. So in practice, the Pauli exclusion principle is taken into account by accepting only secondary nucleons which have $E_N > E_f$ **[II]**.

During propagation, particles may be reflected from, as well as transmitted through, the shell boundaries mentioned above. Listing 2.1 demonstrates how the reflection and transition between different zones is implemented.

```
void G4NucleiModel::boundaryTransition(G4CascadParticle& cparticle) {
  G4int zone = cparticle.getCurrentZone();

  if (cparticle.movingInsideNuclei() && zone == 0) {
    G4cout << " boundaryTransition-> in zone 0 " << G4endl;
  } else {
    std::vector<G4double> mom = cparticle.getMomentum();
    std::vector<G4double> pos = cparticle.getPosition();

    G4int  type = cparticle.getParticle().type();
    G4double pr = 0.0, r = 0.0;
    G4int i(0);

    for (i = 0; i < 3; i++) {
      pr += pos[i] * mom[i + 1];
       r += pos[i] * pos[i];};

    r = std::sqrt(r);
    pr /= r;
    G4int next_zone = cparticle.movingInsideNuclei() ? zone - 1 : zone + 1;
    G4double dv = getPotential(type,zone) - getPotential(type, next_zone);
    G4double qv = dv * dv - 2.0 * dv * mom[0] + pr * pr;
    G4double p1r;

    if (verboseLevel > 2){
      G4cout << " type " << type << " zone " << zone << " next " << next_zone
             << " qv   " << qv   << " dv   " << dv   << G4endl;}

    if(qv <= 0.0) { // reflection
      p1r = -pr;
      cparticle.incrementReflectionCounter();
    } else {        // transition
      p1r = std::sqrt(qv);
      if(pr < 0.0) p1r = -p1r;
      cparticle.updateZone(next_zone);
      cparticle.resetReflection(); };

    G4double prr = (p1r - pr) / r;
    for (i = 0; i < 3; i++) mom[i + 1] += pos[i] * prr;
      cparticle.updateParticleMomentum(mom);
    };
}
```

Listing 2.1: *BoudaryTransition*-method of *G4NucleiModel*-class implements of an algorithm used by the Bertini nuclear model to simulate a particle reflection and transition between different zones in the nuclei.

Intra-nuclear cascade

The INC model consists of following basic steps:

1. The spatial point, where the incident particle enters, is selected uniformly over the projected area of the nucleus.
2. Total particle-particle cross-sections and region-dependent nucleon densities are used to select a path length for the projectile particle.
3. The momentum of the struck nucleon, the type of reaction, and the four momenta of the reaction products are determined.
4. The exciton model is updated as the cascade proceeds.
5. If the Pauli exclusion principle allows and $E_{particle} > 2$ MeV step 2 is performed to transport the products.

Each secondary particle from initial and subsequent interactions is also propagated in the nuclear potential until it interacts or leaves the nucleus.

After INC, the residual excitation energy of the resulting nucleus is used as input for the pre-equilibrium model.

Pre-compound

Below 0.2 GeV the incident hadron energy of the pre-compound treatment becomes increasingly important. The Bertini-style cascade has its own exciton routine which is used to collapse the particle-hole states and de-excite the residual nucleus. This routine is based on that of Griffin [69, 70]. In this model the nucleon states are characterised by the number of excited particles and holes, the excitons. Intra-nuclear collisions give rise to a sequence of states characterised by an increasing exciton number, eventually leading to an equilibrated nucleus. As cascade collisions occur, an excited residual nucleus is built up. In the exciton model the possible selection rules for particle-hole configurations are:

$$\Delta p = 0, \pm 1 \qquad \Delta h = 0, \pm 1 \qquad \Delta n = 0, \pm 2, \tag{2.8}$$

where p is the number of particles, h is the number of holes and $n = p + h$ is the number of excitons. The most important assumption made by Griffin is that, for a given number of exitons, n, every particle-hole configuration consistent with the total energy is equally probable.

For a practical implementation of the exciton model we use published parameters from Ref. [86] for matrix elements. Parametrisation of the level density is tabulated with both A and Z dependence using data from Ref. [27]. The high-temperature behaviour for the nuclear binding energy uses a smooth liquid high energy formula [**II**].

The Bertini cascade pre-equilibrium model uses target excitation data, an exciton configuration to produce non-equilibrium evaporation. The angular distribution is isotropic in the rest frame of the exciton system. An example of pre-compound model performance is shown in Fig. 4.3b.

Fermi break-up and fission

Fermi break-up is allowed only in some extreme cases for light nuclei ($A < 12$ and $3(A - Z) < Z < 6$) and for high excitation energies. The model is a simple explosion which decays the nucleus and suppresses the exotic evaporation processes.

Fission in the Bertini cascade is a phenomenological model using potential minimisation. Binding energy parametrisation is used and some features of the fission statistical model [65] are incorporated [**II**].

Evaporation and gamma de-excitation

The statistical theory for the particle emission of the excited nucleus remaining after the INC was originally developed by Weisskopf [111]. This model assumes complete energy equilibration before the particle emission and re-equilibration of excitation energies between successive evaporations. As a result the angular distribution of emitted particles is isotropic.

The Geant4 evaporation model for cascade implementation adapts an often-used computational method developed by Dostrowski [15, 82]. The emission of particles is computed until the excitation energy falls below some specific cutoff. If a light nucleus is highly excited the Fermi break-up model is executed. Additionally, fission is performed if the channel is open. The main chain of evaporation is followed until the excitation energy E^* falls below the cutoff energy 0.1 MeV.

The last part of the evaporation model is a simple γ emission chain, where the gammas produced can have a maximal energy of 0.1 MeV, which corresponds to X-rays. The γ emission chain is followed until $E^* < 10^{-15}$ MeV to ensure a full nucleus de-excitation [**II**].

2.2 Cross-sections

The path lengths of nucleons in the nucleus are sampled according to the local density and to free N-N cross-sections. Angles after collisions are sampled from the experimental differential cross-sections. Tabulated total reaction cross-sections are calculated by Letaw's formulation [32, 33, 96]. For N-N cross-sections the parametrisations are based on the experimental energy and isospin-dependent data. The parametrisation described in [57] is used.

For pions the INC cross-sections are provided to treat elastic collisions and following inelastic channels

$$\pi^0 n \to \pi^- p \qquad \pi^+ n \to \pi^0 p \qquad \pi^0 p \to \pi^+ n \qquad \pi^- p \to \pi^0 n. \tag{2.9}$$

Multiple particle production is also implemented and reported in Publication [**II**]. The pion absorption channels are

$$\pi^- pp \to np \qquad \pi^- np \to nn \qquad \pi^+ nn \to pn \qquad \pi^+ np \to pp, \tag{2.10}$$

and

$$\pi^0 pp \to pp \qquad \pi^0 np \to np. \tag{2.11}$$

2.3 Design of Bertini sub-models

Figure 2.2 shows the general design of Bertini sub-models in Geant4. Notice the competitive nature between the evaporation and fission models. The sub-model management is handled by the *G4InuclCollider* class [72]. Class *G4CascadeInterface* is used to provide the Bertini cascade functionality to Geant4 hadronic framework (Listing 2.2).

Table 2.1 summarises the sub-models available in Geant4 version 9.1. The design allows the model to be extended to any particle for which there is a sufficient amount of double-differential cross-section measurements.

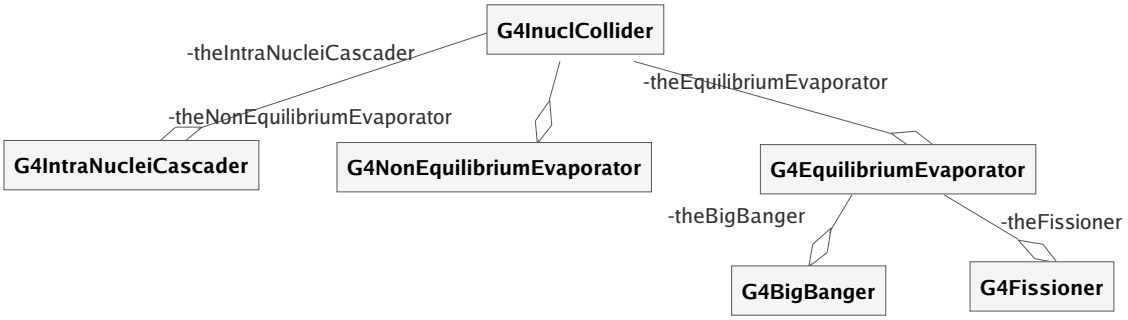

Figure 2.2: General relationships with Bertini cascade classes. Sub-model management is handled by the *G4InuclCollider* class (for details see Listing 2.2) [72].

Bertini cascade sub-models in Geant4 9.1		
Responsibility	Class name	Note
Interfacing	*G4CascadeInterface*	Interface using all Bertini sub-models providing a full treatment for inelastic scattering
	G4PreCompoindCascade-Interface	Interface to INC and pre-compound models only, subsequent evaporation-fission phase is not performed
	G4ElasticCascadeInterface	Interface to elastic scattering model
Colliding particles	*G4ElementaryParticle-Collider*	
Reaction channel management	*G4CascadeChannel*	Treats p, n, $\pi^{0,\pm}$, and K, Λ, and Ξ
Kaon extension with:	*G4CascadeK**	$K^{\pm}$, K^0,$\bar{K}^0$ channels (8 classes)
- Λ treatment	*G4CascadeL**	Λ channels (2 classes)
- Ξ treatment	*G4CascadeX**	Ξ channels (4 classes)
Sub-model manager	*G4InuclCollider*	
Nuclei model	*G4InuclNuclei*	
INC model	*G4IntraNucleiCascader*	Actual Bertini intra-nuclear cascade
Exciton model	*G4NonEquilibrium-Evaporator*	Excitons integrated with INC model
Explosion model	*G4BigBanger*	Multi-fragmentation for highly excited nucleus
Fission model	*G4Fissioner*	Uses *G4FissionConfiguration*-class
Evaporation model	*G4EquilibriumEvaporator*	De-excitation of equilibrated nucleus
De-excitation model	*G4EquilibriumEvaporator*	Simple γ de-excitation

Table 2.1: Summary of Bertini cascade sub-models.

```
G4HadFinalState* G4CascadeInterface::ApplyYourself(
                  const G4HadProjectile& aTrack, G4Nucleus& theNucleus) {
  // [...]
  G4InuclElementaryParticle *  bullet = new G4InuclElementaryParticle(
                                momentumBullet, bulletType);
  G4double theNucleusA = theNucleus.GetN();

  // Collider initialisation
  G4ElementaryParticleCollider*   colep = new G4ElementaryParticleCollider;
  G4IntraNucleiCascader*            inc = new G4IntraNucleiCascader; // Actual INC
  inc->setInteractionCase(1); // Interaction type is particle with nuclei
  G4NonEquilibriumEvaporator*     noneq = new G4NonEquilibriumEvaporator;
  G4EquilibriumEvaporator*         eqil = new G4EquilibriumEvaporator;
  G4Fissioner*                     fiss = new G4Fissioner;
  G4BigBanger*                     bigb = new G4BigBanger;
  G4InuclCollider*             collider = new G4InuclCollider(
                                                colep, inc, noneq, eqil, fiss, bigb);
  G4CollisionOutput output;
  output = collider->collide(bullet, target);

  // Convert cascade data to use hadronics interface
  std::vector<G4InuclNuclei>             nucleiFragments =output.getNucleiFragments();
  std::vector<G4InuclElementaryParticle> particles =      output.getOutgoingParticles();

    for (ipart = particles.begin(); ipart != particles.end(); ipart++) {
      outgoingParticle = ipart->type();

      std::vector<G4double> mom = ipart->getMomentum();
      G4double ekin = ipart->getKineticEnergy() * GeV;
      G4ThreeVector aMom(mom[1], mom[2], mom[3]);
      aMom = aMom.unit();

      switch(outgoingParticle) {
      case proton:
        cascadeParticle = new G4DynamicParticle(
                             G4Proton::ProtonDefinition(), aMom, ekin);
  break;
      case neutron:
        cascadeParticle = new G4DynamicParticle(
                             G4Neutron::NeutronDefinition(), aMom, ekin);
  break;
      } // [...]
      theResult.AddSecondary(cascadeParticle);

    for (ifrag = nucleiFragments.begin(); ifrag != nucleiFragments.end(); ifrag++) {
        G4double eKin = ifrag->getKineticEnergy() * GeV;
        std::vector<G4double> mom = ifrag->getMomentum();
        eTot   += std::sqrt(mom[0]*mom[0]);

        G4ThreeVector aMom(mom[1], mom[2], mom[3]);
        aMom = aMom.unit();
        G4int A = G4int(ifrag->getA()); G4int Z = G4int(ifrag->getZ());
        aIonDef = theTableOfParticles->FindIon(Z, A, 0, Z);
        aFragment =  new G4DynamicParticle(aIonDef, aMom, eKin);
       }
    theResult.AddSecondary(aFragment); // [...]
  return &theResult;
}
```

Listing 2.2: *G4CascadeInterface*-class mediates all information between the Geant4 hadronic framework and internal description of Bertini sub-models.

Bertini physics lists

The Geant4 toolkit offers a variety of options for physics processes and models over a wide range of energies for electromagnetic and strong interactions. For the same combination of projectile and target at a given energy, there can be several models or processes applicable with different accuracy, strengths, and computational costs. It is possible to create numerous configurations of models in order to address the needs of a particular use case. Making an optimal selection of a set of models from among those available can thus be a challenging task, especially for hadronic interactions.

Choosing among the Geant4 hadronic models is made easier by a number of physics lists, which are included in the Geant4 toolkit release. Each physics list is a complete and consistent collection of models chosen to be appropriate for a given use case.

Hadronic use cases relevant to high-energy physics applications include calorimeters, trackers, and a typical general-purpose detector. At low energy the use cases of neutron dosimetry applications and nucleon penetration shielding are covered.

Bertini sub-models are utilised in validated Geant4 physics lists:

GQSP_BERT This physics list uses a Bertini cascade below 9.9 GeV and QGSP for energies that are higher, but below 25 GeV.

GQSP_BERT_HP This is basically a similar physics list to GQSP_BERT, except that below 20 MeV a high-precision neutron model HP is used. Listing 2.3 demonstrates how this physics list is defined in the Geant4.

Listing 1.1 demonstrates how the user can select the wanted physics lists with macro commands.

```
void HadronPhysicsQGSP_BERT_HP::CreateModels()
{
  theNeutrons = new G4NeutronBuilder;
  theNeutrons->RegisterMe(theQGSPNeutron = new G4QGSPNeutronBuilder(QuasiElastic));
  theNeutrons->RegisterMe(theLEPNeutron = new G4LEPNeutronBuilder);

  theLEPNeutron->SetMinEnergy(19.9*MeV);
  theLEPNeutron->SetMinInelasticEnergy(9.5*GeV);
  theLEPNeutron->SetMaxInelasticEnergy(25*GeV);

  theNeutrons->RegisterMe(theBertiniNeutron = new G4BertiniNeutronBuilder);

  theBertiniNeutron->SetMinEnergy(19.9*MeV);
  theBertiniNeutron->SetMaxEnergy(9.9*GeV);

  theNeutrons->RegisterMe(theHPNeutron = new G4NeutronHPBuilder);

  thePro=new G4ProtonBuilder;
  thePro->RegisterMe(theQGSPPro = new G4QGSPProtonBuilder(QuasiElastic));
  thePro->RegisterMe(theLEPPro = new G4LEPProtonBuilder);

  theLEPPro->SetMinEnergy(9.5*GeV);
  theLEPPro->SetMaxEnergy(25*GeV);

  thePro->RegisterMe(theBertiniPro = new G4BertiniProtonBuilder);
  theBertiniPro->SetMaxEnergy(9.9*GeV);

  thePiK = new G4PiKBuilder;
  thePiK->RegisterMe(theQGSPPiK = new G4QGSPPiKBuilder(QuasiElastic));
  thePiK->RegisterMe(theLEPPiK = new G4LEPPiKBuilder);

  theLEPPiK->SetMaxEnergy(25*GeV);
  theLEPPiK->SetMinEnergy(9.5*GeV);

  thePiK->RegisterMe(theBertiniPiK = new G4BertiniPiKBuilder);

  theBertiniPiK->SetMaxEnergy(9.9*GeV);

  theMiscLHEP = new G4MiscLHEPBuilder;
}
```

Listing 2.3: An implementation of the GQSP_BERT_HP physics list. Notice how minimum and maximum energies are set for each model and the particles in it.

Chapter 3

Applications for Geant4 Bertini Cascade

This chapter introduces an extension to the Bertini cascade to model kaon-induced interactions. The discussion is based on Publication [126] and [**III**]. An application to simulate the CMS hadronic calorimeter using Bertini models is also reported.

3.1 Kaon extension

Background

Simulating the propagation of the cascade range kaons ($\mathrm{E_{kin}} < 5\ \mathrm{GeV}$) in material is an important part of the design of new high-energy physics detectors and the validation of results from existing detectors.

In the year 2002 the Geant4 toolkit provided several hadronic cascade models, which apply to pions, protons, and neutrons. These models were the low-energy parametrised model (LEP), the Binary cascade, and the Bertini cascade. Only the LEP model could be applied to the incident kaons that are of interest in the SLAC BaBar experiment. However, the LEP model is not especially suited for these energies, and was known to perform poorly for kaons. For example, for a 0.705 GeV incident kaon there were no $\mathrm{K^+}$ particles produced in the quasi-elastic peak. In fact, no $\mathrm{K^+}$ appeared in the spectrum at any value of the nuclear excitation energy. Instead, the model converted the $\mathrm{K^+}$ into $\mathrm{K^0_L}$, $\mathrm{K^0_S}$, and pions. The incident $\mathrm{K^+}$ momentum had to be raised from 0.705 GeV to 2 GeV before any $\mathrm{K^+}$ appeared at all in the final state spectrum [126].

At this time Geant4 Bertini models had already been adopted in the BaBar experiment, and were found to provide a much better performance for pion-, proton-, and neutron-induced reactions in comparison to the original LEP model [21]. Combining this finding with the fact that the Bertini models are designed to have a transparent architecture, making further extension feasible, SLAC initiated the development of Bertini kaon extension [126].

Cross-sections

The Bertini cascade assumes that particle-particle interaction cross-sections and branching ratios within the nucleus are given by their free-space counterparts.

So, in order to extend the model to include kaons, $\mathrm{K^+p}$, $\mathrm{K^-p}$, $\mathrm{K^+n}$, and $\mathrm{K^-n}$ cross-section measurements are required.

An extensive list of these cross-sections and branching ratios is provided in the CERN catalogue [58]. Above an incident momentum of about 15 GeV/c the data begin to thin out significantly, setting an upper bound on the applicability of the extended model. Incident K^0_L and K^0_S must also be included in the model, thus requiring the K^0 and $\overline{K^0}$ cross-sections for intra-nuclear propagation.

After the initial interaction with a nucleon, hyperons may be produced and subsequently interact with other nucleons before leaving the nucleus. Hence, Λ-, Σ-, and Ξ-nucleon cross-sections are also needed. Many of these were taken from Ref. [48].

Many of the required cross-sections have never been measured, and estimates or guesses are required to fill in the missing information. Where there are gaps in the energies at which measurements were made, a simple linear interpolation of the cross-sections is employed in the extended model. If there are unmeasured channels from a given reaction, the channel cross-sections are filled in by using the total cross-section measurements as a constraint [**III**]. As far as possible, missing cross-sections were estimated by using isospin and strangeness conservation [126]. For example, it was assumed that

$$\sigma_{K^0 p} = \sigma_{K^+ n} \quad \text{and} \quad \sigma_{\overline{K^0} n} = \sigma_{K^- p}. \tag{3.1}$$

Cross-sections in kaon extension have been developed in synchronisation with other Bertini sub-models, and the kaon extension supports the same interface. The validation of the Bertini cascade model for projectiles up to 10 GeV was announced in Publication [**III**].

Final State Generation

For each interaction type, the model has a list of final state channels and particle types. For incident pions, protons, and neutrons, the existing model keeps track of one- through to six-body final states up to 10 GeV. In the extended model the number of particle types was increased to include kaons (K^0_L, K^0_S, K^+, and K^-) and the lowest mass hyperons (Λ, Ξ^0, and Ξ^-).

The maximal final state multiplicity was increased for incident strange particles from six to seven. This reflects the fact that the sum of seven-body final states represents a significant fraction of the total cross-section.

The final state momenta are sampled from parametrised angular and momentum distributions. The extended model uses the same distributions, despite the fact that they were derived from pion, proton, and neutron data. A summary of the Bertini kaon extension is given in Table 2.1.

3.2 Quasi-elastic K^+ scattering from lead

Tests of the extended Bertini model were compared to inelastic K^+ scattering data [20]. These data for the quasi-elastic peak in D, C, Ca, and Pb targets provides a useful test of the intra-nuclear kinematics in the model. The results for a Pb target are shown in Fig. 3.1. As the data for the 43°scattering angle indicate, the Bertini model with kaon extension gets the energy of the quasi-elastic peak more or less correct.

The model is found to overestimate the quasi-elastic peak width. This was suspected to be related to the too-shallow nuclear potential for kaons. Furthermore, it was known that the real part of the optical potential for kaons should be deeper than the 7 MeV used in this simulation. For the more recent implementation of Bertini kaon extension, a slightly improved performance is achieved with modified extension potentials of 15 MeV for kaon and 30 MeV for hyperons.

The overall normalisation was low by about 30%. The data had a systematic error of 11%, so most of the difference was probably due to the model or the value of the total inelastic cross-section.

At 24°the model also seems to show the quasi-elastic peak in the right place. This is harder to estimate, because the data include elastic scattering and scattering from low-lying collective levels in the nucleus, while the model deals only with inelastic, incoherent scattering. It also appears that the width was overestimated at 43°. Similar results were observed for the D, C, and Ca targets [126].

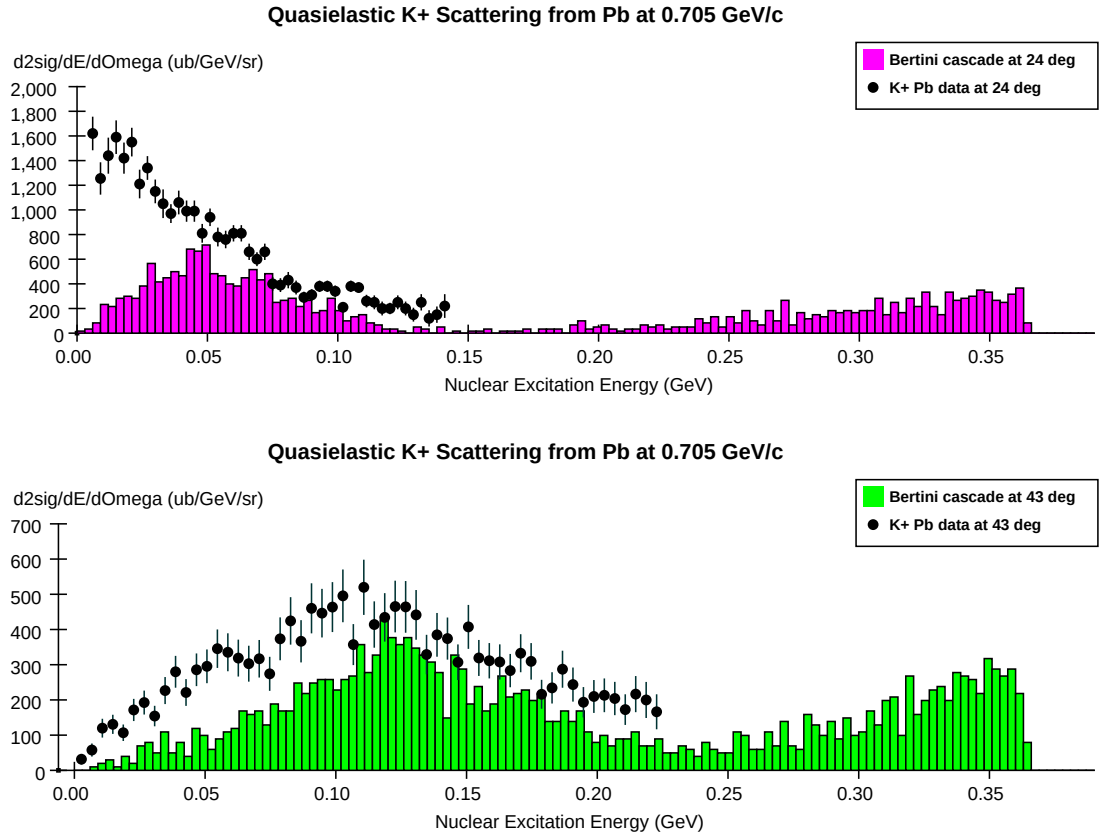

Figure 3.1: Bertini kaon extension in action. Inelastic K^+ scattering from Pb at 24°and 43°. The incident K^+ momentum was 0.705 GeV/c. The horizontal axis is the nuclear excitation energy in GeV, so that elastic scattering would appear at 0 GeV. The vertical axis is the double differential cross-section, $d^2\sigma/dE/d\Omega$, in μb/GeV/sr units. In comparison with the experimental data [20], the Bertini model reproduces the energy of the quasi-elastic peak relatively well. When the same target configuration was tested using the Geant4 LEP model, K^+ was not produced at all.

3.3 Simulation of the CMS hadronic calorimeter

Background

Among the different high-energy physics sub-detectors, calorimeters play an important role, as they provide an energy deposition profile and measure the energy of the incoming particles.

The most obvious reason for us to study and simulate particle showers is to design and develop hadronic calorimeters. For example, to optimise the performance of hadronic calorimeters, alternative arrangements of the detector components can be studied. Further, accurate shower understanding is demanded when estimating radiation damage and activation. One of the early motivations for the development of cascade Monte Carlo codes was to simulate how the particle shower penetrates the entire block of matter. These punch-through studies are particularly important in radiation protection and shielding [12].

Advances in high-energy physics demands an understanding of hadronic interactions at even higher energies in order to probe deeper into the structure of matter. Increasingly energetic hadron showers and particle multitudes pose a challenge for shower simulation. Simulation codes representing state-of-the-art programming practices and a high level of details in physics modelling are needed to respond to this challenge.

The level of detail to which the investigator takes the simulation depends crucially on the particular application. When only the relevant details are simulated, one can save large quantities of computer time. It is often necessary to rely on parametrisations of data or phenomenological models. In recent years we have seen signs of a transition from parametrisation-driven modelling, which provides fast performance, towards more physically sound modelling, providing the potential for a deeper understanding of calorimetry.

In hadronic calorimeters two extreme types of cascades can occur. In the first type the shower energy is largely converted into EM energy, typically through the generation of pions. In the second type EM sub-showers make only a small contribution. The cascades are opposite in many of their properties. For example, showers of the second type tend to be significantly longer than showers of the first type. Particularly in calorimeter design, a non-linearity compensation scheme has to be provided in order to deal with non-linearities arising in calorimeter design. The goal of good linearity and resolution is achieved in Geant4 by a balanced combination of EM and hadronic models.

Geant4 simulation of CMS hadronic calorimeter

At the CMS a good description of the electromagnetic calorimeter ECAL and hadronic calorimeter HCAL [59, 118] energy resolution is important for several physics studies. In particularly, the HCAL is needed for hadronic channels, such as $Z/W \rightarrow jet + jet$, and to understand the missing transverse energy of the detector. Thus, a large number of experiments have been performed in order to arrive at a detailed understanding of the CMS calorimetry. Key parameters for the CMS H2 test beam data from the year 2006 (TB2006) were:

H2 beam 1-350 GeV,

ECAL super module of PbWO4 crystals,

HCAL brass (50 mm) - scintillator (3.7 mm) sampling [49].

The basic properties of simulated hadron showers compared with experimental data are the transverse and longitudinal distributions. Figure 3.2 presents a longitudinal shower profile initiated by 20 GeV π^-. Data from the CMS TB2006 facility [120] are compared to a Geant4 simulation using various physics lists: QGSP, LHEP, QGSP_BERT, and FTFP. The QGSP_BERT physics list is found to give the best overall agreement with the data. Here we see a reason why the focus in the CMS Geant4 HCAL studies has shifted from QGSP to QGSP_BERT.

The response of TB2006 HCAL to 1–350 GeV protons is shown in Fig. 3.3a. The corresponding resolution is shown in Fig. 3.3b. Again, the QGSP_BERT physics list is used to simulate the test beam setup with reasonable agreement in comparison with the measurements. Analysis of the more recent data sets have lead to a more detailed understanding of CMS HCAL resolution.

In general, the CMS HCAL Monte Carlo simulation shows reasonable agreement with the TB2006 data. The most serious problem is the discontinuity seen in the particle event rates around 10 GeV. This is the energy at which the transition between the Bertini model and the higher-energy model QGSP is located in the QGSP_BERT physics list. Improvements to this Geant4 problem are still under investigation.

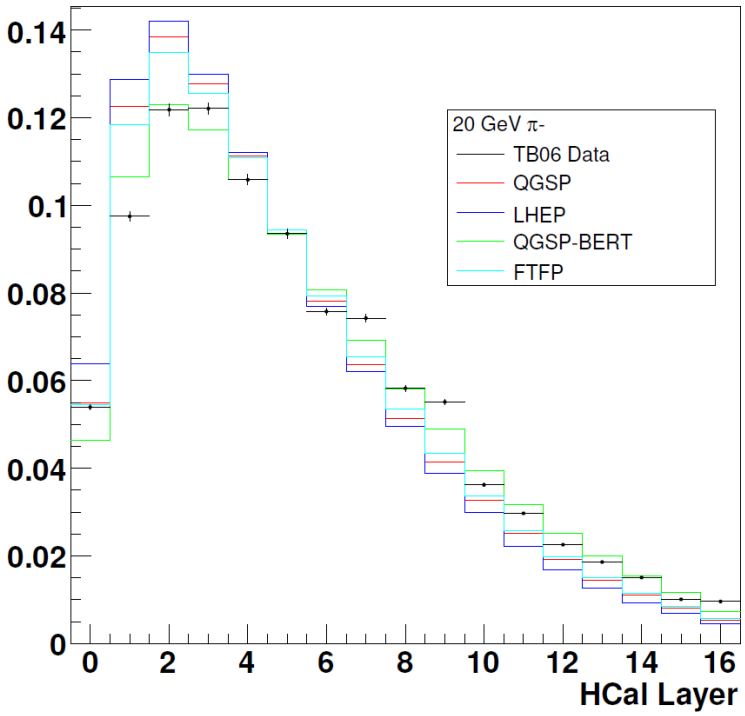

Figure 3.2: CMS HCAL longitudinal shower profile. The QGSP_BERT physics list gives the longest shower profiles and best agreement with the TB2006 data. (Courtesy of S. Kunori [50])

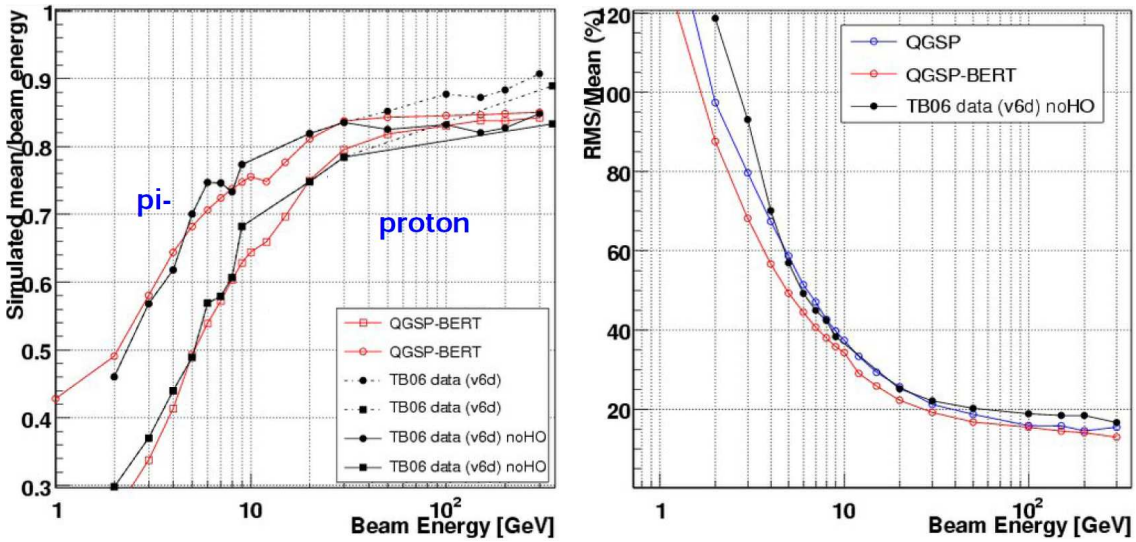

Figure 3.3: **a)** CMS HCAL response (linearity) to protons. A Monte Carlo simulation using Geant4 QGSP_BERT physics is compared to test beam data from the year 2006. Reasonable agreement is seen. **b)** HCAL resolution. (Courtesy of S. Kunori [49])

Chapter 4

Validation of Geant4 Hadronic Models

In this chapter we discuss the issue of Geant4 hadronic physics validation. On the basis of Publication [**IV**] and other references we describe how Bertini cascade models have been validated against experimental data.

4.1 Validation suite for intermediate energy interactions

Before being put into production, each new Geant4 version is subjected to a series of validation tests focusing on the validation of the detector model, as well as the tracking, reconstruction, and physics processes. In the cascade energy region the Geant4 collaboration has prepared a validation suite for the hadronic physics validation [84]. The validation suite is designed also to aid users in selecting optimal physics models.

Validation tests can be classified into two categories: thin-target experiments and thick-target experiments. Thin-target experiments are often used, because they allow a clean and detailed study of single hadronic interactions. The Geant4 suite includes a large set of experimental data for 22 MeV–3 GeV projectile hadrons from thin-target scattering experiments [84]. The complete detector setup is another type of validation, which typically utilises test beam data from calorimeters and tracking devices. In this case, the observables (CMS H2 beam line data, for example) are the convolution of many interactions; therefore, the whole functionality of Geant4 is validated at once [**III**].

Figure 4.1 is an example of a plot made by the validation suite. It shows the validation of the Bertini cascade for double differential neutron production cross-sections. In most cases good agreement is found; however, relatively large disagreements exist at the most forward scattering angles. Another plot demonstrating the systematic approach to the validation is shown in Fig. 4.2. Exceptionally good performance is shown for the Bertini cascade as a result of the accurate cross-section parametrisation used for iron, which is based on Pearlstein's systematics [96].

4.2 Validation of Bertini cascade models

Publication [**IV**] reports on extensive validation over the energy range 100 MeV to 1 GeV. One such validation of Geant4 Bertini and Binary models for p(800 MeV)+Al $\rightarrow$ n+X reaction is shown in Fig. 4.3a.

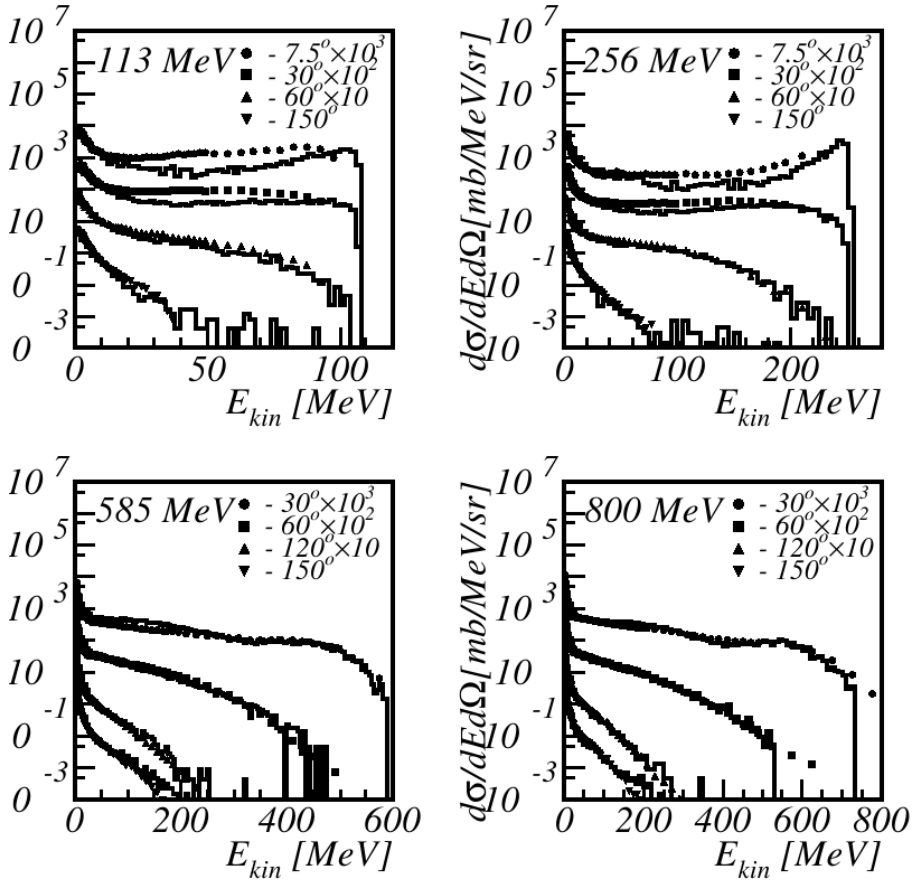

Figure 4.1: Double differential cross-section for neutrons produced in 113 - 800 MeV proton scattering off aluminium. The histograms are Geant4 Bertini cascade Monte Carlo predictions [124], while the data points are from [39]. Particularly good agreement with experimental thin-target data is shown for large angle scattering.

A verification of the secondary neutrons created in the Bertini pre-compound phase (exciton model) and evaporation models is presented in Fig. 4.3b. Neutron production cross-section result from protons bombarding bismuth target, and secondary neutrons created in the exciton and evaporation parts are identified. A corresponding performance was shown in Fig. 1.5 for the standard Geant4 pre-compound and evaporation models.

Figure 4.5 demonstrates the performance of Geant4 Bertini INC model for simulation of $\mathrm{p}(256\ \mathrm{MeV}) + \mathrm{Fe} \rightarrow \mathrm{n} + \mathrm{X}$ in comparison with experimental data, while Fig. 4.6 shows pion production for reaction $\mathrm{p}(585\ \mathrm{MeV}) + \mathrm{Pb} \rightarrow \pi^{+} + \mathrm{X}$.

Additional validations of the Bertini models implemented in Geant4 has been performed independently by several investigators:

- The LHC Computing Grid (LCG) Simulation Physics Validation Project has become the primary forum for validating the detector simulation tools used in LHC.

  LCG has studied the performance of Bertini cascades against thin-target data [7]. An important benchmark has been neutron production from proton bombardment, and particularly a comparison with double-differential cross-section measurements, $d^2\sigma/d\Omega dE_n$, i.e. neutron spectra at fixed angles. In comparison with the measurements made at the Los Alamos Meson Physics Facility (LAMPF) for 113-800 MeV proton beams and for 7.5–150° scattering an-

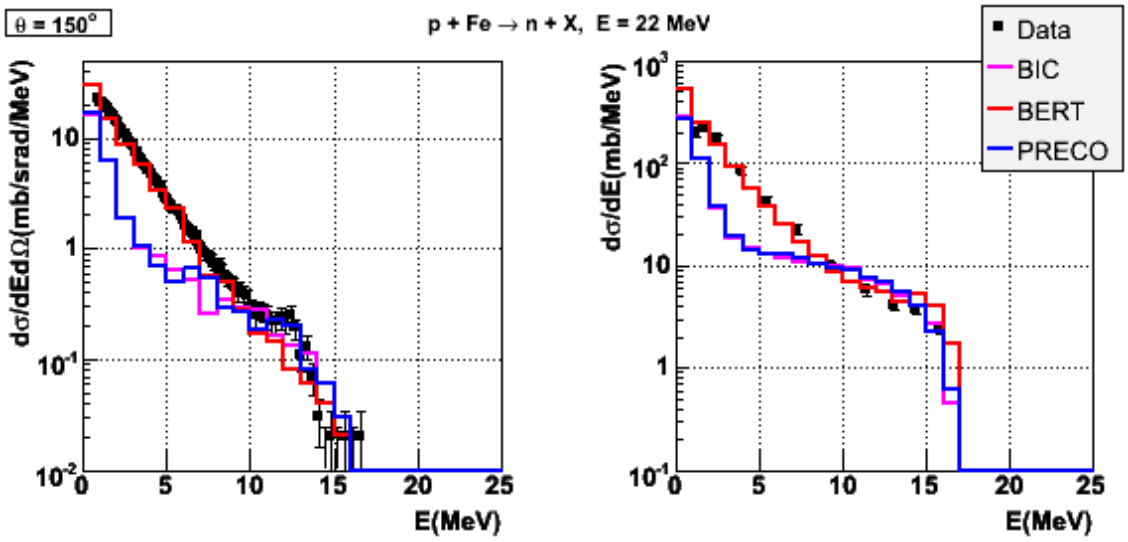

Figure 4.2: System test for Geant4 9.1 release to validate models of low-energy hadronic scattering. Exceptionally good agreement with the data is shown for the Bertini cascade because of the accurate cross-section parametrisation used for iron, which is based on Pearlstein's systematics [96]. **a)** Energy spectrum of neutrons scattering to θ=150°for p(22 MeV)+Fe $\rightarrow$ n+X. **b)** Angle integrated neutron energy spectrum. The results from the Binary cascade and standard Geant4 pre-compound model are shown. (Courtesy of V. Ivanchenko.)

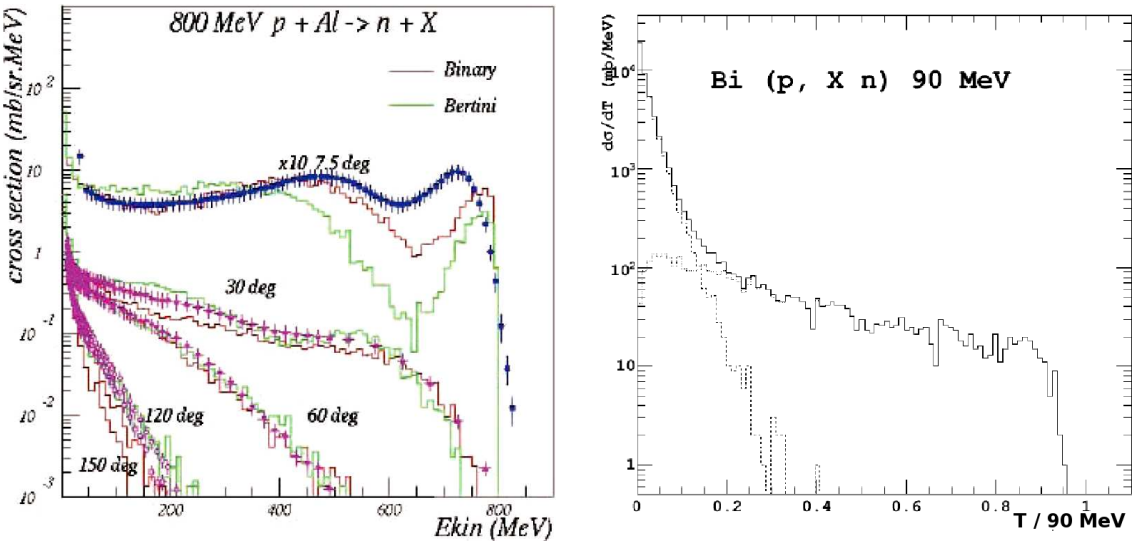

Figure 4.3: **a)** Validating Geant4 Bertini and Binary models: neutron production from 800 MeV protons on Al [**IV**]. **b)** Secondary neutrons created using Bertini pre-compound model and evaporation model ($E < 20$ MeV) in proton-induced Bi interactions. This can be compared to the simulation of standard Geant4 pre-compound and evaporation models shown in Fig. 1.5.

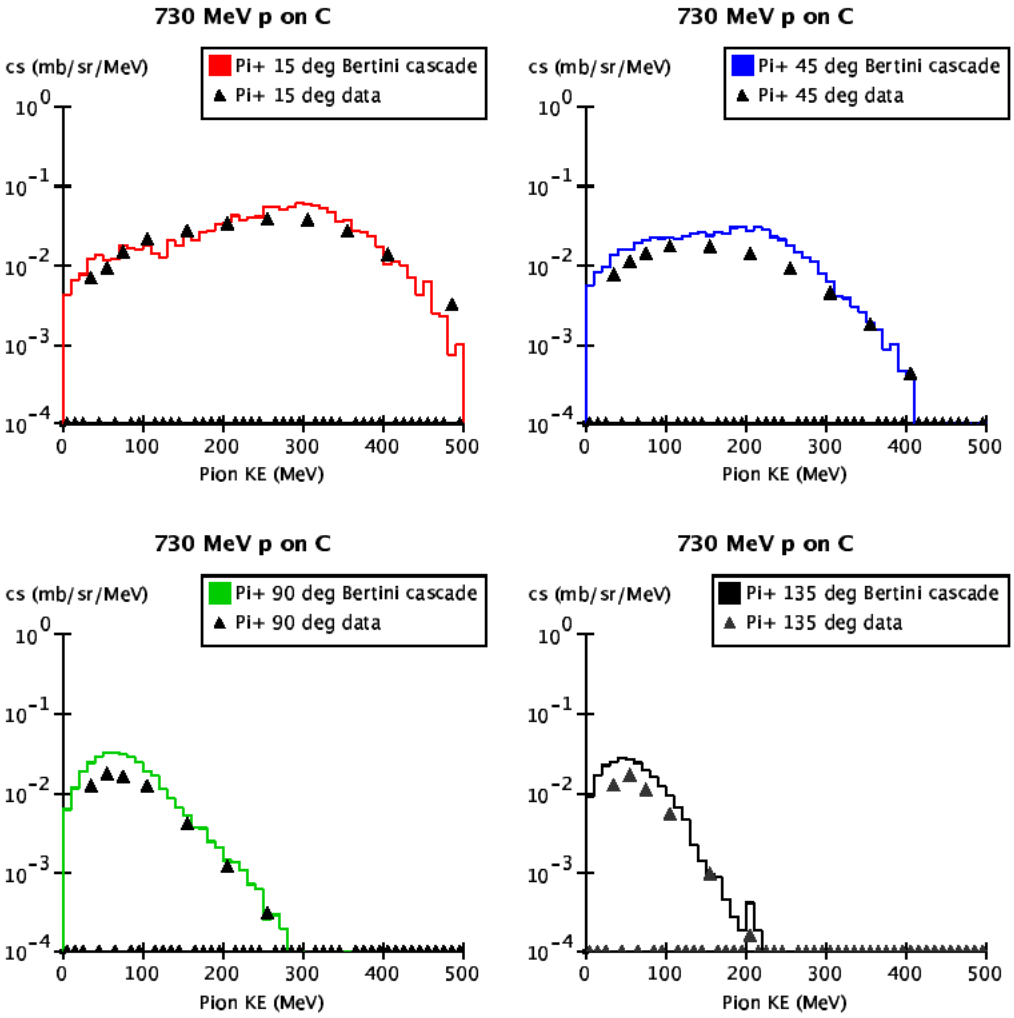

Figure 4.4: Double-differential cross-section for π^+ production from 0.73 GeV protons incident upon a carbon target. The Bertini cascade is compared with the data from [22]. Because of its good accuracy, which was found to be significantly better compared to standard treatment with the Low Energy Parametrised (LEP) model based on the GEANT3 GHEISHA implementation, BaBar was the first experiment to utilise the Bertini cascade [21]. (Courtesy of D. Wright.)

gles, the GQSP_BERT physics list was found to reproduce double-differential cross-section data at the level of 20-50% [6].

LCG has also made comparison studies between the Geant4 and LHC subdetector test-beam data, such as the response of LHC calorimeters to pions [98].

- SLAC has validated a double-differential cross-section for a π^+ production from 0.7-2 GeV protons incident upon various targets [21]. In comparison with the experimental data [20] Bertini was found to have good accuracy. Figure 4.4 demonstrates the performance for a π^+ production from 0.73 GeV protons incident upon a carbon target.

- The CMS H2 test beam has initiated a significant validation process, since the QGSP physics list was found to produce profiles that were too shallow. This finding ended up in the creation of the QGSP_BERT physics list, which improves the shower profile in comparison with the H2 test beam data.

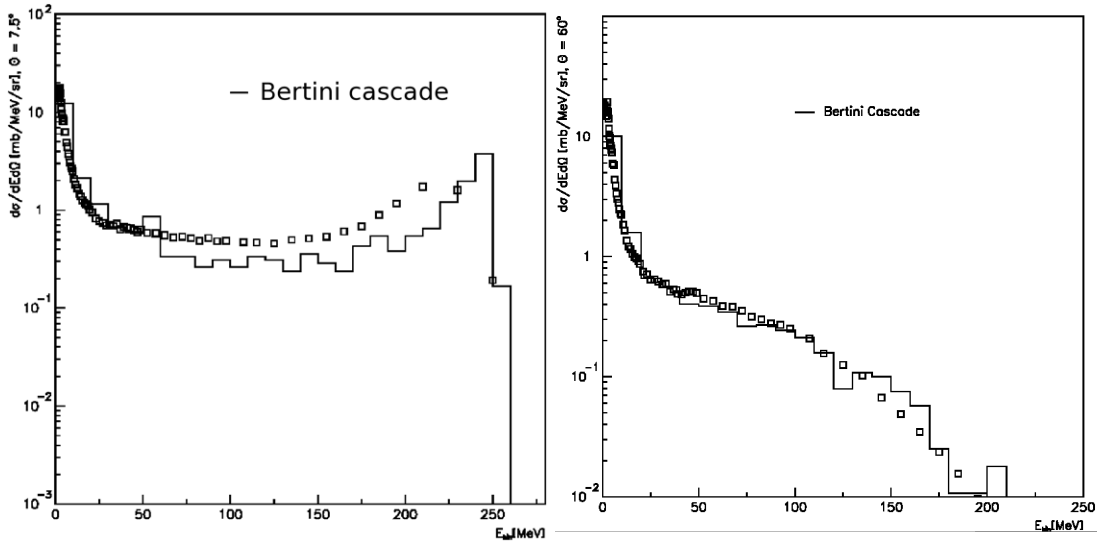

Figure 4.5: **a)** Geant4 Bertini INC model simulation of p(256 MeV)+Fe → n(θ = 7.5°)+X in comparison with experimental data [40]. **b)** θ = 60°[**II**].

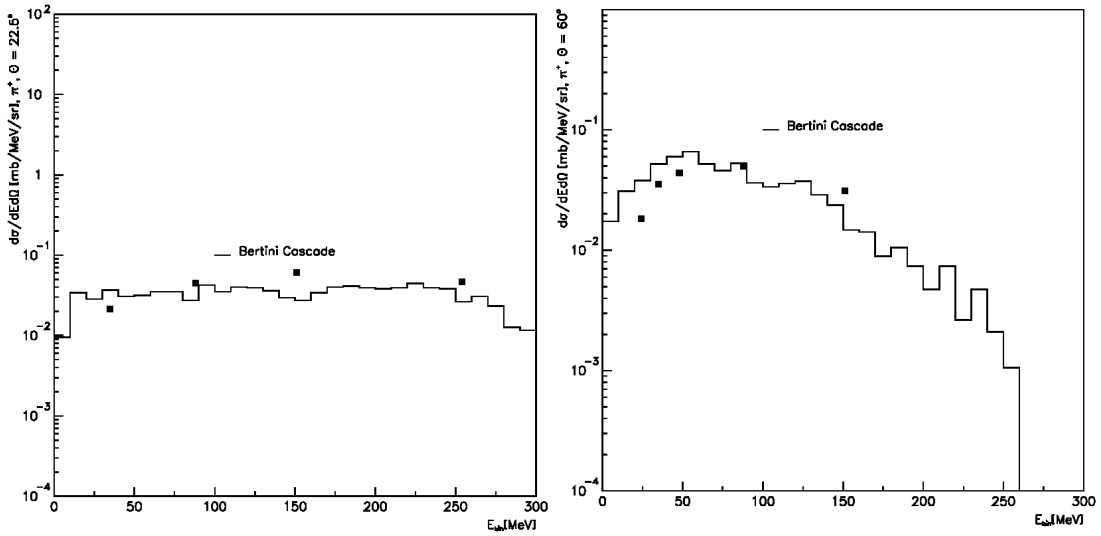

Figure 4.6: **a)** Geant4 Bertini INC model simulation of p(585 MeV)+Pb → π^+(θ = 22.5°)+X in comparison with experimental data [31]. **b)** θ = 60°[**II**].

- The high energy performance of the Bertini model has been validated in Ref. [101]. This study used a data set from ITEP [19], which consists of inclusive proton and neutron production from π and p beams on a variety of nuclear targets (C, Cu, Pb, U) with beam momenta in the range 1-9 GeV/c. The data have a statistical error of 1-10% and systematic uncertainty of 5-6%.

  In comparison with other Geant4 cascade models, the Bertini cascade model was found to give the best overall description of the data. For light targets Bertini underestimates the production of protons and neutrons in the backward hemisphere. Bertini is faster than the QGSC and Binary models but significantly slower than the LEP model which is using a parametrisation approach.

4.3 Isotope production

Accumulated data on fission yields, together with spallation and fragmentation products, are important for understanding the mechanisms of the formation of nuclei, and for the development of reliable models of intermediate-energy nuclear reactions. Medium-energy nuclear data are useful in many applications, such as the design of accelerator shielding, the effects of cosmic radiation on astronauts, accelerator-based nuclear waste transmutation studies, the interpretation of the reaction products of cosmic ray particles, the production of medical isotopes, and radiation therapy.

In Ref. [77] a validation of the radionuclide production of the Bertini model for U and Tc targets irradiated by 0.1-1.6 GeV protons is discussed. The findings in this work are supported by inter-code comparisons in Refs. [61, 62], the indication being that Bertini modelling provides a physics performance comparable with other relevant software packages, such as CEM, LAHET, HETC, CASCADE, ALICE, and YIELDSX.

In Ref. [78] we particularly investigated nuclide production in proton-induced reactions on various target elements in the energy range 0.04–3.0 GeV. Characteristic features of high-energy reactions for the excitation function and mass-yield curve are shown in Fig. 4.7.

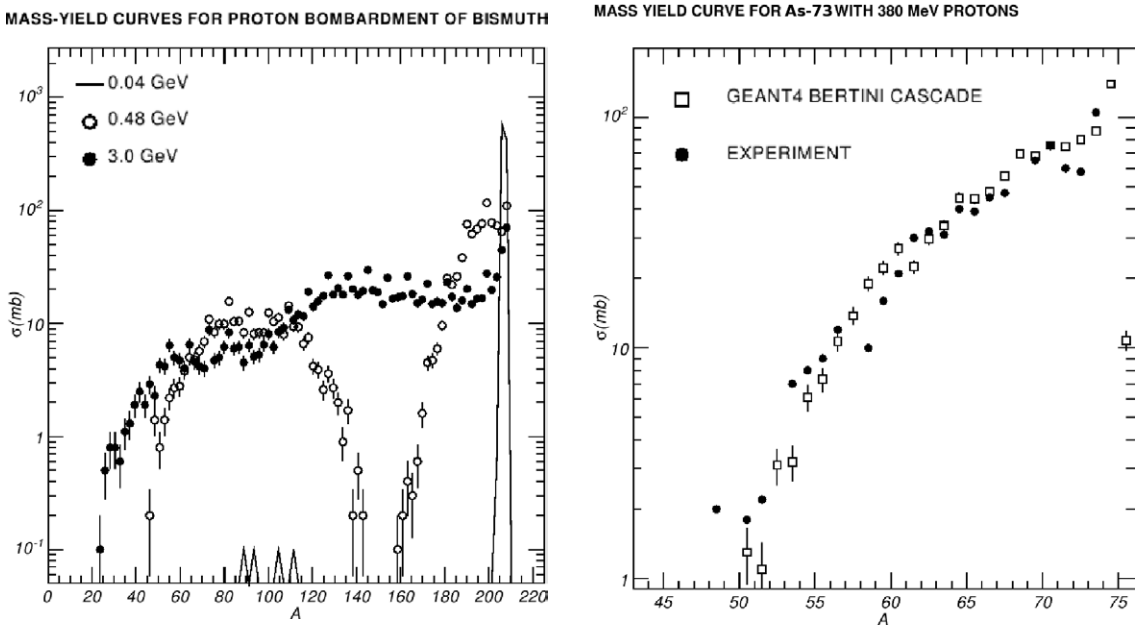

Figure 4.7: **a)** Mass-yield curves for proton bombardment of a bismuth target. For the case of 0.48 GeV protons we see spallation products for $A > 160$ and a fission region for $A < 140$. While the energy is increased to the GeV region the clean-cut distinction between these regions vanishes [74]. **b)** Yields of residual products nuclei for thin-target experiment p(380 MeV)+^{73}As. In comparison with experimental data from [54], Bertini shows reasonably good agreement.

Figure 4.8 shows another validation of isotope production resulting from the bombardment of aluminium by protons. Monte Carlo predictions are obtained from the Bertini and Binary cascade models. Since the pre-compound model often plays the most important role in the isotope distribution from highly excited nucleus, plots indicate that the independent pre-compound models that were validated have a comparable performance.

In Geant4 neutron-induced isotope production is usually treated with the Geant4 isotope production model, which used evaluated data libraries. Thus isotope validation indicates that in some cases Bertini models could be used instead.

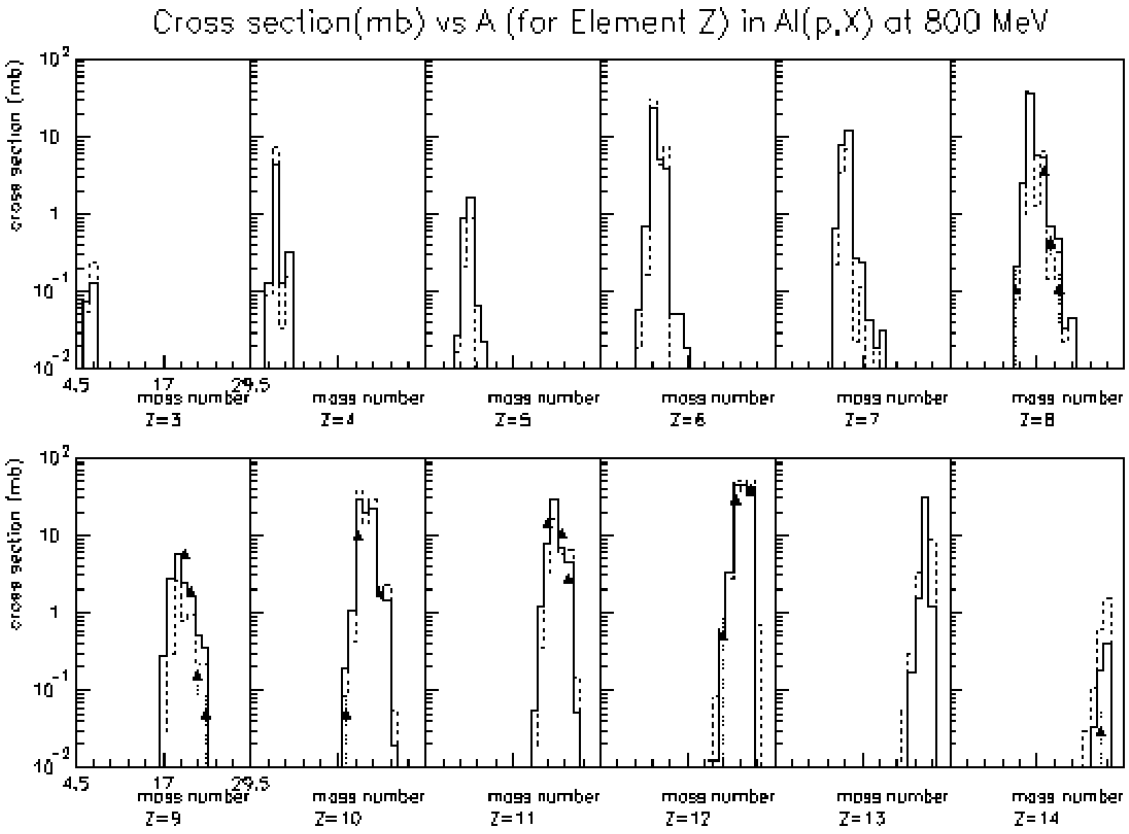

Figure 4.8: Comparison of isotope production resulting from 0.8 GeV protons bombarding aluminium among Geant4 models. Histograms show the prediction of the Bertini cascade (solid line) and the Binary cascade (dashed line) [124]. A good performance is seen when Monte Carlo simulation is compared with the experimental data from [26].

An example of validating isotope production on an yttrium target is given in Fig. 4.9. The power of the cluster computing environment (see Fig. 8.1) was needed to estimate and validate the cross-sections of the rarest isotopes produced by Geant4 Bertini models. Figure 4.9 also demonstrates a relatively successful isotope production from an 8.1 GeV proton projectile. This energy is often considered too high for INC models; the validity of the Bertini cascade is extended to this energy with the help of cross-section tabulations up to 15 GeV.

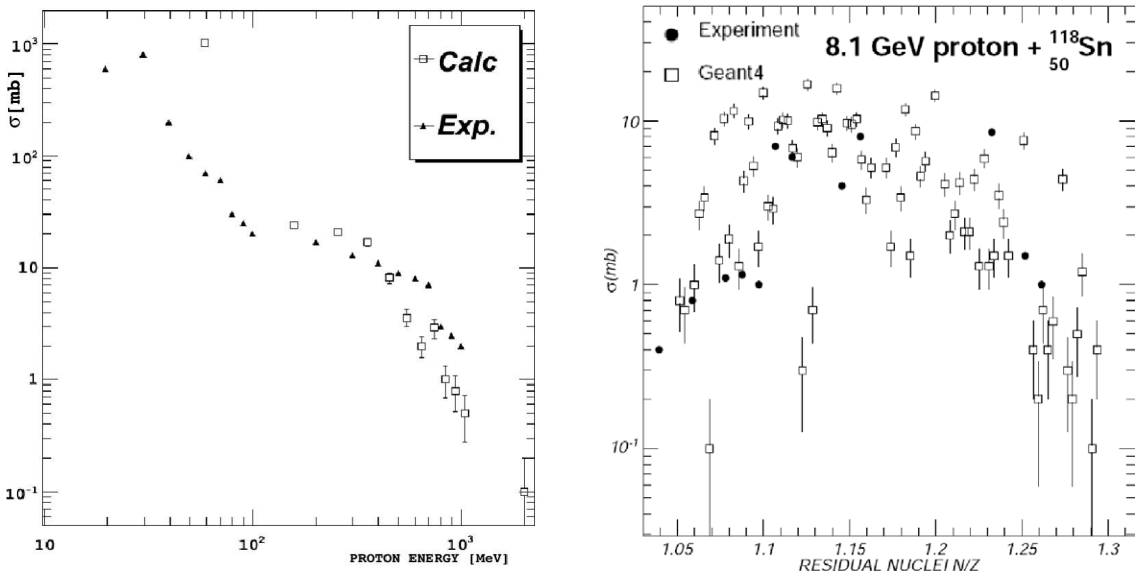

Figure 4.9: **a)** Example of Bertini proton-induced isotope production p+^{89}Y $\rightarrow$ ^{88}Zr+X compared against experimental data [77]. More detailed discussion on the tools and cluster computing environment used to validate the isotope yields is given in Chapter 8. **b)** Comparison of Bertini cascade formation of residual nuclei against data from [56]. Kinetic energy 8.1 GeV for the proton projectile is at the upper limit for the applicability of the Bertini model, and yet we observe a reasonable performance [74].

Part II

ANALYSIS OF THE SiBT DATA AND HIGGS EVENTS IN THE CMS EXPERIMENT

Chapter 5

Helsinki Silicon Beam Telescope for the CMS H2 Beam Line

In the CMS tracker [13, 118] the secondary particles traverse the detector sensors at variable angles. It is therefore important to understand the degradation of the performance of the detectors as a function of the incident angle, i.e. the possible loss of efficiency and position accuracy. We have studied this problem in Publication [**V**] using one of the sensors in the Helsinki Silicon Beam Telescope (SiBT) [114]. In this chapter emphasis is placed on analysing the performance of a single-sided DC-coupled silicon strip detector and the calibration of the detector response. A description of the experimental set-up and the online and offline data analysis is given. Performance results are presented for different angles of incidence for the muon particles.

5.1 Helsinki Silicon Beam Telescope (SiBT)

The SiBT detector, which is based on position-sensitive silicon detectors, has been built to provide high-resolution reference tracks for the detector module tests of the CMS project. Another significant application of the SiBT in the H2 test beam is the characterisation of new silicon detectors [119]. SiBT has allowed us to study the performance of strip detectors processed on silicon wafer grown by the magnetic Czochralski method. These detectors have great potential for radiation hardness [92, 108].

The CERN H2 test beam is derived from a primary proton beam extracted from the CERN Super Proton Synchrotron (SPS). The protons from SPS have an energy of 450 GeV and an extraction cycle length, i.e. the length of the spills, of 16.8 seconds. The primary beam hits the so-called T2 primary target, made of beryllium, and a secondary beam composed of electrons, muons, hadrons, or heavy ions can be extracted.

The experimental set-up at H2 is organised roughly to simulate the conditions inside the CMS detector during its operation. The incoming particle beam passes through four pairs of single-sided silicon strip detectors (Fig. 5.1), ionising charge carriers on its way. Every pair consists of one detector with strips positioned horizontally and another with strips positioned vertically.

In the experimental set-up described in Publication [**V**] SiBT was equipped with single-sided silicon strip detectors that had been processed with the p-side masks of the double-sided AMS detector [5]. One of the sensors was installed in a special support which made it possible to change the angle of the sensor relative to the beam. The rest of the detector was used to measure the reference track. The detectors were DC-coupled with 1024 readout strips of 55-μm pitch. The details of the detector layout and front end electronics in the set-up are available in Publication [**VI**] (pp. 3–4) and Ref. [114].

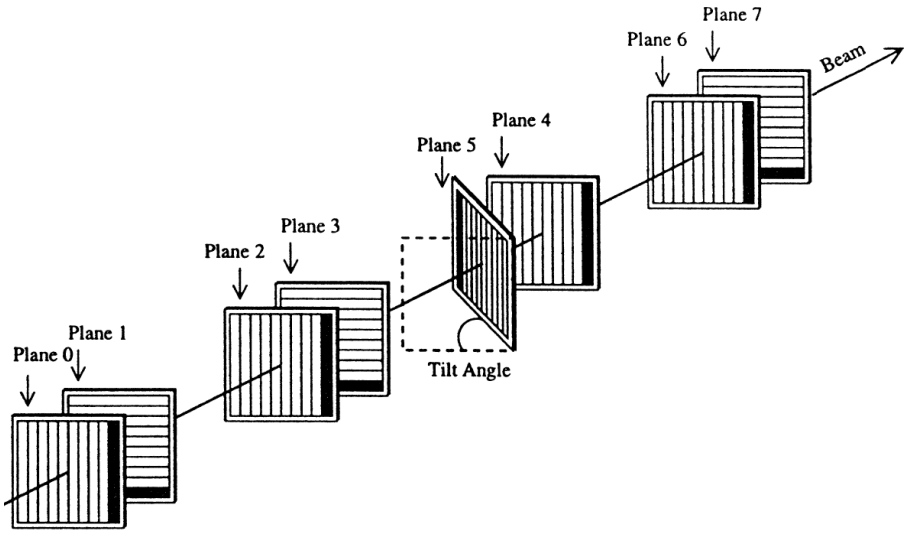

Figure 5.1: A conceptual layout of the Helsinki SiBTused in the CMS H2 test beam to measure the tracks of incoming particles with high resolution. The square-shaped detectors are placed on the support forks in pairs. The vertical and parallel lines indicate the strip orientation [**V**].

The particles used in this experiment were muons coming from the NA49 [46] experiment upstream in the H2 beam line. For this reason, the beam had a rather large ($\sim$10 mrad) angular dispersion of the particle trajectories.

The best accuracy for the fitted track in SiBT was obtained in the middle of the telescope. Therefore, the test sensor was placed near the centre. Plane 5 was chosen for the test device. To gain the best accuracy normal to the strip direction, it was rotated by 90°and moved in front of Plane 4. This configuration allowed a five-point fit of the particle trajectory for the horizontal coordinate. Thus the vertical position was fitted using the remaining three planes. The measurements were performed at six different tilt angles from 0° to 32°.

5.2 SiBT cluster analysis

Correction for common-mode noise was calculated as the chip average of the pedestal subtracted data. The pedestal and common-mode corrected signals exceeding a certain threshold, together with the adjacent strips, were considered to be a cluster. This method roughly corresponded to a 3σ cut on the data, σ being the standard deviation of the signal position. Details of the signal pedestal estimation, cluster-finding algorithm, and the read-out of the telescope are given in Ref. [114].

The track length inside the sensor is proportional to $\cos^{-1}\beta$, where β is the track incident angle with respect to normal. The energy deposition is proportional to the track length inside the detector and hence the signal should increase accordingly. The observed cluster signal size is plotted in Fig. 5.2a for a 30° turning angle. As expected, the mean value of this signal in ADC units was found to be 10% bigger compared to the case of a 0° incidence angle [**V**]. The cluster shapes are demonstrated in Fig. 5.2b, where the pulse heights in each strip of a cluster are presented as bar histograms.

The observed average signal-to-noise ratio was $\sim$29 at 0°, and showed a similar increase with the angle as the cluster signal. The mean number of strips (channels) per cluster also increased with an increasing angle, as is shown in Fig. 5.4a.

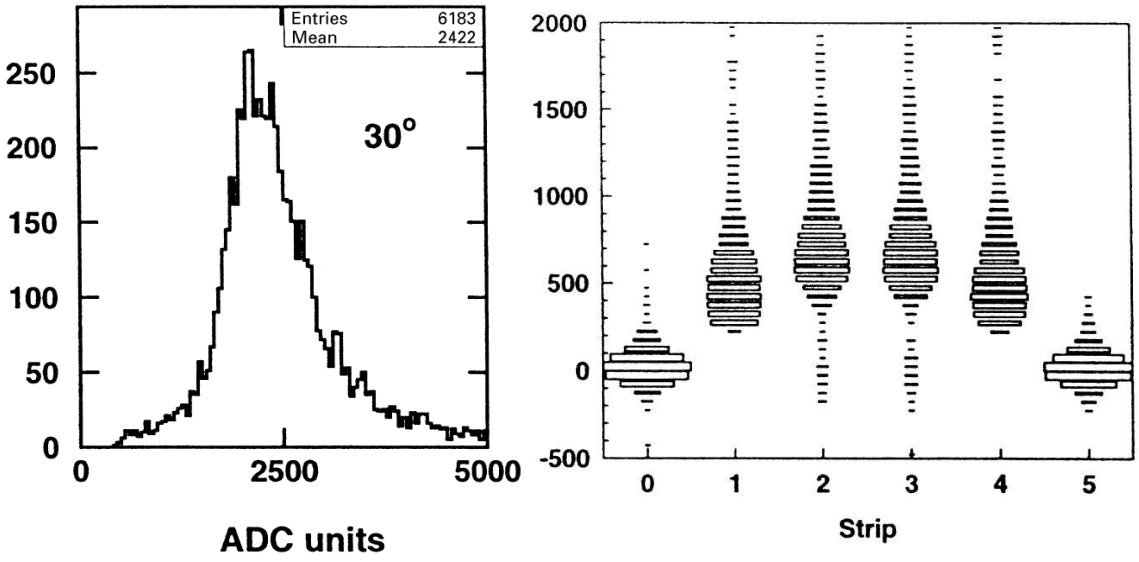

Figure 5.2: **a)** Cluster signal distribution of SiBT test detector for 30°detector turning angle. **b)** Cluster shape for 6-strip clusters at 30°. The signal distribution of each strip in clusters is shown as a bar histogram [V].

5.3 Detector response calibration and resolution

The calibration of the telescope sensors for geometric misalignment and for nonlinear response is important in order to attain the best-possible resolution of the detectors. A dedicated track reconstruction algorithm, adopted for the variable orientation of the detector planes, was used, together with a special calibration procedure [75], to precisely determine the geometric offsets in the position and orientation of the sensors relative to each other.

The nonlinear response appears as a systematic offset of the measured cluster position from the particle impact position between any two strips. This effect was manifested in the distribution of the η function defined as

$$\eta = \frac{S_2}{S_1 + S_2}, \tag{5.1}$$

where S_1 and S_2 are signals in two consecutive strips with a maximal sum $S_1 + S_2$. The variable η represents an estimate of the particle hit position between two strips (Fig. 5.3a).

In the event of an ideal response of linear charge sharing the η distribution should be flat. The departure from uniformity is particularly important for narrow clusters. The variable η defined by Eq. (5.1) makes sense in the case of narrow clusters, but for broader clusters at large angles we used the cluster-weighted mean

$$<i> = \frac{\sum_i iS_i}{\sum_i S_i} \tag{5.2}$$

as an estimate for the position rather than η. In Eq. (5.2) the sum goes over the cluster channels i.

The difference between the mean and the nearest strip below the mean is an estimate of the particle hit position between two strips

$$\eta' = mod(<i>, 1). \tag{5.3}$$

This quantity is plotted in Fig. 5.3b for a 30° turning angle.

Two different methods to estimate the detector resolution exist. Both of these methods are based on investigating the residuals of the track fit, and the methods take into account the so-called impact point error, i.e. the error in the position of the fitted trajectory.

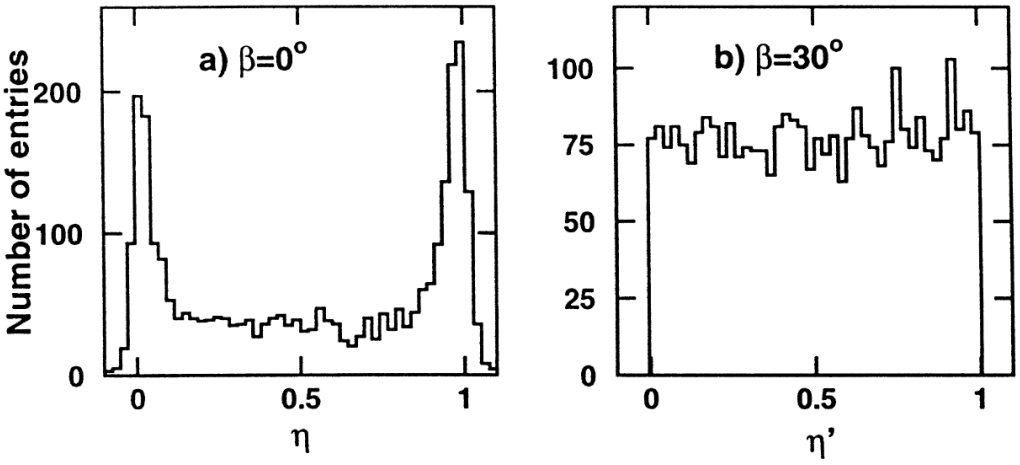

Figure 5.3: **a)** Distribution of variable η, as defined by Eq. (5.1), representing an estimate of the particle hit position between two strips at 0°. **b)** Distribution of variable η', defined by Eq. (5.3), at 30° [**V**].

In the first method, the sensor under study is omitted in the track fit. The fit residual r is

$$r = u_m - u_f, \tag{5.4}$$

where u_m is the measured u-coordinate, and u_f is the impact point coordinate of the fitted trajectory. These quantities are independent, since the sensor under study is removed from the fit. Hence the correlation term in the error estimation vanishes, so that the detector resolution is

$$\sigma_m = \sqrt{{\sigma_r}^2 - {\sigma_f}^2}, \tag{5.5}$$

where the impact point error σ_f is computed using the track parameters covariance matrix from the fit.

In the second method, the hits from the sensor being studied are included in the fit. Since in this case the fitted coordinate u_f depends on the corresponding measurement u_m, the correlation term must be taken into account, and we have

$${\sigma_r}^2 = {\sigma_m}^2 - 2{\sigma_{mf}}^2 + {\sigma_f}^2. \tag{5.6}$$

The correlation term σ_{mf} can be calculated from the χ^2 fit formalism, giving $\sigma_{mf} = {\sigma_f}^2$, so that in this case we have the detector resolution

$$\sigma_m = \sqrt{{\sigma_r}^2 + {\sigma_f}^2}. \tag{5.7}$$

We used the second method, which is somewhat more precise, because it uses all the points in the fit, so that the error σ_f is smaller. It should be noticed that the impact point error depends on the weights ${\sigma_m}^{-2}$ used in the fit and the weights depend on the detector resolution.

In order to correctly estimate the detector resolution with the second method, we determined σ_m by analysing the pull distribution

$$pull = \frac{u_m - u_f}{\sqrt{{\sigma_m}^2 - {\sigma_f}^2}}. \tag{5.8}$$

In the ideal case of Gaussian statistics of the measurement errors, the pull distribution should be standard normal. However, we observed the central Gaussian distribution with rather large

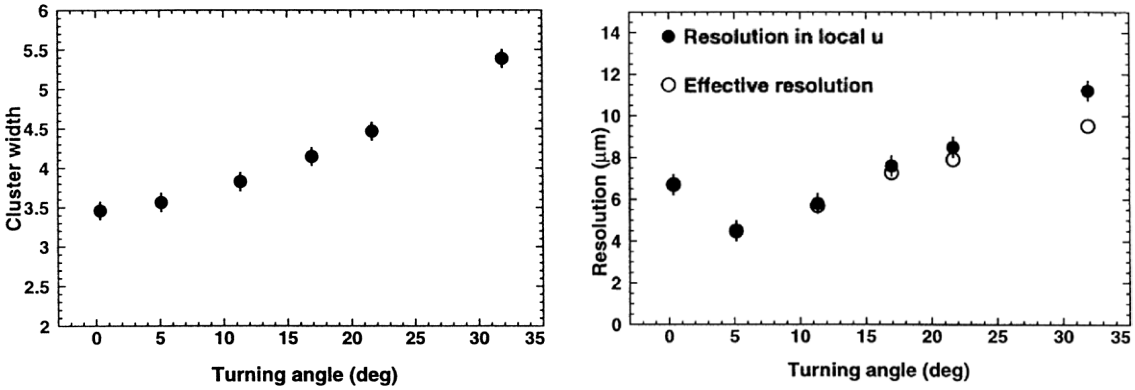

Figure 5.4: **a)** Mean number of channels in an SiBT cluster as a function of turning angle. The average cluster width increases by two strips between 0°and 30°. **b)** Detector resolution as a function of the turning angle. The resolution in the u-coordinate is measured in the detector plane, while the effective resolution is measured perpendicular to the tracks [**V**].
.

tails, which were due to non-Gaussian effects ([**V**], p. 542). The pull distributions were fitted with Gaussian distribution ignoring the tails outside two standard deviations.

Similarly, we defined the detector resolution as the Gaussian width of the central peak within two standard deviations. The detector resolution σ_m is plotted in Fig. 5.4b as a function of the turning angle. Since the algorithm using Eq. (5.1) for the cluster mean deteriorates quickly with an increasing turning angle, we used the cluster-weighted mean defined by Eq. (5.3) for the broader clusters with β>10°. In the plot, we used the calibrated angles rather than the measured angles.

The calibration corrections were of the order 1°–2°. The observation was that the resolution improved by 30% with an increasing turning angle from 0° to 5°. Another significant observation was that the effective resolution degraded by only ∼30% between 0° and 30°. Since the effective resolution is proportional to $\cos\beta$, it is ∼1 μm better than the u-resolution at $\beta = 30°$.

It is important to estimate the precision with which the SiBT can measure the trajectory position as a function of the distance from the telescope, since it used as a reference detector for other devices in the beam line. The analysis yielded resolutions of 6.5±0.3 μm for six sensors out of eight. The transverse precision of the trajectory position was also estimated as a function of the distance from the Helsinki Silicon Beam Telescope at the CMS H2 test beam (Publication [**V**], p.543). For example, for beam momenta of 100 GeV, SiBT was able to provide a trajectory position with a 25-μm transverse precision at a distance of 1 m from the centre of the telescope.

The main results achieved in Publication [**V**] for the Helsinki SiBT operated at the CERN CMS H2 beam line, based on careful geometric calibration [75, 89, 109] include characterisation of the hit clusters and the detector resolution:

- The size of the cluster signal increased by some 10% with an increase in the detector tuning angle from 0°to 30°. The signal-to-noise ratio was close to 30, also showing a slight increase with increasing tilt angle. The mean width of the clusters increased from 3.5 to 5.4 within the same angular range.
- The resolution for 55-μm pitch detectors in SiBT was about 6.5 μm at a normal angle of incidence. It was found to improve down to 4.5 μm at 5°, above which the resolution deteriorated, so that at 30° it was ∼9.5 μm.

Chapter 6

H2 Test Beam Software for the SiBT

This chapter is dedicated to a discussion on Publication **[VI]**, which describes the architecture and configuration of the object-oriented online and offline software prepared for the Helsinki Silicon Beam Telescope. The aim of the project was to upgrade the old FORTRAN -based GEANT3 simulation of SiBT and offline analysis code to use Geant4 simulation and the C++ language. In the following sections a SiBT software module for simulation is discussed, together with modules for online and offline analysis. Examples are given to illustrate the adopted structural features of the program to monitor the quality of the measured SiBT data in the CMS H2 test beam.

6.1 Geant4 simulation of the SiBT

A motivation to prepare a new simulation tool using Geant4 was to understand the tracking of particles through the experimental setup, to simulate the detector response, and to improve the graphical representation of the SiBT with the particle trajectories [122]. The main functionality implemented in the simulation included:

- Definition of the geometrical layout of the SiBT telescope and the materials used in the simulation. The detector geometry was implemented as a singleton design pattern, i.e. as a class that has one globally accessible instance.
- The visualisation of the detector setup.
- Simulation of the random distribution for the incoming H2 test beam.
- Computation of the SiBT hit position in the silicon wafers for the particles used in the tracking. Monte Carlo generation of some ghost hits in order to simulate noise in the DAQ system.
- A simple Geant4-based digitisation was prepared to model the energy deposit into strips by the beam particles. Generation of the associated clusters was also included in the simulation.
- An interface was prepared to connect the Geant4 simulation module to offline monitoring tools, and provide output of the simulation results.

In order to model the CMS H2 test beam, the particles that hit the beam telescope were generated from Gaussian distribution. The divergences of the incoming pion and muon beams were set in such a way as to have a similar position and angle distributions as the H2 beam. A visualisation of a muon passing through the SiBT using the Geant4 simulation setup is given in Fig. 6.1.

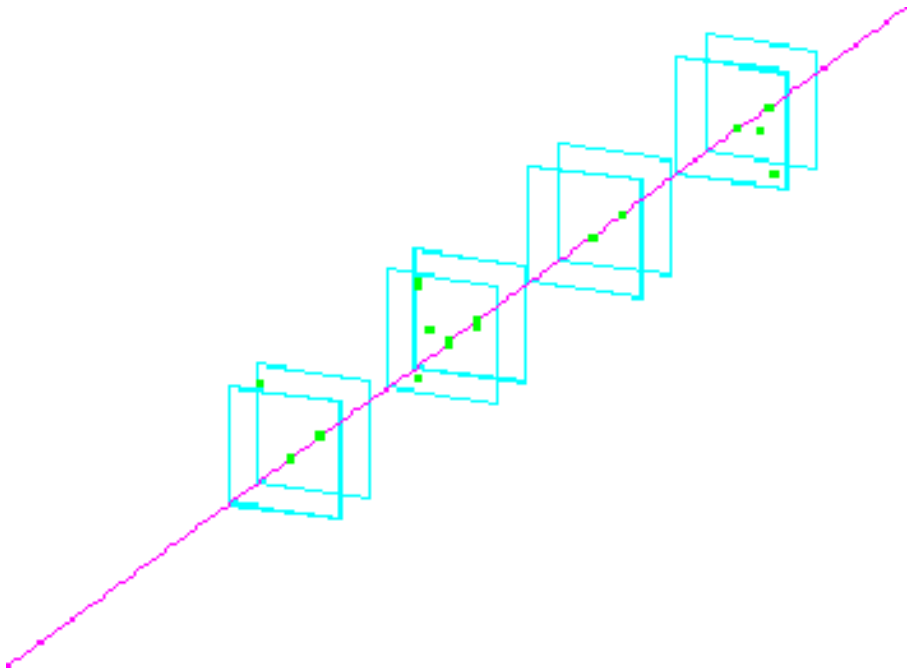

Figure 6.1: Geant4 simulation of a muon passing through the SiBT with eight silicon planes and generating signal hits. Some randomly generated ghost hits are also visible [122].

6.2 Online software for the SiBT

Data acquisition

The DAQ software in the SiBT H2 beam test reads, processes, and stores the acquired data once the spill is over. In order to achieve consistency with other CMS software systems, the DAQ software was realised in a Linux -platform using CMS C++ coding guidelines of object-oriented methodology and modular design.

During our measurements, presented in Publication [**VI**], the intensity of the primary proton beam was typically $4 \cdot 10^{11}$ protons per spill. In our experiment the energy of the chosen muon beam was 225 GeV and the beam intensity varied between 200 and 2000 muons per spill. The DAQ software provided key statistics on the current SiBT status in the muon beam, including the detector efficiencies, the size of the data, and the number of events read.

Online monitoring

To overcome the information gap between the detector hardware and the offline analysis, a new online monitoring program was developed for SiBT to provide fast feedback of the data, to tune the detector hardware, and to monitor the quality of the data captured (Fig. 6.2). This monitoring software provided detailed information on the cluster data. Since detailed track fitting was not included in the online monitoring, it was fast enough to provide information on the detector status in real time.

In monitoring applications the graphical user interface (GUI) plays an important role. For SiBT we used Qt -programming and a light histogramming tool, Histo-Scope. The design of the SiBT software was accomplished with a CASE tool, Rational Rose, using the unified modeling

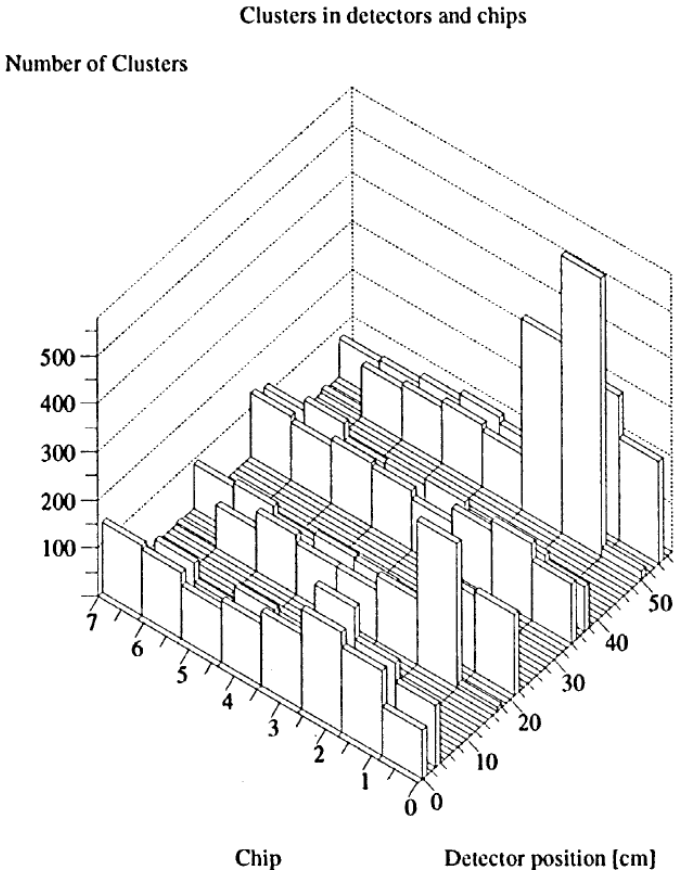

Figure 6.2: Example of SiBT online graphical user interface. The number of clusters per chip is shown for each of the eight detector planes, revealing a current CMS H2 muon beam profile. Online histograms based on the Histo-Scope package are interactive, allowing different viewing-angles and scaling [114].

language UML. Technical details of the GUI (Qt/X11) and the Histo-Scope histogramming tool are given in Publication [**VI**], p.5. Details on the other tools used for the development of the SiBT software are available in Ref. [66].

Several new histograms were prepared to improve the online monitoring quality. One significant feature in the new monitoring interface was a coarse track monitor. It visualised the particle hit positions on different detector layers, allowing rough estimates of the efficiencies of the layers, as well as of the beam profile and direction.

The online monitoring proved highly necessary during the test beam period, since it provided valuable information about the performance of the detectors and helped to pinpoint problems and to optimise the noise thresholds of the readout clusterisation algorithm during the hardware tuning phase. During the data capture phase the online monitoring was successfully used to control the quality of the data for possible hardware malfunctions.

The offline monitoring software, discussed in the following section, has many features in common with the online analysis code, which further facilitated its development.

6.3 Offline monitoring

Subsystems

The offline analysis for the SiBT was divided into two subsystems, one with the responsibility for the monitoring and the other focusing on the analysis. The monitor subsystem is responsible for managing the user interface. It provides a graphical user interface (GUI) and another interface to a non-interactive batch mode. The analysis subsystem provides a code for SiBT data analysis. This subsystem is further divided into six packages (Fig. 6.3):

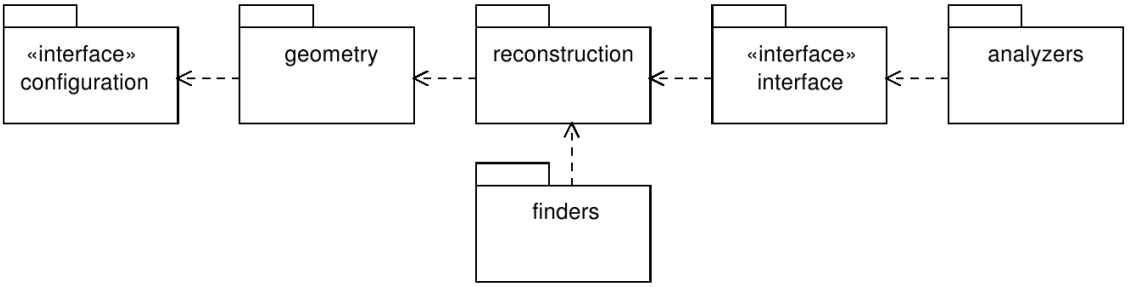

Figure 6.3: Package structure of the SiBT analysis software subsystems. Dependencies between the packages are indicated with arrows. The monitor subsystem uses interface packages [**VI**].

Configuration The configuration package provides a framework to manipulate the SiBT analysis configuration information.

Geometry This package provides C++ -classes that describe the geometry of the SiBT telescope. The package manages the geometries and provides the correct geometry to the analysis subsystem for each run.

Finders This package contains implementations of the cluster- and track -finding algorithms.

Reconstruction This package defines a framework to reconstruct clusters, tracks, and eventually full events from the raw SiBT data.

Analysers The analyser package has concrete analyser classes, which are used to process reconstructed SiBT events.

Interface The interface package mediates classes between the monitor and the analysis subsystem. The most important of these classes is the *SiBTAnalyserManager*, used to manage different analysers.

Configuration framework

The SiBT software was designed to be used by a configuration framework, which organises the configuration information into a tree structure. Each node in this tree is an object that can contain objects and detector parameters. Each node also provides a reference to a type object, providing meta-information about nodes. This information is used to indicate what parameters the specific node has and what objects can be inserted as children of that node.

The power of this configuration system lies in the fact that it provides a natural way to insert new objects into the configuration. This is done in such a way that the GUI and related routines are dynamically updated without any additional coding. The key classes needed to manage configuration information include:

SiBTVConfigurable This is an abstract base class for all configuration nodes. Accessing and describing the parameters is delegated to concrete subclasses ([**VI**], p.6). An example of a concrete subclass is the *SiBTTrackFinder*, which is used to find tracks.

SiBTVConfigurableType is also an abstract class, and it is used to provide meta-information about nodes.

SiBTConfigurableType This is a concrete subclass of *SiBTVConfigurableType*. Being a template class, it can automatically create new instances of its parameter class. (Details of the configuration framework are given in [**VI**], p.14.)

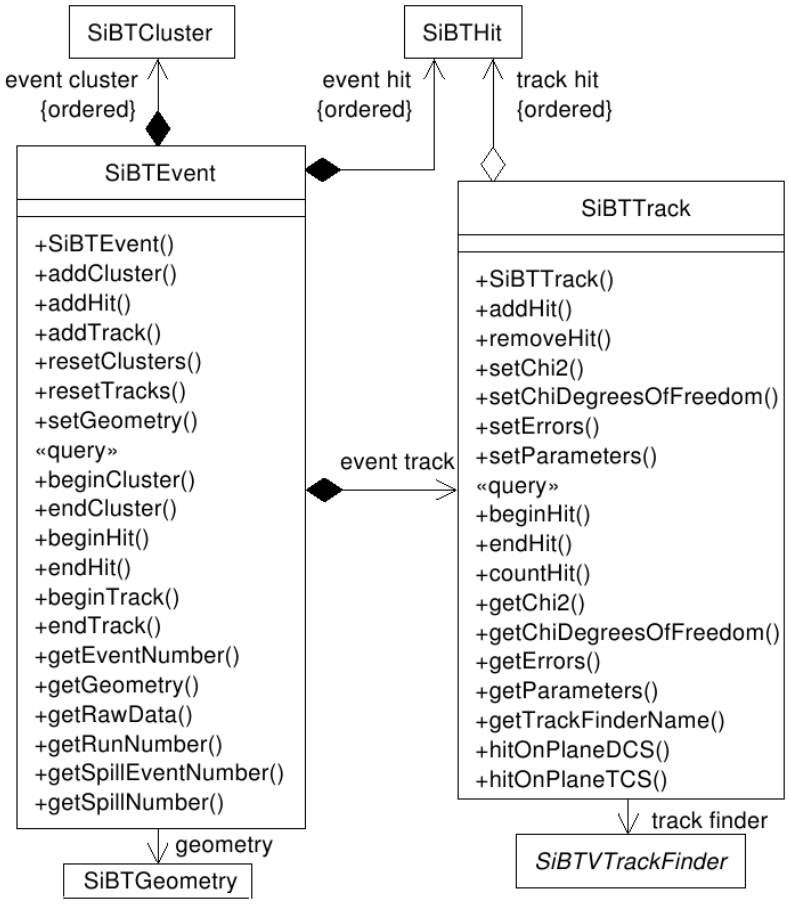

Figure 6.4: Offline monitoring software for SiBT: class diagrams for *SiBTEvent* and *SiBTTrack* are shown with their relations to *SiBTCluster* and *SiBTHit* [**VI**].

Track-finding framework

We developed an analysis model for SiBT H2 test beams, where the clusters, hits, tracks, and other objects needed by the track-finding process are parts of an event object (Fig. 6.4). The key classes are:

SiBTEvent This class is used to access all the information about a single event, such as the event number and raw data. It provides methods to access hits made from the raw data and tracks fitted to these hits.

SiBTTrack A single reconstructed track is described with *SiBTTrack*. Reconstruction data are saved into a parameter vector and an error matrix. The track class can determine the intersection points between the trajectory and the SiBT detector planes.

SiBTVTrackFinder This class is an abstract class, defining an interface for different track-finder implementations, such as the default *SiBTTrackFinder* or an alternative method using a parabola fit (Fig. 6.5).

SiBTTrackFinder This class defines a default implementation of the SiBT track-finding. The method is suitable only for a low-intensity H2 beam, since it uses brute force by going through all the hit combinations and fits a straight line to each combination. The method of least squares is used, and the tracks with the best χ^2 value are selected.

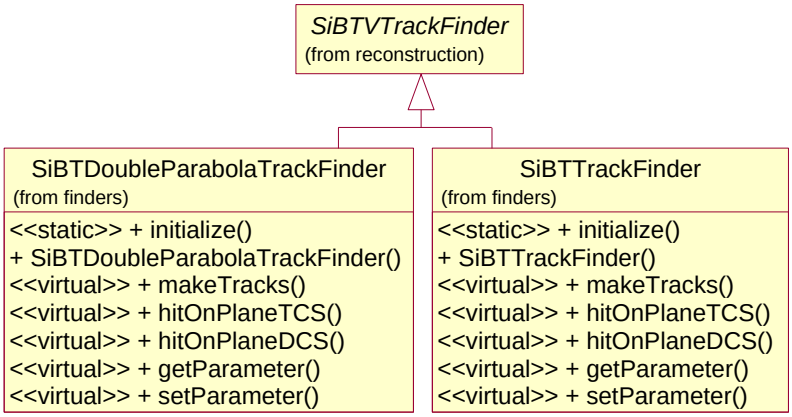

Figure 6.5: Two different track-finder methods prepared for the SiBT reconstruction software [123].

Monitoring cluster properties

Clusters of fired strips were identified by an online algorithm, performing an effective 3σ cut on individual strip signals. The strips above the cut were considered to make a cluster, together with the two adjacent strips on both sides [114].

The distribution of SiBT cluster sizes is plotted in Fig. 12 in Publication [**VI**], p.22. Clusters with 3 or 4 strips represent more than 90% of the data. A long tail represents clusters probably resulting from γ-rays. Broad clusters having more than 5 strips ($\sim$1% of the clusters) were ignored in the analysis.

The cluster position profile reflects the beam profile, as the H2 beam is highly collimated. The profile plots prepared with monitoring software clearly reveal the parts of the detector which were not fully working. Detector 6 had sections of dead strips or dead electronics, which are visible as gaps in the profiles (Fig. 6.6a). The strip coordinate η, which is calculated with the standard algorithm (5.1), is shown in Fig. 6.6b also for SiBT Plane 7, which worked almost perfectly.

Track reconstruction

Despite the fact that some of the detectors and read-out chips had deficiencies, tracks could be reconstructed successfully for a sizable sample of events. Track reconstruction involved an automatic calibration procedure for geometrical alignment of the SiBT ([**VI**], p. 9).

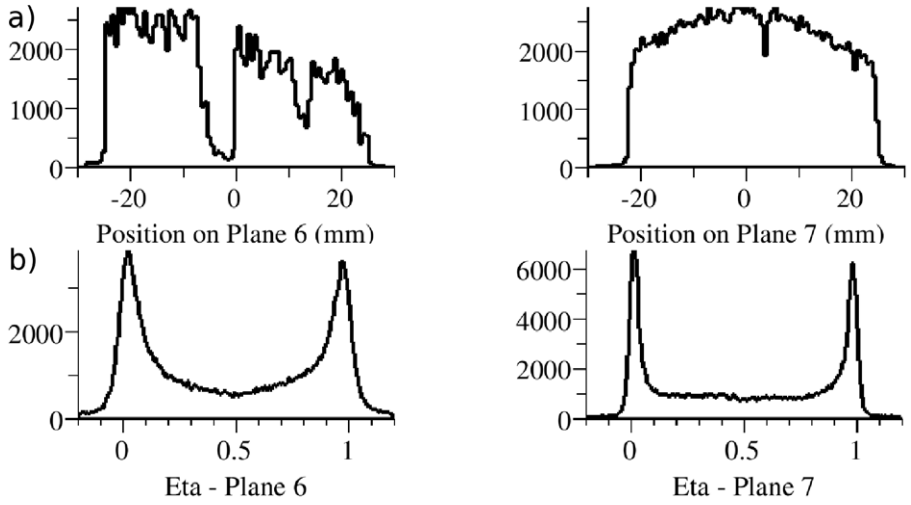

Figure 6.6: **a)** Hit profiles for SiBT Detector Planes 6 and 7 at CMS H2 test beam. Notice the sections of dead strips in Detector Plane 6. **b)** Corresponding η variables estimating a hit position between two strips [**VI**].

The detector resolution σ_{m} was determined from Eq. (5.5), and the pull distribution was calculated using Eq. (5.8). The distributions of pull values were found to follow the standard normal distribution, as expected, when the fit weights are properly set and the detector is aligned.

The fit quality is reflected in the χ^2 probability distribution. The probability distribution was reasonably flat, except for a small peak near zero resulting from hit offsets with non-Gaussian tails (Fig. 6.7a). The normalised χ^2 peaks near one, as it should (Fig. 6.7b).

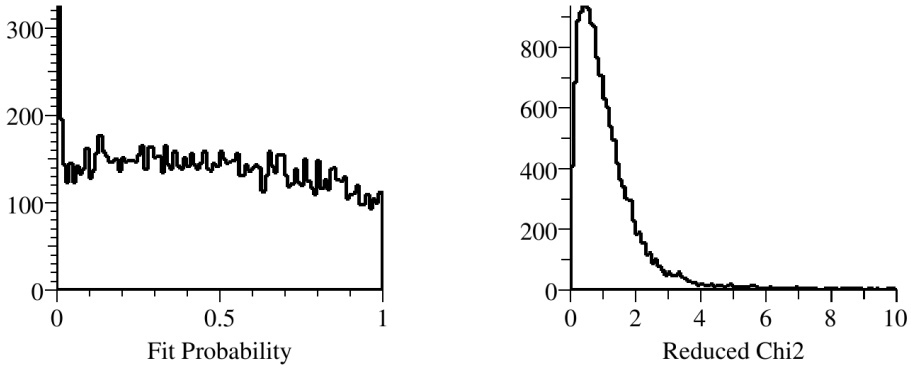

Figure 6.7: **a)** Track fit probability distribution. A peak near zero is due to hit offsets with non-Gaussian tails. **b)** Normalised $\chi^2 = \chi^2/\mathrm{NDF}$ [**VI**].

From the track fit analysis we deduced that the SiBT detector resolution was $\sim$10 μm for the installation of the apparatus ([**VI**], p. 10). Further, on the basis of reconstructed impact points in SiBT Detector Plane 0, we were able to estimate the location and profile of the CMS H2 muon beam (Fig. 6.8).

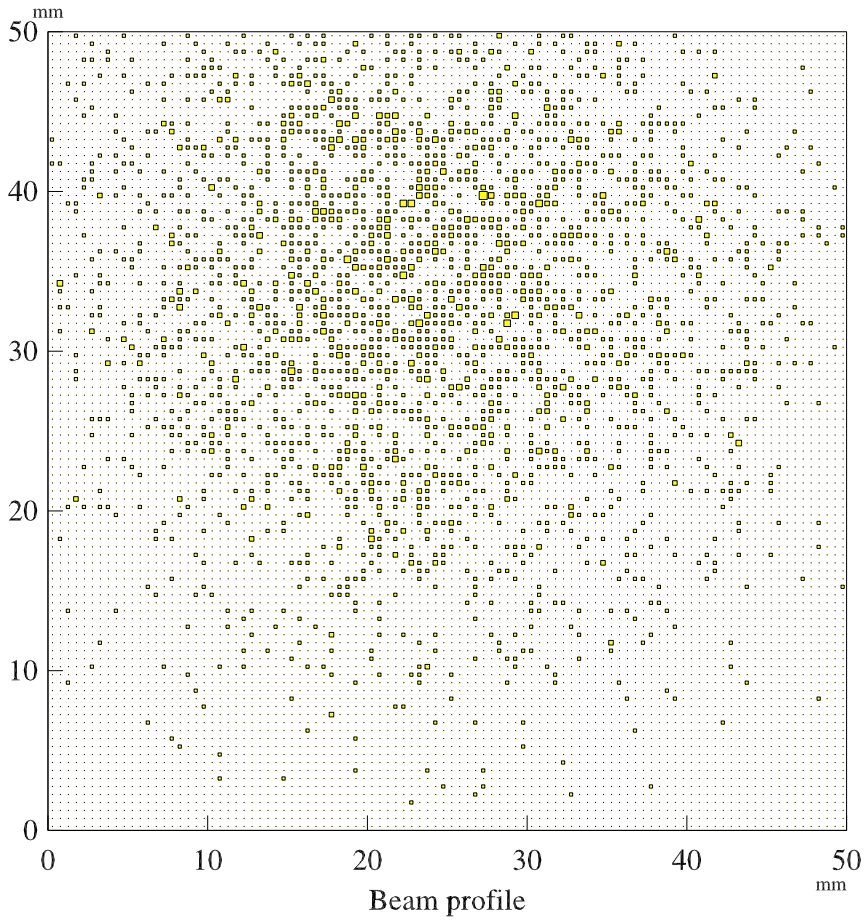

Figure 6.8: Reconstructed impact points for the first SiBT detector plane revealing the location and profile of the CMS H2 muon beam [122].

Chapter 7

Neural Networks for Higgs Signal b-tagging in the CMS Experiment

B-tagging is an important method to separate Higgs events with associated b-jets from the Drell–Yan background $\mathrm{Z}, \gamma^* \to \tau\tau$, for which the associated jets are mostly light quark and gluon jets. In Publication **[VII]** we studied the use of artificial neural networks (ANNs) in tagging b-jets using the process $\mathrm{pp} \to \mathrm{b\bar{b}H_{SUSY}} \to \tau\tau$ in the simulated CMS experiment [23, 91].

The b-tagging approach consisted of two different types of neural networks. First, multilayer perceptrons classifiers available in the data analysis framework ROOT [43, 44] were used. Various learning methods were evaluated, such as the steepest descent algorithm and variants of the conjugate gradients method, to find optimal classification results. Second, the applicability of the self-organising map (SOM) algorithm together with learning vector quantisation in the b-tagging problem was demonstrated.

7.1 Tagging of b-jets in $\mathrm{pp} \to \mathrm{b\bar{b}H_{SUSY}} \to \tau\tau$ channel

At the LHC the neutral MSSM Higgs boson production $\mathrm{pp} \to \mathrm{b\bar{b}H_{SUSY}}$ in association with b-quarks is the most important production mechanism for Higgs bosons at large $\tan\beta$ [30]. One of the most promising decay modes for discovering heavy neutral Higgs bosons is $\mathrm{H_{SUSY}} \to \tau\tau$. The tau decays either leptonically, or into hadrons, forming a tau-jet. These events can be triggered using a lepton trigger or a tau-jet trigger.

B-jets associated with the Higgs boson provide an additional tool to separate the Higgs events from the Drell–Yan background, in which Z,γ^* decay into a tau pair has a large cross-section compared to the Higgs production. This background can be suppressed by requiring reconstructed jets to be present at the event, and further by requiring associated jets to be identified as b-jets. Knowing whether a jet of hadrons originates from a quark or a gluon can also shed light on the hadronisation mechanism. The b-flavour identification of a jet is called b-tagging. The b-tagging performance of various channels has been studied extensively in the CMS [102, 110].

The Drell–Yan background events are mostly produced with no associated jets, or, if jets are present, they are due to light quarks and gluons. B-tagging effectively suppresses the Drell–Yan background, for which the associated jets are mostly light quark and gluon jets. The effectiveness of the algorithm is based on the relatively long lifetime of the b hadrons. The situation is demonstrated for the CMS detector in Fig. 7.1.

B-jets associated with Higgs bosons are generally very soft, which makes their tagging a demanding task. In a low E_T jet the track multiplicity and momenta are low, and many jets do not

have enough tracks within a fixed cone around the jet axis to be reconstructed using a combinatorial trajectory builder [115] and to be identified as a b-jet. As a consequence, the b-tagging efficiency (the fraction of jets tagged as b in $b\bar{b}$ samples) is not very high, if the mistagging rate (the fraction of non b-jets tagged as b in background samples) is to be kept below a typical 1% level.

The impact parameter ip is defined as the minimum distance between the track trajectory and the primary interaction point. The impact parameter significance σ_{ip} is the ip value divided by the estimated error. Figure 7.2a shows leading track σ_{ip} for b-jets and background events used in our application [**VII**].

The simplest b-tagging algorithms count the number of tracks within a jet cone with a high enough impact parameter significance σ_{ip}. A jet is identified as a b-jet if a number of tracks with σ_{ip} exceeding a chosen threshold is found. In Ref. [91] using track counting algorithms, the b-tagging efficiency for the associated jets was found to be 35% with a mistagging probability of $\sim$1%.

In addition to impact parameter, reconstructed secondary vertices can be used to tag the b-jets. Thus, best results are achieved using sophisticated probabilistic algorithms combining track counting and secondary vertex information [102].

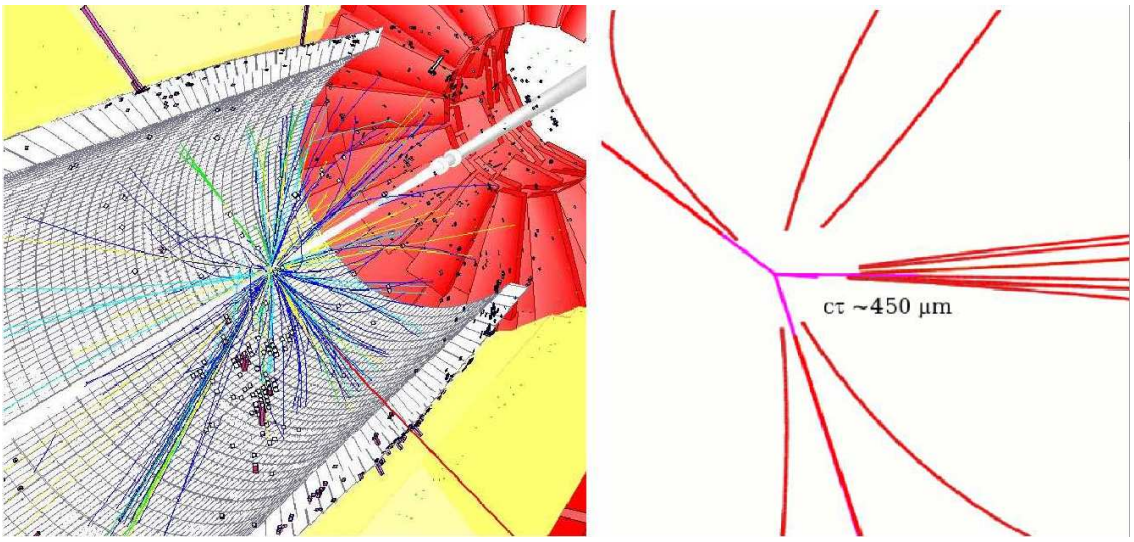

Figure 7.1: **a)** Geant4-based simulation of a Higgs event in the CMS [118] detector. **b)** A primary vertex region for an LHC Monte Carlo event containing a b-jet. B-tagging exploits the relatively long lifetime of the b hadrons [**VIII**].

7.2 Multi-layer perceptrons for a signal vs. background classification

Pattern recognition with multi-layer perceptrons

In Publication [**VII**] we report on neural network-based b-tagging in the CMS experiment. For this application we chose to use the feed-forward neural network (FFNN) algorithm for multi-layer perceptrons (MLPs) with error back-propagation.

This algorithm is summarised for a basic one hidden layer network as follows:

1. Neuron weights ω_{ji} and ω_{kj} are initialised with random values. Here i is data vector index corresponding the number of network neuron or node in the input layer, j is a index of hidden layer node, and kth node in the output layer.

2. We write lth event as $\mathbf{x}_l$. On the basis of the data sample layers' responses are calculated

$$y_j = \sum_i \omega_{ji} x_i, \text{ and } z_k = \sum_j \omega_{kj} h_j. \tag{7.1}$$

The outputs for the hidden nodes are mapped as $h_j = g(y_j/T)$. Correspondingly for the output node vector $\mathbf{o}$ the mapping is $o_k = g(z_k/T)$, where T is a parameter for temperature, or inverse gain, used in the sigmoid-shaped transfer function

$$g(y) = \tanh(y/T) \qquad \text{or} \qquad g(y) = \frac{1}{2}[1 + \tanh(y/T)]. \tag{7.2}$$

A low temperature corresponds to a steep sigmoid, $T \to 0$ corresponds binary neurons, and a high temperature corresponds to an approximately constant value of Eq. /7.2).

3. Teaching cycle error E is calculated. For example, the summed square error

$$E = \frac{1}{2} \sum_l \sum_k (o_k - o'_k)^2, \tag{7.3}$$

where o'_k denotes known target patterns, or correct classifications, for events used in the cycle.

In gradient descent back-propagation method E is minimize by changing weights

$$w_{ji}(t+1) = w_{ji}(t) + \Delta\omega_{ji}. \tag{7.4}$$

Updating reads

$$\Delta\omega_{ji} = -\eta \frac{\partial E}{\partial \omega_{ji}} = -\eta \sum_k \omega_{kj} \delta_k g'(y_j) x_i. \tag{7.5}$$

where $\eta < 1$ is a learning rate parameter, and

$$\delta_k = (o_k - o'_k) g'(\sum_j \omega_{kj} x_j). \tag{7.6}$$

Further

$$w_{kj}(t+1) = \omega_{kj}(t) - \eta \delta_k h_j. \tag{7.7}$$

During the training the network passes through the energy landscape, and the learning parameters should be allowed to change dynamically.

4. Teaching is cycles are repeated from Step 2 until weights ω connecting the neurons have converged.

Simulation of the CMS events

The b-tagging efficiency and mistagging rate in CMS were studied using simulated data with low luminosity conditions. The events were simulated using PYTHIA 6.215 [55] with CTEQ5 structure functions [25]. The CMS detector response was simulated using full Geant4 simulation within the ORCA framework [117].

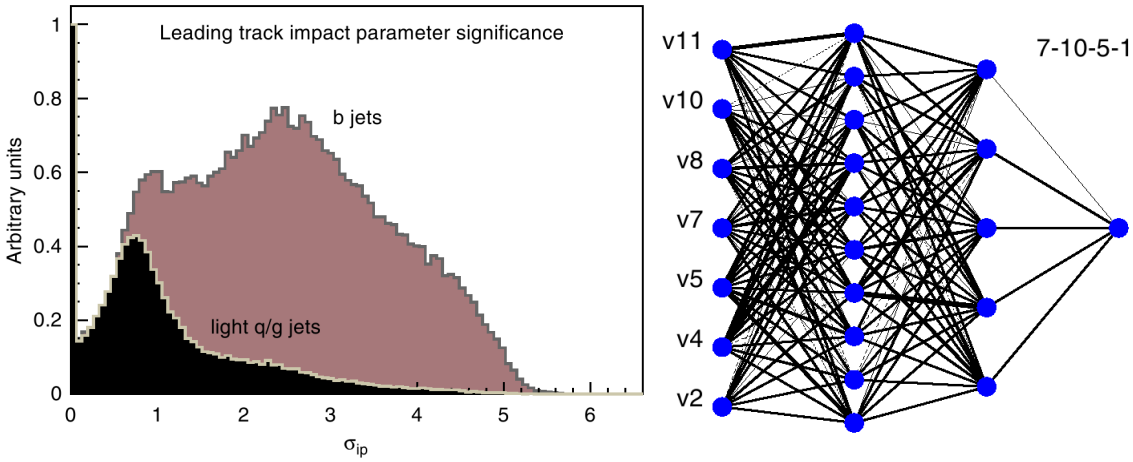

Figure 7.2: **a)** σ_{ip} of leading track for b-jets and background events. **b)** MLP 7-10-1 configuration. The seven input variables are mapped through a hidden layer of 10 neurons. Line thickness indicates the strength of the connection between corresponding neurons [**VII**].

The simulated events consisted of $\mathrm{pp} \rightarrow \mathrm{b\bar{b}H_{SUSY}}, \mathrm{H_{SUSY}} \rightarrow \tau\tau \rightarrow \mathrm{ll} + \mathrm{X}$ events, $\mathrm{t\bar{t}} \rightarrow \mathrm{ll} + \mathrm{X}$ events and Z,$\gamma^* \rightarrow \mu\mu$ events. The simulated samples consisted of ∼8k b-jets associated with the Higgs boson, 135k b-jets from the $\mathrm{t\bar{t}}$ events, and 89k light quark and gluon jets from the Drell–Yan events.

The events were required to pass the lepton trigger and to have a successfully reconstructed primary vertex. The jet reconstruction was done using an iterative cone algorithm, and the tracks within a $\Delta R < 0.7$ cone around the jet axis were reconstructed using a combinatorial trajectory builder [115]. The quantity ΔR is defined as

$$\Delta R = \sqrt{\Delta\varphi^2 + \Delta\eta^2}, \tag{7.8}$$

where $\Delta\varphi$ is an azimuthal angle and $\Delta\eta$ a pseudorapidity relative to the jet axis. The details of the CMS track selection algorithm are given in [102].

Application of the MLP for the b-tagging problem

In the ANN approach to the b-tagging problem we feed the networks the same events as used in the traditional track counting algorithm. This made possible an unbiased performance comparison between the two approaches. The $\mathrm{t\bar{t}}$ events with harder and more central b-jets were used as the signal and the light quark and gluon jets associated with Drell–Yan as the background. The choice of using $\mathrm{t\bar{t}}$ events is justified in this application, since topologically they are close to the actual signal pp $\rightarrow b\bar{b}H_{SUSY}, H_{SUSY} \rightarrow \tau\tau$. Seven variables (Fig. 7.3) were chosen and fed to the neural networks:

- number of tracks with transverse momenta $p_T >$ 0.5 GeV in the jet cone $\Delta R = 0.7$, and
- impact parameter ip together with ip significance σ_{ip} for the three leading tracks with the highest p_T, with the best σ_{ip}.

ROOT provides a flexible object-oriented implementation of multi-layer perceptrons (MLPs). Various learning methods, such as the Steepest Descent algorithm, Broyden–Fletcher–Goldfarb–Shanno algorithm (BFGS) [60], and variants of conjugate gradients are provided with a visualisation of the network architecture and learning process. An example of a visualised network

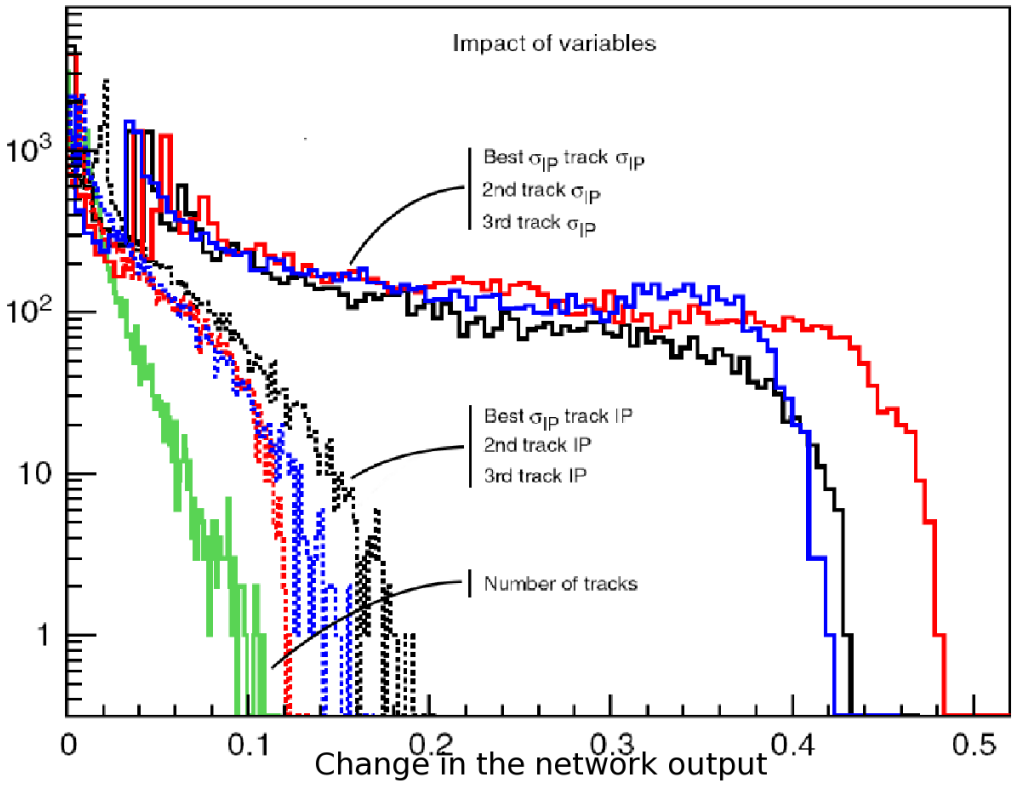

Figure 7.3: The track impact parameter significances σ_{ip} were found to have the best classification power. Visualisation by the ROOT MLP tool [**VIII**]. The method *DrawDInputs* of the *TMLPAnalyzer* class is used to show the impact a small variation to test sample variable has on the network output.

architecture is shown in Fig. 7.2b. A nice feature of this implementation is that a stand-alone C++ -code of the network can be exported.

From different ROOT MLP learning algorithms BFGS [60] was found to have the best performance. The simplest learning method, stochastic minimisation, also performed relatively well for this set of variables. This learning algorithm uses Robbins–Monro stochastic approximation [99] applied to MLPs.

The entire set of statistics of the background jets was used, with an equal number of signal jets. Half of the statistics were used for training, and the other half for validation. The generator-level Monte Carlo -truth was used to identify the true b, c, and light quark and gluon jets.

The trained network and the weights of the nodes were saved into a stand-alone b-tagging algorithm, which was used to b-tag the b-jets associated with the Higgs boson. This served as an independent and additional validation method for estimating the actual b-tagging performance of the neural network algorithm.

Performance of the MLP network

We performed a cut to the network response by assigning any event with an output bigger than a selected cut to be the signal. Events with

output smaller than this cut were considered to be background. Typical quantities that mea-

sure the effectiveness of this cut (Refs. [42, 45]) include signal efficiency, signal mistagging, background efficiency, and background mistagging.

The best algorithm is the one which provides the highest signal tagging efficiency at a chosen mistagging rate. A typical value required in b-tagging for the mistagging rate is 1%. For the analysis the cut in the NN output variable was selected, so that a signal mistagging probability 1% was achieved, and comparison with the traditional track-counting method was straightforward.

The corresponding b-tagging efficiency is shown in Fig. 7.4. The performance of the NN algorithms was observed to be relatively constant signal efficiency $\sim 40\%$ as a function of network size. The best configuration, 7-10-5-1, has 42% efficiency at a 1% mistagging probability. The impact parameter significances σ_{ip} were the input variables with the best classification power, as shown in Fig. 7.3.

Results from Publication **[VII]** indicate that the ANN classification can be used successfully in the b-tagging problem in the CMS experiment, and the MPL classification power is competitive with the traditional track-counting method.

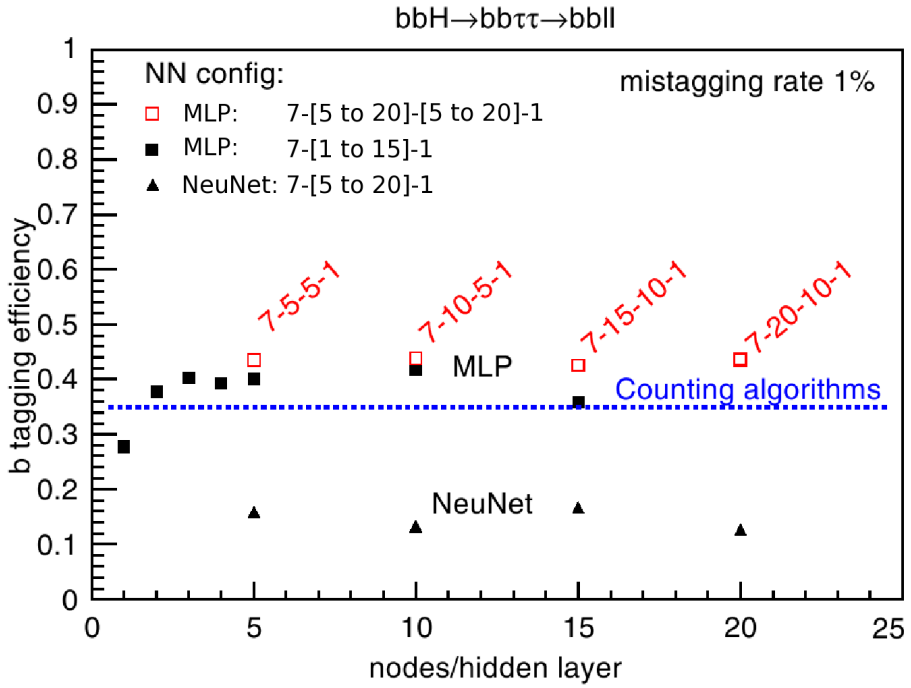

Figure 7.4: Tagging efficiency as a function of nodes in a one-hidden-layer architecture. The teaching and validation were performed using associated jets in $\mathrm{t\bar{t}}$ (signal) and Drell–Yan (background) events. The performance of MLP is compared to the typical tagging efficiency achieved (line) in the CMS with the standard counting algorithm. The weaker performance of the optional ROOT MLP tool NeuNet is also shown **[VII]**.

7.3 Separation of Higgs signal from the QCD -background with self-organising maps

Background rejection with SOM

The MLP is an appealing tool with an impressive track record, and yet it suffers from severe limitations since the learning has to be done in a supervised manner and the features have to be known beforehand. It is also difficult to analyse the internal representation built up by the hidden nodes. A self-organising map (SOM) operates in a different way, which complements the MLP approach.

The SOM is the most popular unsupervised NN algorithm because:

- SOM naturally performs exploratory data analysis, corresponding to a search for new physics;
- autonomous organisation of the events in clusters makes possible the emulation of clustering algorithms. For example, it was demonstrated in Ref. [42] that SOM shows significant similarities to the jet $k_\perp$ clustering algorithm.
- SOM analysis can be used as a novel technique to find new cut variables to be used in a standard analysis [36], and
- it offers the possibility of a parallel algorithm on a cluster platform [34].

The goal of the SOM is to transform an incoming pattern vector of arbitrary dimensions into a two-dimensional discrete map. This is done using units called nodes or neurons, which can be viewed as points in the i-dimensional input space representing a cell, also called the Voronoj cell, around it. The input data are quantised, the number of nodes n determining the accuracy of binning.

Mathematically, the SOM can be regarded as the non-liner mapping of the i-dimensional input vector. Since this mapping is known to be topology-preserving, even complex data clusters can be mapped. For an event vector the Euclidean distances d_n to all nodes are calculated, and the minimum distance d_m is used for classification.

Competition and co-operation between the neurons in the network, together with synaptic adaptation, results in the formation of a topographic map of the input patterns. The topographic map is autonomously organised by a cyclic process of comparing the input patterns to the vectors stored at each node. Being inherently nonlinear, this mapping may be viewed as a nonlinear generalisation of a principal component analysis [71].

The SOM algorithm can be summarised as follows:

1. Initial random weight vectors $\mathbf{w}_j(0)$ are chosen, where $j = 1...l$ and l is the number of neurons in the lattice.
2. The sample is drawn from the input vectors $\mathbf{x}$.
3. The best-matching winning node m at time step t is found by using the minimum-distance Euclidean criterion
$$m(\mathbf{x}) = \arg\min_j \|\mathbf{x}(t) - \mathbf{w}_j\|. \tag{7.9}$$
4. The weight vectors of nodes are updated
$$\mathbf{w}_j(t+1) = \mathbf{w}_j(t) + \Delta\omega_j h_j(t), \tag{7.10}$$

where

$$\Delta\omega_j = \eta(t)\ (\mathbf{x}(t) - \mathbf{w}_j(t)). \tag{7.11}$$

In Eq. (7.11) η is a learning-rate parameter, typically decreasing in value as the training proceeds. h_j is the neighbourhood centered around the winning node. Thus the weight vector and its neighbourhood belonging to the winner unit are moved closer to data vector $\mathbf{x}$.

Typically, general rules for optimising the time dependence of free parameters do not exist [35], so various ways to tune parameters during learning exist.

5. Continue to Step 2 until the changes $\Delta\omega$ in Step 4 are below the pre-defined cut value.

One of the early SOM studies in heavy quark jet tagging introduced a plane of 7x7 feature nodes that was used to disentangle b-, c-, and light (usd) quarks [38]. Momentum information for the six leading particles was used as inputs.

Learning Vector Quantisation

Although SOM is an unsupervised learning algorithm, for practical classification one typically augments it with supervised learning for fine-tuning. Learning vector quantisation (LVQ), which amounts to learning correct answers and unlearning incorrect answers, is often used to calibrate the feature map.

Contrary to collective SOM with the neighbourhood function, LVQ introduces a competitive self-organisation, where only one unit is selected as the winner. The key virtue of this method is that the final network will be easy to analyse by inspecting the weight vectors, since they mimic the specific features that the units are most sensitive to.

Application of the SOM for b-tagging

The performance of self-organising maps in our b-tagging problem was studied using the public-domain program package SOM_PAK [87], which provides a compact implementation of the unsupervised learning of the SOM algorithm. We confined our unsupervised teaching to using the same seven variables that were used in MLP classification.

We estimated the performance of our unsupervised competitive neural architecture using a technique introduced in [90]. The statistical significance r_i comparing the node activation between background and signal events in this method is defined as ratio

$$r_i = \frac{|N_i^b - N_i^s|}{\sqrt{N_i^b + N_i^s}}, \tag{7.12}$$

where N_i^b is the number of winning background events for node i, and similarly N_i^s is the number of winning signal events. A node mask m was prepared for cut value c, such that

$$m_i = \begin{cases} 0 & r_i \leq c \\ 1 & r_i > c. \end{cases} \tag{7.13}$$

Using this method unseen events were classified with a b-tagging efficiency of 72% and with a 12% mistagging rate. SOM was able to filter away 44% of the background events, with a 0.2% probability of the signal being misclassified.

Figure 7.5 visualises a semantic map that is divided into two regions, representing the signal and the background. Figure 7.6 lists the number of signal events associated with the winning

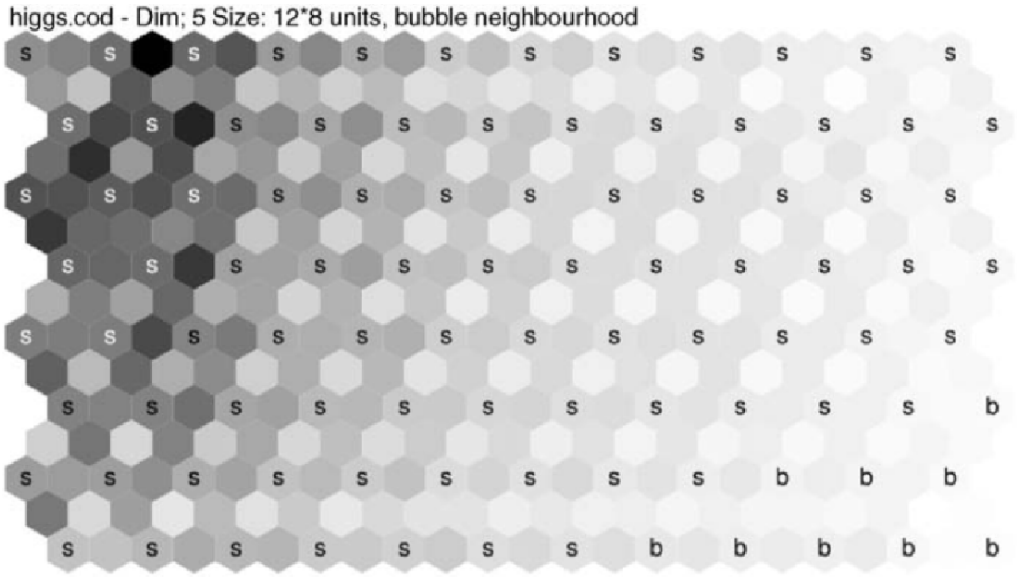

Figure 7.5: Visualisation of SOM map regions sensitive to signal (s) and background (b) events. A clear separation can be noticed between the signal and background regions [**VII**].

node, while testing the mapping of 15x15-node SOM performance. Similarly, background events are associated with a different area in the SOM [**VII**].

The technique based on learning vector quantisation (LVQ), which utilises the Monte Carlo truth of signal and background event information, can be used to further tune the SOM classifier decision regions. We found that subsequent tuning (SOM -calibration) of the SOM classifier with the LVQ_PAK -tool improved the b-tagging efficiency by $\sim$2%.

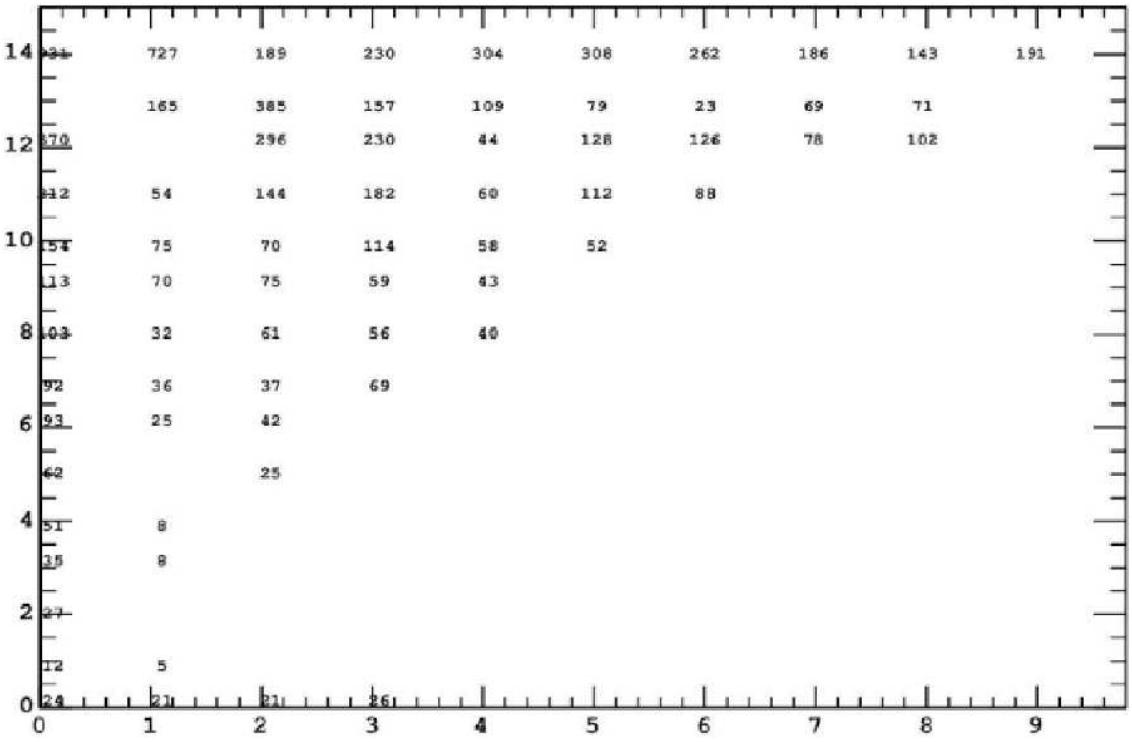

Figure 7.6: Number of signal events associated with the winning node, while testing the mapping of 15x15-node SOM performance. The 10x15 fraction on the map is shown where the activation to signal events was present. For example, we see that 727 events from the test sample activated the SOM node (1, 14) [76].

Chapter 8

Cluster Computing and the CMS Data Analysis

In Chapter 8 we present a study to further optimise the neural networks discussed in the previous chapter. Publication **[VIII]** reports how the performance of Higgs particle -associated neural network b-tagging was enhanced using a high-throughput Linux cluster at the Finnish CMS Tier-2 computing facility. The power of cluster computing and the ROOT data analysis toolkit was used to create a large number of neural classifiers with different configurations. Our approach was to prepare repeated computer experiments for network training. This method was used to verify that our neuro-classifiers have a stable physics performance for signal recognition and background rejection.

8.1 ROOT-based CMS data analysis in a cluster environment

The ROOT data analysis framework [43] was developed at CERN to respond to the new requirements emerging in the LHC era. It has replaced many old FORTRAN -based CERNLIB tools, such as fitting algorithms.

The benefits of this framework include optimised treatment of large and complex data-sets, benchmarking tools, and support for C++ scripting and compiled code. Perhaps the most significant practical consequence that comes with the use of ROOT is that physicists can now use the C++ -language coherently, from simulation to data management, data analysis, plotting, and scripting.

One of the advanced ROOT features is the Parallel ROOT Facility (PROOF), which supports the cluster and grid computing needed in challenging simulation and data analysis tasks at LHC. A key feature of the used data model is the concept of a tree. Thus, input and output data should be organised using the *TTree* -class, to benefit fully from the functionality provided by ROOT. The *TChain* -class, which is a collection of files containing *TTree* -objects, must be utilised to make possible parallel processing in a cluster or PROOF grid environment.

The most ambitious collection of multivariate analysis tools in HEP is the ROOT -based toolkit TMVA [79]. This software provides more than ten different MVA methods, and supports three different neural network implementations.

8.2 Computational environment for the Ametisti Linux cluster

Helsinki Institute of Physics will manage one of the CMS Tier-2 computing facilities needed in the CMS detector response simulation and analysis of LHC data. The Ametisti Linux cluster is part of this facility. It has 132 CPUs in 66 computational nodes of 64-bit 1.8/2.2 GHz AMD Opteron CPUs with 2/4 GB RAM (Fig. 8.1).

The Ametisti cluster is based on the National Partnership for Advanced Computational Infrastructure (NPACI) Rocks Cluster Distribution. NPACI Rocks provides a cluster management software for scientific computation based on Red Hat Linux, supporting cluster installation, configuration, monitoring, and maintenance. Rocks comes preconfigured with the Sun Grid Engine batch queue system, which supports advanced features such as back filling, fair share usage, array jobs, and even interactive usage. The Ametisti cluster is a powerful tool for LHC-era computing with the software tools developed at CERN.

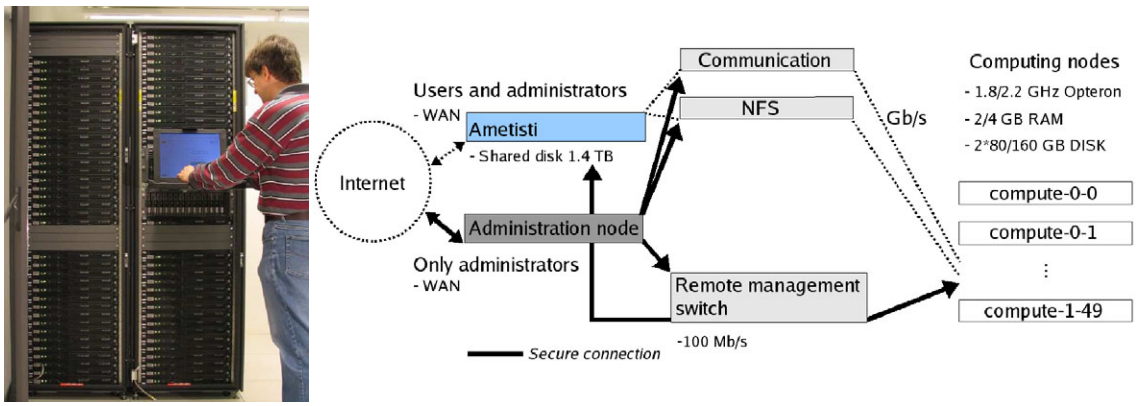

Figure 8.1: **a)** The 132-CPU Opteron Ametisti cluster at the University of Helsinki, which was used to optimise the neural networks of Higgs classifiers **[VIII]**, and to estimate the cross-sections of rare isotopes produced by Geant4 Bertini models [77]. Ametisti is part of the Finnish M-grid, which currently has more than 1000 AMD CPUs connected with the Advanced Resource Connector middleware. **b)** A schematic picture of the Ametisti cluster computing environment, containing 66+2 node dual AMD Opteron Rocks 1U rack **[VIII]**.

8.3 Optimising Higgs neural network event -classifiers

In Chapter 4 we have already discussed a validation effort for Geant4 intra-nuclear cascade simulation, where millions of events were generated in a cluster environment to create sufficient statistics for rarely-produced isotopes.

We now discuss another case where a cluster environment was found to provide the needed computing power. In Publication **[VII]**, discussed in Chapter 7, we showed that a neural network based on Higgs -related b-tagging provides a promising alternative to standard tagging methods. Finding an optimal network configuration is a multidimensional, computationally demanding optimisation task, so a cluster-based investigation was performed to further optimise the classification power of the neural network.

To perform the optimisation, we made extensive use of the *TMLPAnalyzer* utility class provided by the ROOT MLP package. This class contains a set of useful tests to develop optimal neural network layouts. Furthermore, it allows the user to identify weak, possibly unneeded, variables and to control the network structure. For example, the *DrawDInputs* -method was used to study what kind of impact a small variation in input variables has on the network output [125].

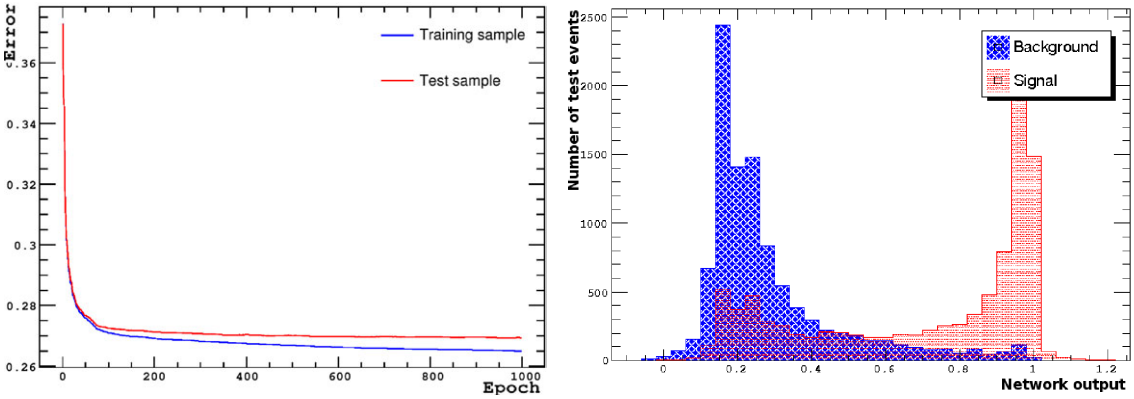

Figure 8.2: **a)** Error observed in network output node for training and test data samples as a function of training epochs. **b)** Classification ability introduced by MLP [**VIII**]. In training the network output was set to represent the background/signal option (background=0 and signal=1). A non-normalized output is shown for the test data.

This kind of sensitivity analysis is useful when selecting an optimal collection of neural network input parameters [**VIII**].

The Ametisti cluster was used to train a large number of neural network architectures, while examining the parameter space (input variables, network size, learning parameters) iteratively and running $\sim$1000 jobs using $\sim$500 CPU hours.

Typically, the training lasted 1000-5000 epochs. An example of the behaviour of training and validation error as a function of training epochs is shown in Fig. 8.2. A clear learning process is observed until epoch $\sim$200, and after this point the test data sample shows no significant improvement. We conclude that, for optimal learning that avoids over-fitting, we should halt teaching at this point.

Compared to the previous study discussed in Chapter 7, larger Geant4 -generated CMS Monte Carlo data sets were used. This made it possible to improve the testing statistics when we optimised the configurations. Naturally, we used independent previously-unseen event samples in the testing phase to measure the generalisation.

Our optimisation procedure included restricting the number of neural network weights for improved generalisation performance, to keep the number of needed training patterns relatively small, and to keep the convergence time short. Networks were trained with the BFGS training algorithm, which was known to perform well (see Sec. 7.2).

The sensitivity analysis of promising neural classifiers was performed by running analysis repeatedly with fresh random number seeds and by changing the input parameters minimally.

Optimisation results

In Publication [**VII**] we reported 42% efficiency at a 1% mistagging probability in the tagging of b-jets in $\mathrm{pp} \rightarrow \mathrm{b\bar{b}H_{SUSY}} \rightarrow \tau\tau$ channel. This result was achieved with an MLP configuration 7-10-5-1.

In Publication [**VIII**] using newly generated Monte Carlo data sets and careful teaching with better statistics, we were able to find a more optimal setup, 7-12-5-1, with a slightly improved performance of 44$\pm$1%. More importantly, we found that a simple three-layered MLP configuration with only one hidden layer (7-15-1) performed quite well with a b-tagging efficiency of 39$\pm$1%. We also found a new promising network configuration, 10-15-5-1, where three additional variables describing the particle momentum were introduced.

```
#ifndef tagger64111_h
#define tagger64111_h

class tagger64111 {
public:
   tagger64111() {}
   ~tagger64111() {}
   double value(int index,double in0,double in1,double in2,double in3,dou\
ble in4,double in5,double in6);
private:
   double input0;
   double input1;
   double input2;
--0-:---F1  tagger64111.h      (C Abbrev)--L1--Top-----------------------
#include "tagger64111.h"
#include <cmath>

double tagger64111::value(int index,double in0,double in1,double in2,doub\
le in3,double in4,double in5,double in6) {
   input0 = (in0 - 0)/1;
   input1 = (in1 - 0)/1;
   input2 = (in2 - 0)/1;
   input3 = (in3 - 0)/1;
   input4 = (in4 - 0)/1;
   input5 = (in5 - 0)/1;
   input6 = (in6 - 0)/1;
   switch(index) {
     case 0:
         return ((neuron0x30e2a80()*1)+0);
     default:
         return 0.;
--0-:**-F1  tagger64111.cxx      (C++ Abbrev)--L1--Top--------------------
```

Figure 8.3: Output for Ametisti cluster job number 64111. Software based on the ROOT MLP neural network was used to generate a stand-alone C++ code, which implements an event classifier. This classifier is fast and optimised to Higgs boson-related b-tagging [**VIII**].

The code generation feature of stand-alone C++ classifiers was utilised. Figure 8.3 gives an example of the ROOT -generated code defining an Higgs event classifier.

These results indicate that semi-automatic optimisation for neural networks using the ROOT MLP implementation in a cluster environment is feasible and that the usage of a cluster environment has enabled us to tune neural classifiers with high accuracy. Yet, further studies are needed to reach a full conclusion of optimal b-tagging efficiency.

Chapter 9

Conclusions

This thesis work has focused on two different computational aspects of particle physics in the LHC era.

First, we have developed hadronic physics models for the Geant4 simulation package. The purpose of this work was to improve the accuracy of Geant4 hadronic physics for applications such as Compact Muon Solenoid hadronic calorimeter HCAL showers. A comparison of Geant4 Monte Carlo simulation with experimental data, such as CMS H2 test beams, has given invaluable feedback, and has led us to further improvements in the Geant4 physics modelling.

Second, we have developed CMS H2 test beam analysis software and a Geant4 -based detector description of the Helsinki SiBT. We have also used a full Geant4 -based simulation of the CMS experiment and demonstrated that neural network -based b-tagging methods can be used to isolate the Higgs signal from the QCD background processes. We have shown that the ANN method is efficient for extracting features in hadronic data and that good performance can be obtained for quark/gluon separation.

Our approach in working with these aspects has been to use systematically object-oriented software technology in response to the computing challenges of the LHC era.

Simulating hadronic physics with Geant4

An important part of this work was to make several intra-nuclear cascade models available in the Geant4 detector simulation framework for use in LHC detector simulations. These Bertini cascade models, now successfully implemented (see Table 2.1 for a summary of sub-models) and documented in Geant4 9.1 [121], include:

- intra-nuclear cascade (INC) of Bertini -type;
- pre-equilibrium treatment with excitons;
- Fermi breakup model;
- fission model,
- evaporation, and
- gamma de-excitation models.

The physics performance of Bertini models was evaluated, and the user community was provided with validated physics lists. In most cases Bertini models for INC, excitation, fission-evaporation were found to be more accurate than the standard GHEISHA model often used in experiments before the LHC era.

Our work has resulted in several model features that were not available in Geant4 before, or in its predecessor GEANT3, thus increasing significantly the ability of Geant4 to simulate LHC experiments accurately. Particularly useful features of Bertini models for the HEP community include:

- an accurate description of pion production (as shown in Fig. 4.4);
- the fact that very good agreement with data is shown for iron targets

  (The good performance as seen in Fig. 4.2 is due to the Bertini cross-section parametrisation using Pearlstein's systematics [96], which was motivated by astrophysical application, such as proton-iron reactions.);
- previously unavailable kaon channels (Fig. 3.1);
- relatively fast performance compared to other microscopic Geant4 models in background radiation studies, and
- good matching with experimental hadronic calorimeter shower shape measurements (Fig. 3.3). High accuracy opens up new possibilities of studying hadronic calorimeter response in detail.

In order to find optimal combinations of Geant4 models to describe experimental data accurately, the Geant4 collaboration has organised an extensive validation programme to study the performance of Geant4. This validation effort includes a study of hadronic shower shapes at the LHC [124], and CMS H2 test beam data have been compared with the predictions of various Geant4 physics lists.

Feedback from various HEP experiments, such as the CMS H2 test beam, has led to further improvements in the Geant4 models. We have shown that the Bertini models can, in many cases, successfully reproduce LHC test beam or thin-target data with an accuracy equal to or better than that given by the old GEANT3.

For example, when the GQSP_BERT physics list is compared with measurements made at the Los Alamos Meson Physics Facility for 113-800 MeV proton beams, and for 7.5–150° scattering angles, the simulation reproduces double-differential cross-section data at the level of 20-50% [6].

Recent LCG evaluation results [29] recommend that LHC experiments performing Geant4 shower shape simulation should use either the LHEP physics list, based on GHEISHA parametrisation, or, if more precise physics is needed for energy response and resolution, the latest QGSP_BERT physics list, where hadron projectiles below 9.9 GeV are treated with the Bertini cascade. Thus, perhaps the most important outcome of our Geant4 research has been the release of Geant4 tools which provide improved accuracy for LHC hadronic calorimeter response simulation.

Analysis of the CERN H2 test beam data and Geant4 simulated CMS data

The online monitoring tool developed for the Helsinki Silicon Beam Telescope in this work proved to be highly necessary during the CMS H2 test beam runs. It provided critical information about the performance of the detector, helping to locate hardware malfunctions (Fig. 6.6)

and to optimise noise thresholds [108]. Additionally, we conducted Geant4 simulations of SiBT to gain insight into the test beam conditions.

We also developed an offline analysis model for SiBT H2 test beams, where clusters, hits, tracks, and other objects needed by the track-finding process are parts of an event object (Fig. 6.4). The software was designed to be used by a configuration framework, which organises the configuration information into a tree structure of nodes. The power of the object-orientation was used in the design of the configuration system to facilitate a natural way to change new objects, such as new detector planes or analysis tools, into the configuration tree. The user can operate the offline analysis tool and configuration in such a way that the GUI and related routines are dynamically updated without any additional coding.

The main results achieved for the Helsinki SiBT operated at the CERN CMS H2 beam line included a characterisation of the hit clusters and an estimation detector resolution. The resolution for 55-μm pitch detectors in SiBT was $\sim$6.5 μm at a normal angle of incidence. The resolution improved down to 4.5 μm at 5°, above which the resolution started to deteriorate (Fig. 5.4).

Furthermore, we applied multi-layer perceptron (MLP) neural network methods to b-jets tagging in pp $\rightarrow b\bar{b}H_{SUSY}, H_{SUSY} \rightarrow \tau\tau$ in the CMS experiment using Monte Carlo data. The most promising finding is that the classification power was found to be competitive with the traditional track counting method, which has given a $\sim$35% b-tagging efficiency with a 1% mistagging rate. In many network configurations studied, the MLP algorithms were found to perform equally well in comparison with the track-counting method (Fig. 7.4). The best MLP classifiers developed in this work were able to outperform standard counting algorithms with a 44% b-tagging efficiency.

A new analysis method, based on an unsupervised learning algorithm of self-organising map SOM [52], was developed for the Higgs search at the LHC [73]. We showed that this kind of unsupervised algorithm, which is rarely used in high-energy physics, can be used to separate Higgs events from the LHC Drell-Yan background in the CMS experiment (Fig. 7.5).

Using the same seven input variables as in the MLP case, a b-tagging efficiency of 72%, with a 12% mistagging rate, was obtained. Finally, a further $\sim$2% efficiency improvement was gained when the SOM classifier, using Monte Carlo data from a full Geant4 simulation, was chained together with a supervised neural network of the learning vector quantisation type [51].

Finally, we have reported on the usage of computer clusters for two particularly CPU - intensive tasks:

- validation of rare isotope production from Geant4 Bertini models (Fig. 4.9), and
- optimisation of neural classifiers for the Higgs signal in CMS b-tagging (Fig. 8.3).

In both cases the Ametisti cluster, which is part of the Finnish Tier-2 computing resource for CMS data analysis, was used. Using ROOT on the Ametisti cluster has enabled us to study the physics performance of the optimised neural network classifiers. We also found a promising neural network configuration with previously unused variables and discovered optimised neural classifiers.

Bibliography

[1] *Computing as a Language of Physics*. Lectures presented at an International Seminar Course, Trieste 2–20 August 1971, IAEA, Vienna, 1972.

[2] P. Kaitaniemi A. Heikkinen and A. Boudard. Implementation of INCL4 cascade and ABLA evaporation codes in Geant4. International Conference on Computing in High Energy and Nuclear Physics (CHEP07), Journal of Physics: Conference Series 119 (2008) 032024, [doi:10.1088/1742-6596/119/3/032024].

[3] R. G. Alsmiller, F. S. Alsmiller, and O. W. Hermann. The high-energy transport code HETC88 and comparisons with experimental data. *Nucl. Instr. and Meth.*, A(295):337–343, 1990.

[4] D. Appleby and J. J. VendeKopple. *Programming Languages: Paradigm and Practice*. WCB / McGraw-Hill, 1997.

[5] R. Battiston. *Nucl. Phys. B (Proc. Suppl.)*, 44:274, 1995.

[6] J. Beringer. (p, xn) Production Cross Sections: A Benchmark Study for the Validation of Hadronic Physics Simulation at LHC. Technical report, CERN-LCGAPP-2003-18, 2003.

[7] J. Beringer. Physics validation of detector simulation tools for LHC. *Nucl. Instr. and Meth.*, A(534):156–161, 2004.

[8] H. W. Bertini. Low-energy intranuclear cascade calculation. *Phys. Rev.*, 131(4):1801–1821, 1963.

[9] H. W. Bertini. Intranuclear-Cascade Calculation of the Secondary Nucleon Spectra from Nucleon-Nucleus Interactions in the Energy Range 340 to 2900 MeV and Comparisons with Experiment. *Phys. Rev.*, 188:1711, 1969.

[10] H. W. Bertini and P. Guthrie. Results from Medium-Energy Intranuclear-Cascade Calculation. *Nucl. Phys.*, A(169), 1971.

[11] E. Boos and L. Dudko. Optimized Neural Networks to Search for Higgs Boson Production at the Tevatron. 2003. [arXiv: hep-ph/0302088].

[12] J. E. Brau. Simulation of hadronic showers and calorimeters. *Nucl. Instr. and Meth.*, A(312):483–514, 1992.

[13] The CMS Collaboration. CMS - The Tracker Project. Technical Report 98-06, CERN/LHCC, April 1998.

[14] G. Daquino. Background radiation studies using Geant4 in LHCb: first results. LCG Physics Validation for LHC Simulations, CERN, January 27th, 2005, 2006. (Unpublished).

[15] I. Dostrovsky, Z. Fraenkel, and P. Rabinowitz. Monte Carlo Calculations of Nuclear Evaporation Processes. V: Emission of Particles Heavier Than ^{4}He. *Physical Review*, 1960.

[16] A. De Angelis et al. Self-organizing networks for classification: developing applications to science analysis for astroparticle physics. *Physics*, A(338):50–53, 2004.

[17] A. Heikkinen et al. Computing revolution in High Energy Physics, Imposed by the Needs of the CMS Experiment at the CERN Large Hadron Collider. In Proceedings of the XXXII Annual Conference of the Finnish Physical Society, March 1998.

[18] A. S. Iljonov et al. *Intermediate-Energy Nuclear Physics*. CRC Press, 1994.

[19] Bayukov et al. *Phys. Atom. Nucl. V42, 116*.

[20] C. M. Kormanyos et al. *Phys. Rev.*, C(51):669, 1995.

[21] D. H. Wright et al. Using Geant4 in the BaBar simulation. Technical report, SLAC-PUB-9862, 2003.

[22] D. R. F. Cochran et al. *Phys. Rev.*, D:3085, 1972.

[23] F. Hakl et al. Application of neural networks to Higgs boson search. *Nucl. Instr. and Meth.*, A(502):489–491, 2003.

[24] G. Alverson et al. IGUANA: a high-performance 2D and 3D visualisation system. *Nucl. Instr. and Meth.*, A(534, Issues 1-2):143–146, 2004. [doi:10.1016/j.nima.2004.07.036].

[25] H. L. Lai et al. Eur. Phys. J. C12 (2000) 375, `hep-ph/9903282`.

[26] H. Vonach et al. *Phys. Rev. C*, (55):2458, 1997.

[27] I. Ribansky et al. Pre-equilibrium decay and the exciton model. *Nucl. Phys.*, A(205):545–560, 1973.

[28] J. Allison et al. The Geant4 Visualisation System. *Comp. Phys. Commun.*, 178(5):331–365, 2008. [doi:10.1016/j.cpc.2007.09.010].

[29] J. Apostolakis et al. Hadronic Shower Shape Studies in Geant4. *CERN-LCGAPP-2007-02*, 2007.

[30] J. Campbell et al. Higgs boson production in association with bottom quarks. [arXiv: hep-ph/0405302], May 2004.

[31] J. F. Crawford et al. Measurement of Cross Sections and Asymmetry Parameters for the Production of Charged Pions from Various Nuclei by 585-MeV Protons. *Phys. Rev. C*, (22):1184, 1980.

[32] J. R. Letaw et al. *The Astrophysical Journal Supplements*, 51:271, 1983.

[33] J. R. Letaw et al. *The Astrophysical Journal*, 414:601, 1993.

[34] J. S. Lange et al. *Nucl. Instr. and Meth.*, A(389):74, 1997.

[35] J. S. Lange et al. Transputer self-organizing map algorithm for beam background rejection at the BELLE silicon vertex detector. *Nucl. Instr. and Meth.*, A(420):288–309, 1999.

[36] K.-H. Becks et al. Separation of hadronics W-decays from QCD-background with self-organizing maps. *Nucl. Instr. and Meth.*, A(426):599–604, 1999.

[37] K. Hultqvist et al. Using a neural network in the search for the Higgs boson. *Nucl. Instr. and Meth.*, A(364):193–200, 1995.

[38] L. Lönnblad et al. Self-organizing Networks for Extracting Jet Features. Lund Preprint LU TP 91-4, 1991.

[39] M. M. Meier et al. Differential Neutron Production Cross Sections and Neutron Yields from Stopping-length Targets for 113-MeV Protons. *Nucl. Scien. Engin.*, (102):310, 1989.

[40] M. M. Meier et al. Differential Neutron Production Cross Sections and Neutron Yields from Stopping-length Targets for 256-MeV Protons. *Nucl. Sci. Eng.*, (110):289, 1992.

[41] P. Boinee et al. Automatic Classification using Self-Organising Neural Networks in Astrophysical Experiments. 2003. [arXiv: cs.NE/0307031].

[42] P. De Felice et al. Jet analysis by neural networks in high energy hadron-hadron collisions. *Physics Letters*, B(354):473–480, 1995.

[43] R. Brun et al. ROOT–An Object Oriented Data Analysis Framework. *Nucl. Instr. and Meth.*, A(389):81, 1997.

[44] R. Brun et al. ROOT Status and Future Developments. Technical report, CHEP'03 proceedings, 2003. [arXiv: cs.SE/0306078].

[45] R. D. Field et al. Using neural networks to enhance the Higgs boson signal at hadron colliders. *Physical Review D*, 53(5):2296–2308, 1996.

[46] S. Afanasiev et al. *Nucl. Instr. and Meth.*, A(430):210, 1999.

[47] S. Guatelli et al. Dosimetry for interplanetary manned missions. *IEEE Nuclear Science Symposium Conference Record*, Volume 4:2169–2173, 2004.

[48] S. I. Alekhin et al. Compilation of Cross-Sections IV: γ, ν, Λ, Σ, Ξ, and K^0_L Induced Reactions. *CERN-HERA*, 87-01, 1987.

[49] S. Kunori et al. G4 vs tb2006: linearity / resolution / eta-dependence. Talk given in April 2008 (Unpublished).

[50] S. Piperov et al. CMS hadron shower studies: linearity, shower shapes. Talk given November 21, 2007 (Unpublished).

[51] T. Kohonen et al. LVQ_PAK: the learning vector quantization program package. Technical report, A30, Laboratory of Computer and Information Science, Helsinki University of Technology, 1996.

[52] T. Kohonen et al. SOM_PAK: the self-organizing map program package. Technical report, A31, Laboratory of Computer and Information Science, Helsinki University of Technology, 1996.

[53] T. Maggipinto et al. Role of neural networks in the search of the Higgs boson at LHC. *Physics Letters*, B(409):517–522, 1997.

[54] T. Schiekel et al. Nuclide production by proton induced reactions on elements ($6 \leq \mathrm{Z} \leq 29$) in the energy range from 200 MeV to 400 MeV. *Nucl. Instr. and Meth.*, B(114):91–119, 1996.

[55] T. Sjostrand et al. PYTHIA 6.2 Physics and Manual. *LU TP 01/21, 3rd ed.*, April 2003. [arXiv: hep-ph/0108264].

[56] V. Aleksandryan et al. *Nuclear Physics*, A(674):539–549, 2000.

[57] V. Barashenkov et al. Interaction of high-energy radiation with substance. In *Dubna Report P2-5719*. 1971.

[58] V. Flaminio et al. Compilation of Cross-Sections II: K^+ and K^- Induced Reactions. *CERN-HERA*, 83-02, 1983.

[59] V. V. Abramov et al. Studies of the response of the prototype CMS hadron calorimeter, including magnetic field effects, to pion, electron, and muon beams. *Nucl. Instr. and Meth.*, A(457):75–100, 2001.

[60] W. H. Press et al. *Numerical Recipes in C: The Art of Scientific Computing*. Prentice-Hall, 2nd edition, 1992.

[61] Y. E. Titarenko et al. Experimental and Computer Simulations Study of Radionuclide Production in Heavy Materials Irradiated by Intermediate Energy Protons. 1999. [arXiv: nucl-ex/9908012].

[62] Y. E. Titarenko et al. Study of residual product nuclide yields from 0.1, 0.2, 0.8, and 2.6 GeV proton-irradiated ^{nat}Hg targets. *LANL Report LA-UR-00-3600*, 2000. [arXiv: nucl-ex/0008012].

[63] A. Kling *et al.* (eds.). *Advanced Monte Carlo for Radiation Physics, Particle Transport Simulation and Applications*. Proceedings of the Monte Carlo 2000 Conference, Lisbon, 23–26 October, 2000. Springer, 2001.

[64] H. Fesefeldt. The Simulation of Hadronic Showers – Physics and Application. Technical report, PITHA 85-02, Physikalisches Institut, RWTH Aachen, 1985.

[65] P. Fong. *Statistical Theory of Fission*. Gordon and Breach, New York, 1969.

[66] A. Heikkinen for the Geant4 Collaboration. Geant4: an Object-Oriented Toolkit for Simulation in High Energy Physics. *Proceedings of the XXXIII Annual Conference of the Finnish Physical Society, March 4-6 1999, Turku, Finland*, TURKU-FL-L28:7.9, 1999.

[67] E. T. Booth G. Bernardini and S. J. Lindenbaum. The Interactions of High Energy Nucleons with Nuclei. II. *Phys. Rev.*, 88(5):1017–1026, 1952.

[68] M. Goldberger. The Interaction of High Energy Neutrons and Heavy Nuclei. *Phys. Rev.*, 74:1269, 1948.

[69] J. J. Griffin. Statistical model of intermediate structure. *Physical Review Letters*, 17(9):478–481, 1966.

[70] J. J. Griffin. Statistical model of intermediate structure. *Physics Letters*, 24B(1):5–7, 1967.

[71] S. Haykin. *Neural Networks*. Prentice-Hall, Englewood Cliffs, NY, 1999.

[72] A. Heikkinen. Implementing the Bertini intra-nuclear-cascade in the Geant4 hadronic framework. In *Proceedings of the Monte Carlo Method: Versality Unbounded in a Dynamic Computing World, Chattanooga, Tennessee, April 17-21, 2005, on CD-ROM*. American Nuclear Society, LaGrange Park, IL, USA.

[73] A. Heikkinen. Separation of Higgs boson signal from Drell-Yan background with self-organizing maps. Published in the proceedings of the ACAT'07, NIKHEF, Amsterdam, April 23–27, 2007.

[74] A. Heikkinen. Validation of Geant4 Bertini cascade nuclide production. In *Proceedings of the Fourth International Workshop on Frontier Science 2005, New Frontiers in Subnuclear Physics, Università di Milano-Bicocca, Italia, September 12–17, 2005*, Frascati Physics Series Vol. XL (2006), pp. 259–264.

[75] A. Heikkinen and V. Karimaki. Fine Calibration of Detector Positions by Tracks in Helsinki Silicon Beam Telescope. Technical report, CMS NOTE-1999/029, 1999.

[76] A. Heikkinen and S. Lehti. Self-organized maps for tagging b jets associated with heavy neutral MSSM Higgs bosons. In *XVth International Conference on Computing in High Energy Physics and Nuclear Physics, CHEP'06, Volume I*, 2006. Proceedings of the CHEP 2006, Mumbai, India, February 13-17, 2006.

[77] A. Heikkinen and T. Lindén. Validation of Geant4 Bertini cascade nuclide production using parallel ROOT facility. In *XVth International Conference on Computing in High Energy Physics and Nuclear Physics (CHEP-06), Volume I*.

[78] A. Heikkinen and T. Lindén. Validation of the Geant4 Bertini Cascade model and data analysis using the Parallel ROOT Facility on a Linux cluster. In *Proceedings of CHEP'04, Interlaken, Switzerland, 27 September - 1 October, 2004. CERN-2005-002 Vol. 1 (2005) pp.306–309*, 2005.

[79] A. Hocker. TMVA - Toolkit for Multivariate Data Analysis. *CERN-OPEN-2007-007*, 2007. [arXiv: physics/0703039].

[80] A. Howard. Final Geant4 Benchmark Comparison with TARC data. LCG Physics Validation for LHC Simulations, CERN, November 21st, 2007, 2006. (Unpublished).

[81] A. Howard. Validation of Neutrons in Geant4 Using TARC Data - production, interaction and transportation. 2006 IEEE Nuclear Science Symposium Conference Record N38-3, 2006.

[82] Z. Zraenkel I. Dostrovsky and G. Friedlander. Monte Carlo Calculations of High-Energy Nuclear Interactions. III: Application to Low-Energy Calculations. *Physical Review*, 116(3):683–702, November 1959.

[83] I. Iashvili and A. Kharchilava. CMS TN-1996/100, 1996.

[84] V. N. Ivanchenko. The Geant4 hadronic verification suite for the cascade energy range. Technical report, CHEP'03 proceedings, 2003. [arXiv: nucl-th/0306016].

[85] V. N. Ivanchenko. Geant4: physics potential for instrumentation in space and medicine. *Nucl. Instr. and Meth.*, A(525):402–405, 2004.

[86] C. Kalbach. Exciton Number Dependence of the Griffin Model Two-Body Matrix Element. *Z. Physik*, A(287):319–322, 1978.

[87] T. Kohonen. *Self-Organizing Maps*. Springer, 1995.

[88] J. Lakos. *Large-Scale C++ Software Design*. Addison-Wesley, 2000.

[89] T. Lampén. Detector Alignment Studies for the CMS Experiment. Doctoral thesis, Helsinki University of Technology, April 2007. HIP-2007-02.

[90] M. J. Lang. Application of a Kohonen network classifier in TeV γ-ray astronomy. *J. Phys*, G: Nucl. Part. Phys.(24):2279–2287, 1998.

[91] S. Lehti. Tagging b-jets in $b\bar{b}h_{SUSY} \rightarrow \tau\tau$. *CMS NOTE 2001/019*, 2001.

[92] P. Luukka. Characterization of Czochralski Silicon Detectors. Doctoral thesis, Helsinki University of Technology, May 2006. HIP-2006-04.

[93] R. G. Alsmiller M. P. Guthrie and H. W. Bertini. *Nucl. Instr. and Meth*, (66):29, 1968.

[94] M. Mjahed. *Nucl. Phys.*, B(140):799, 2005.

[95] R. Jones on behalf of the CERN Beam Instrumentation Group. *Status Report on LHC Beam Instrumentation*. LHC Machine Advisory Committee, MAC, 6th December 2007 (Unpublished).

[96] S. Pearlstein. Medium-energy nuclear data libraries: a case study, neutron- and proton-induced reactions in ^{56}Fe. *The Astrophysical Journal*, 346:1049–1060, 1989.

[97] M. G. Pia and J. Knobloch. Particle physics software aids space and medicine. *CERN Courier*, June 2004.

[98] A. Ribon. Physics validation of the simulation packages in a LHC-wide effort. In *Proceedings of CHEP'04, Interlaken, Switzerland, 27 September - 1 October, 2004. CERN-2005-002 Vol. 1 (2005) pp.203–206*, 2005.

[99] H. Robbins and S. Monro. *Annu. Math. Stat.*, (22):400, 1951.

[100] C. Rubbia. CERN 96-97, 1997.

[101] V. D. Elvira S. Banerjee and J. Yarba. Talk given at Geant4 Hadronics Meeting, February 27th 2008. (Unpublished).

[102] G. Segneri and F. Palla. Lifetime based b-tagging with CMS. CMS NOTE 2002/046, 2002.

[103] R. Serber. Nuclear Reactions at High Energies. *Phys. Rev.*, 72:1114, 1947.

[104] N. Srimanobhas. Neutron Background Studies at CMS. LCG Physics Validation for LHC Simulations, CERN, September 20th, 2006. (Unpublished).

[105] N. V. Stepanov. ITEP Preprint, ITEP-55, 1988.

[106] B. Stroustrup. Speaking C++ as a Native. In *Advanced Computing and Analysis Techniques in Physics Research, VII International Workshop ACAT 2000, Batavia, Illinois, USA, October 16-20, 2000*, AIP Conference proceedings Vol. 583. American Institute of Physics, 2001.

[107] H. Katajisto T. Brander, A. Heikkinen and F. García. Geant4 shielding simulation of graphite-epoxy composite material for a satellite electronics housing. In *Proceedings of the XXXVIII Annual Conference of the Finnish Physical Society, March 18-20, 2004, Oulu, Finland*, number 25 in Report series in physical sciences, 2004.

[108] E. Tuominen. Development of Radiation Hard Radiation Detectors – Differences Between Czochralski Silicon and Float Zone Silicon. Doctoral thesis, Helsinki University of Technology, September 2003. HIP-2003-2.

[109] T. Lampén V. Karimäki, A. Heikkinen and T. Lindén. Sensor Alignment by Tracks. Technical report, CMS CR-2003/022, 2003.

[110] C. Weiser. A Combined Secondary Vertex Based B-Tagging Algorithm in CMS. *CMS NOTE 2006/014*, 2006.

[111] V. Weisskopf. Statistics and Nuclear Reactions. *Physical Review*, 52:295–302, August 1937.

[112] J. P. Wellisch. Hadronic shower models in Geant4 - the frameworks. *Comp. Phys. Commun.*, 140:65–75, 2001.

[113] J. P. Wellisch. Geant4 physics validation for large HEP detectors. *Nucl. Instr. and Meth.*, A(502):669–672, 2003.

[114] A. Heikkinen with C. Eklund et al. Silicon Beam Telescope for CMS Detector Tests. *Nucl. Instr. and Meth.*, A(430):321–332, 1999.

[115] A. Heikkinen with CMS collaboration. The TriDAS Project - Technical Design Report, Volume 2: Data Acquisition and High-level Trigger. CERN/LHCC 02-26, CMS TDR 6, 2002.

[116] A. Heikkinen with CMS collaboration. CMS – The Computing Project Technical Design Report. CERN/LHCC 2005-023, CMS TDR 7, 20 June 2005.

[117] A. Heikkinen with CMS collaboration. Physics Technical Design Report Vol. I, Detector Performance and Software. CERN/LHCC series, 2006-001 (2006) 522 pp., 2006.

[118] A. Heikkinen with CMS collaboration. The CMS experiment at the CERN LHC. *The Journal of Instrumentation*, JINST 3 S08004, 2008.

[119] A. Heikkinen with E. Tuominen et al. Test beam results of a large area strip detector made on high resistivity Czochralski silicon. *Nucl. Phys. B (Proceedings Supplements)*, 125C:175–178, 2003.

[120] A. Heikkinen with G. Folger et al. Progress in hadronic physics modeling in Geant4. *Submitted to Journal of Physics*, 2008.

[121] A. Heikkinen with Geant4 Collaboration. Geant4 Physics Reference Manual – Geant4 9.1, December 2007. (Available at Geant4 Collaboration Webpage).

[122] A. Heikkinen with M. Haapakorpi et al. New Object Oriented Software for Silicon Beam Telescope. Technical report, (Unpublished), 1999.

[123] A. Heikkinen with M. Haapakorpi et al. Object Oriented Reconstruction and Analysis for the Helsinki Beam Telescope. *Proceedings of the International Europhysics Conference on High Energy Physics, EPS99, Tampere, Finland, 15-21 July 1999*, IOP Publishing, 1999.

[124] A. Heikkinen with T. Koi et al. Validation of Hadronic Models in Geant4. In *AIP Conf. Proc., Hadronic Shower Simulation Workshop, March 19, 2007*, volume 897, pages 31–40, 2007.

[125] A. Heikkinen with T. Lampen et al. Testing TMVA software in b-tagging for the search of MSSM Higgs bosons at the LHC. International Conference on Computing in High Energy and Nuclear Physics (CHEP07), Journal of Physics: Conference Series 119 (2008) 032028, [doi:10.1088/1742-6596/119/3/032028].

[126] D. Wright and A. Heikkinen. Adding Kaons to the Bertini cascade model. In *Proceedings of CHEP'04, Interlaken, Switzerland, 27 September - 1 October, 2004. CERN-2005-002 Vol. 1 (2005) pp.215–218*, 2005.

Publications I–VIII

ISBN 978–952–10–5675–8 (paperback)
ISBN 978–952–10–5676–5 (pdf)
ISSN 1455–0563
http://ethesis.helsinki.fi
Helsinki University Print 2009